DEPTH AND BOTTOM PRESSURE FLUCTUATIONS IN A HYDRAULIC JUMP

A Thesis Submitted

in Partial Fulfilment of the Requirements

for the Degree of

MASTER OF TECHNOLOGY

by

RAVI BHUSHAN KUMAR

to the

Department of Civil Engineering

Indian Institute of Technology, Kanpur

July, 1996

CERTIFICATE

This is to certify that the present M.Tech thesis work entitled **Depth and Bottom Pressure Fluctuations in a Hydraulic Jump** *has been carried out by* **RAVI BHUSHAN KUMAR** *under our supervision and it has not been submitted elsewhere for a degree.*

S. Surya Rao

Dr.S.SURYA RAO
Professor
Dept. of Civil Engineering
Indian Institute of Technology
Kanpur

K Muralidhar

Dr.K.MURALIDHAR
Professor
Dept. of Mechanical Egineering
Indian Institue of Technology
Kanpur

July, 1996

ACKNOWLEDGMENTS

I express my deepest sense of gratitude to my thesis advisors Dr. S. Surya Rao and Dr. K. Muralidhar for their constant help and encouragement in the successful completion of this work. I am grateful to all my teachers at I.I.T Kanpur for helping me in shaping my professional skills in the field of Hydraulics and Water Resources Engineering.

I would like to thank my Lab Staff Mr. Kalyan Das, Mr. Ramashankar and Mr. R. B. Singh for their sincere help.

I would like to thank all the people who have been friends and helped me during my stay at I.I.T. Kanpur especially Sanjay, Rajesh, Khalil, Bovin, Sandeep, Karunakar, Narayana and Avadhesh. I would never forget the memories of all the interesting, endless chats we shared during our long evening strolls.

I can never thank enough my parents and brothers. Their inspiration, expectation and confidence have been a pillar of strength to me all the time.

ABSTRACT

The present work is concerned with the statistical characterization of fluctuations in depth and bottom pressure in a free and steady hydraulic jump. The hydraulic jump was formed in a horizontal laboratory flume just downstream of a sluice gate. The state of incident supercritical flow was undeveloped. Continuous record of instantaneous depth and pressure fluctuation was acquired and the digital data was analysed for certain statistical characteristics. Results have been presented for two different Froude numbers.

The structure of fluctuation of bottom pressure and depth is discussed in the form of evolution of probability density function, variation of skewness and kurtosis with distance along the jump, the space correlation function, the autocorrelation function and the spectra. The interrelation between two fluctuating quantities is presented in the form of a crosscorrelation coefficient and its variation with distance along the jump. With the reduced data the air concentration in the region of hydraulic jump has been successfully determined. Also presented is the apparent unit weight of the air water mixture.

Experimental results obtained in the present work match well with those presented by past investigators. Original finding of the study are : 1. Depth and bottom pressure fluctuation are initially uncorrelated; the correlation increases almost linearly with distance. 2. Turbulence is initially anisotropic with transverse scales greater than longitudinal scales; turbulence decays in the downstream direction and becomes increasingly isotropic. 3. The evolution of turbulence towards a fully developed state is seen in the power spectra of both depth as well as bottom pressure. 5. Air content monotonically decreases with distance.

CONTENT

LIST OF FIGURES

LIST OF TABLES

LIST OF PHOTOGRAPHS

LIST OF SYMBOLS

a,b,c	constant coefficient in Equations 3.35 & 3.36
a_c	air content in airwater mixture in hydraulic jump
$B_u( )$	probability density function
$E(f)$	spectrum amplitude
f	frequency
h	depth
h_1	depth before jump
h_2	depth after jump
I_x, I_y, I_t	integral scale of correlation function in corresponding direction
p	base pressure
p_2	base pressure after jump
N	total number of points in sample space
Q	discharge
$R( )$	correlation coefficient
R_{XY}	crosscorrelation coefficient for two signal X(t) & Y(t)
T	total time of record
t	instantaneous time
t_u	time for which a signal value remains in a infinitesimal interval about u
u	an arbitrary value
$X(t)$	any arbitrary signal
$X'(t)$	fluctuating component of signal X(t)
$\bar{X}$	mean value of signal X(t)
X_{max}	statistical maximum value of signal X(t)

X_{min}	statistical minimum value of signal X(t)
X_{RMS}	root mean square value of signal X(t)
X_{3m}	skewness coefficient of signal X(t)
X_{4m}	kurtosis coefficient of signal X(t)
$X^{\#}(f)$	frequency spectrum of signal X(t)
z	normal variate
σ	standard deviation
τ	lag time
η	lag distance in longitudinal direction
ξ	lag distance in transverse direction
λ_t	time micro scale
γ_a	unit weight of air
γ_m	unit weight of airwater mixture in jump
γ_w	unit weight of water

superscript $'$ denotes the fluctuating component of the signal

superscript * denotes the nondimensional form of the quantity

CHAPTER - 1

INTRODUCTION

1.1 Preliminaries

The hydraulic jump is a common method of dissipating energy in a large number of applications. It is also used for mixing of chemicals in industrial processes. The generation of large scale turbulence and subsequently its conversion to heat results in dissipation of energy in the flow. This gives rise to severe pressure fluctuation and thus also the depth fluctuation in the region of a hydraulic jump. Also, this process entrains some quantity of air. All above mentioned facts cause adverse loading condition on the floor, resulting in its damage through the mechanism of fatigue, structural resonance, cavitation and erosion. It is of utmost interest for a hydraulic engineer to know the stochastic characteristics of depth and base pressure fluctuation in the region of a hydraulic jump and their interrelationship.

1.2 Literature Review

The hydraulic jump is defined as sudden and turbulent transition of flow of fluid from supercritical state to subcritical state. The flow in a hydraulic jump is accompanied by extremely turbulent roller eddy. The flow can be characterised as non homogeneous turbulent aerated flow. Intense turbulence in the region of hydraulic jump causes a number of features of concern to engineers. Notable among these are energy losses occurring due to turbulence, air content of the air water mixture in the jump region, statistical character of forces acting on floor etc.

In the literature available in this field, most investigators were interested in finding the statistical character of flow, losses occurring in jump and its interaction with the rigid boundary, i.e., bed and sides. From the extensive literature

available in this field it becomes clear that the hydraulic jump was first described by Leonardo Da Vinci. Ever since and until 1965, the studies in this field were limited only to understanding of macroscopic structure of the hydraulic jump.

The first attempt to study the microscopic structure of turbulence in a hydraulic jump is due to Rouse (1965). He along with Siao and Nagaratnam published their work in which they presented the differential and integral form of the pertinent momentum and energy equations involving the mean and fluctuating part of velocity and pressure. Due to nonavailibility of instruments to perform the measurement in water, they simulated the jump configuration in an airduct. Later on with the development of pressure transducers that can be used in water, studies were conducted on a hydraulic jump itself. Vasiliev and Bukreyev (1967) conducted experiments on jumps using strain gauge type transducers. They presented results in the form of autocorrelation function and spectral density estimates. They also gave example to calculate the load on the apron. Leutheusser and Kartha (1972) studied the effect of inflow condition on the hydraulic jump. They have shown the effect of the state of flow development of the incident supercritical stream on mean characterestics of jump phenomena. Abdul Khader and Elango (1974) conducted important experiments in this field using sophisticated transducers and data acquisition system. They conducted the experiment at three different Froude numbers. They presented results in the form of autocorrelation function and spectral density estimates. They also determined the temporal micro scales. Lopardo and Henning (1985) conducted similar studies and presented some guidelines for performing experiments in this field. Bower and Toso (1988) performed experiments for Froude numbers from 3-10, with both developed and undeveloped incident flow condition and found the location and magnitude of extreme pressures in the region of hydraulic jump. Fiorotto and Rinaldo (1992) conducted experiments at different Froude numbers from 5-10, with the developed incident flow condition. They presented result in the form of longitudinal space correlation function and probability density function of the pressure fluctuation. They also presented the transverse spatial correlation function at a section where maximum

difference in pressure value was observed. Their main thrust was to find the force on the slab beneath the jump. They have also presented the variation of skewness and kurtosis along the jump for different Froude numbers. Other investigators have also presented their work of a similar nature. Notable among them are Bowers and Tsai (1969), Akbari et al. (1982), Wang et al. (1984) and Kim (1989). Notable work on study of depth fluctuation and its relation to pressure fluctuation has not been reported in past.

1.3 Problem Definition

The present work is a study of the stochastic character of fluctuation of depth and pressure on the floor in a hydraulic jump. After study of extensive literature in the field it is clear that no attempt has been made to study the stochastic character of depth fluctuation. Generally it is assumed to closely follow the pressure fluctuations. Also it is known that flow in a hydraulic jump is aerated. Although the amount of air in water is significant, it is usually ignored in analysis. The main effect of air in water is to decrease the unit weight of air water mixture. An attempt is made to find out the amount of air entrapped in the flow and also to find out the apparent unit weight of air water mixture. In the present work experiments were performed at two different Froude number. The jump was formed just downstream from the sluice gate in a horizontal laboratory flume.

In the present thesis, chapter 2 deals with the experimental apparatus and techniques involved in the present work. Chapter 3 gives a brief description of the statistical analysis and sample calculation. Chapter 4 is concerned with the Results and Discussion. Chapter 5 presents the summary and conclusions given and scope of further study. Appendix A consists of algorithm for statistical analysis and computation of statistical parameters.

CHAPTER - 2

EXPERIMENTAL DETAILS

2.1 Flume

The experiments were carried out in a glass walled rectangular flume having 5 m length, 45 cm width and 90 cm depth, with horizontal floor. Sluice gate was provided at both the ends to form the jump. Water was supplied from a constant head overhead tank. The water at outlet was collected in a covered channel. At the end of the outlet channel a rectangular weir was provided for discharge measurement. The whole experimental setup is shown in Figure 2.1. The experimental test section was made at a distance of 16 cm from the sluice gate. In this area tappings were made in the bottom plate (Figure 2.2). The experimental area was 32 cm wide and 112 cm long. A series of tappings along the longitudinal axis were provided in this work. Transverse tappings lines were provided 16 cm on either side of the longitudinal tapping line. The distance between two transverse tapping lines was kept at 16 cm. A total of 7 (seven) transverse tapping lines were provided in measurement area. The distance between two contiguous taps was 2 cm in both the lines. Tappings were made of copper tubes of 2 mm internal diameter and 3 cm length. The pressure transducer fitted in a socket could be directly connected to the tapping. For the measurement of depth the wave probe was fitted to a rack and pinion gauge which could be lowered in water. It was supported on the floor in order to reduce its longitudinal vibrations.

The measurement for pressure and depth was taken at two points simultaneously through a data acquisition system. This is needed for crosscorrelation between depth and pressure.

2.2 Instrumentation

A block diagram of instruments used and electrical connections is shown in Figure 2.3 . The instrumentation consists

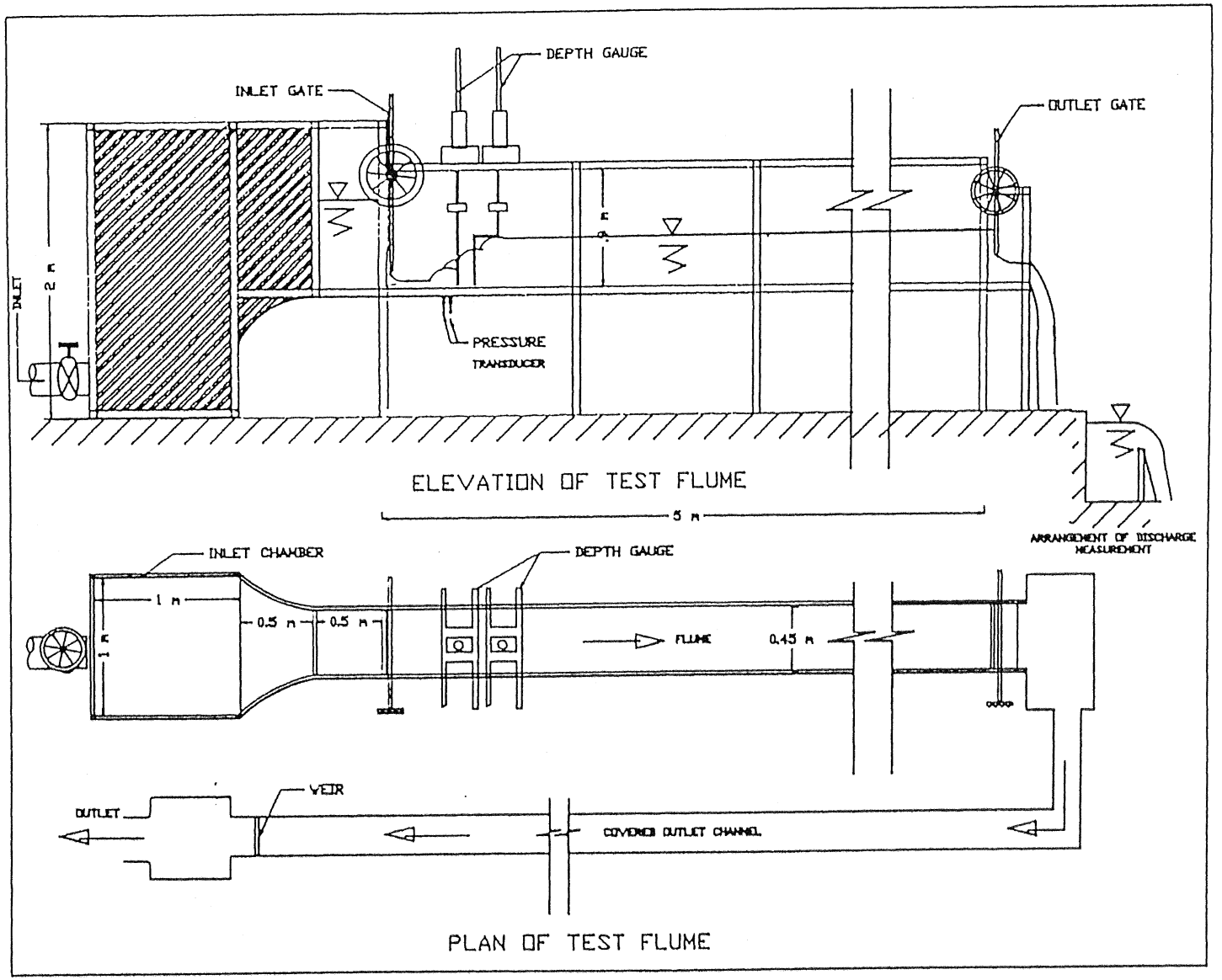

Figure 2.1 : Plan and elevation of experimental setup

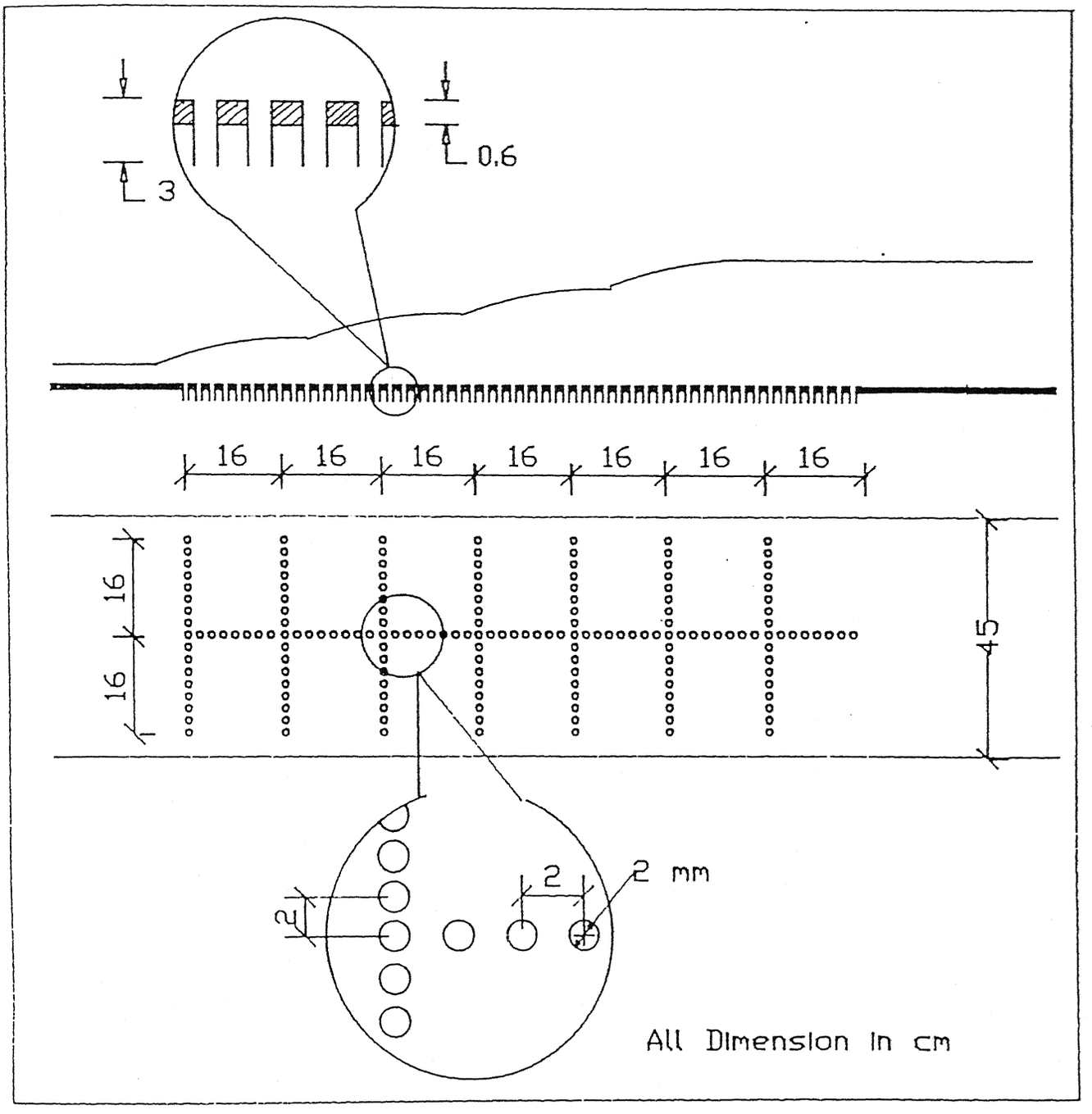

Figure 2.2 : Details of experimental area

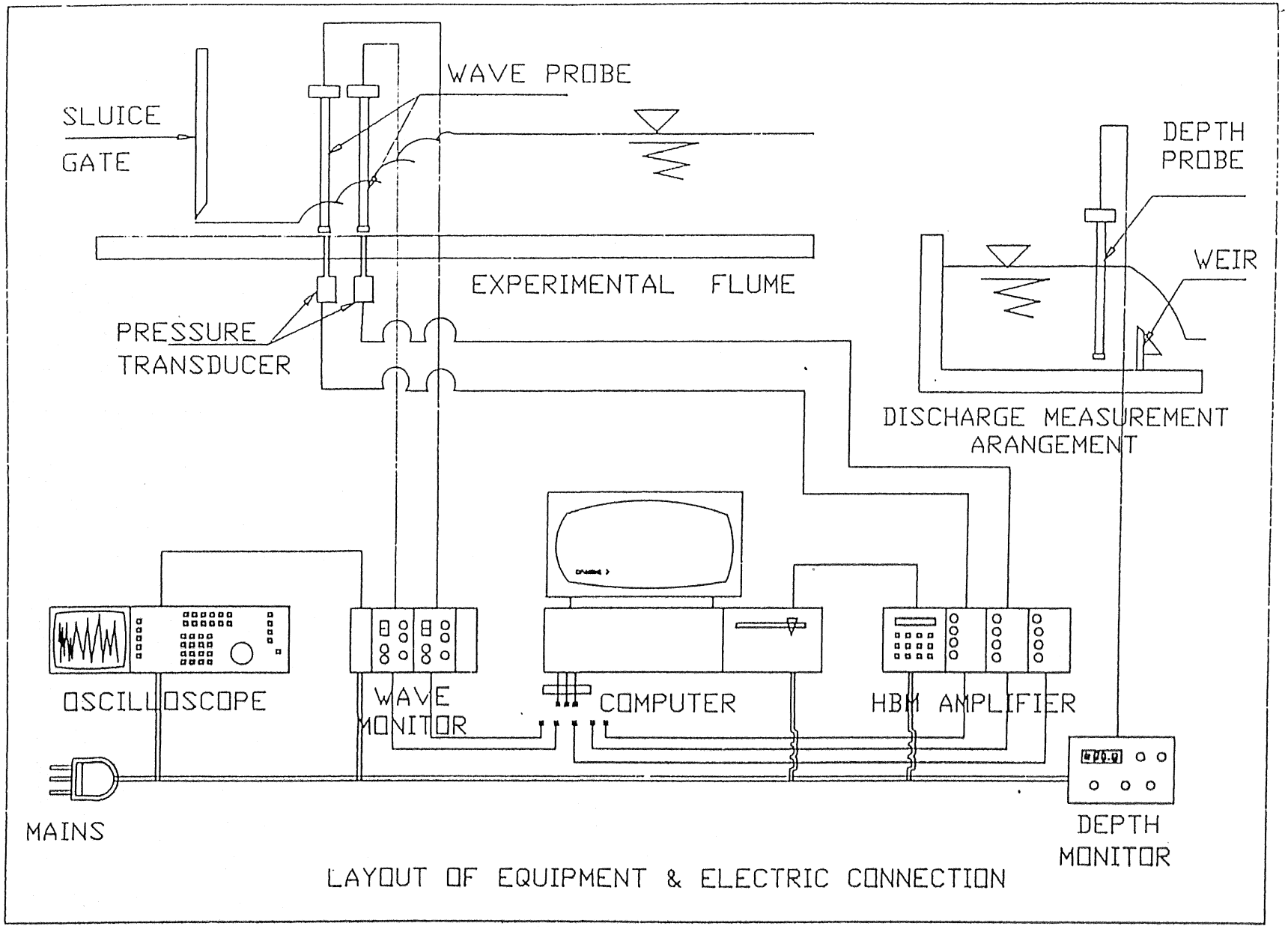

Figure 2.3 : Block diagram of equipment and electrical connection

of a personal computer, pressure transducer, signal amplifier, wave gauge, water level indicator and oscilloscope. Their detailed specifications are provided in Section 2.4 .

Two pressure transducers were used to get the continuous record of pressure fluctuation. The transducer was of HBM make, inductive type with a safe maximum limit of 0.1 bar. The transducer was also capable of recording the suction pressure. The output from the transducer was fed to the signal amplifier. The transducer was screwed in a copper socket which could be directly attached to the tapping made in the flume floor with the help of a rubber tube. Air outlet valve was provided in the socket to expel all air from it before each measurement. The transducer and its connection to tapping is shown in Figure 2.4 .

The signal amplifier was of HBM make, ALPHA 3000 system. It was capable of handling three transducers at a time, connected to the three channels. One CMS32 display interface was also provided for local control and adjustment. The amplifier could also be handled by personal computer using RS232C interface provided with the unit CMS32. The output from the amplifier was linear with respect to pressure with a range of +10 V to -10 V.

Two wave probes were used to get the continuous record of depth fluctuation. The wave probe was connected to a wave monitor which was capable of handling two probes through two modules. The output from the wave monitor was in the range of +10 V to -10 V. Depth in the range of 5 cm to 30 cm could be measured using the probe. The probe is shown in Figure 2.5 .

A water level indicator was used to monitor the head over the weir which in turn was used for finding the discharge. The water level indicator was of capacitance type and was capable of sensing a change in depth of the order of one tenth of a mm.

A storage oscilloscope was used for calibration of above mentioned transducers and probes. It was HP 54501A, capable of handling four channels at a time.

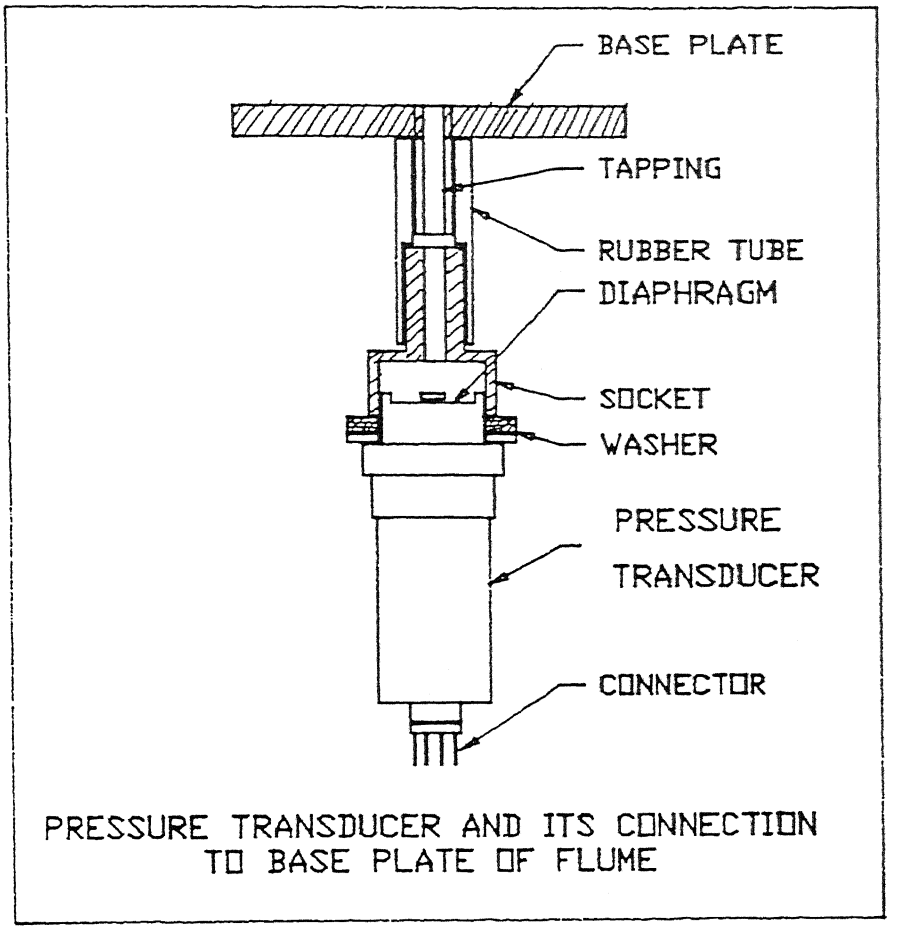

Figure 2.4 : Details of transducer and its mechanical connection

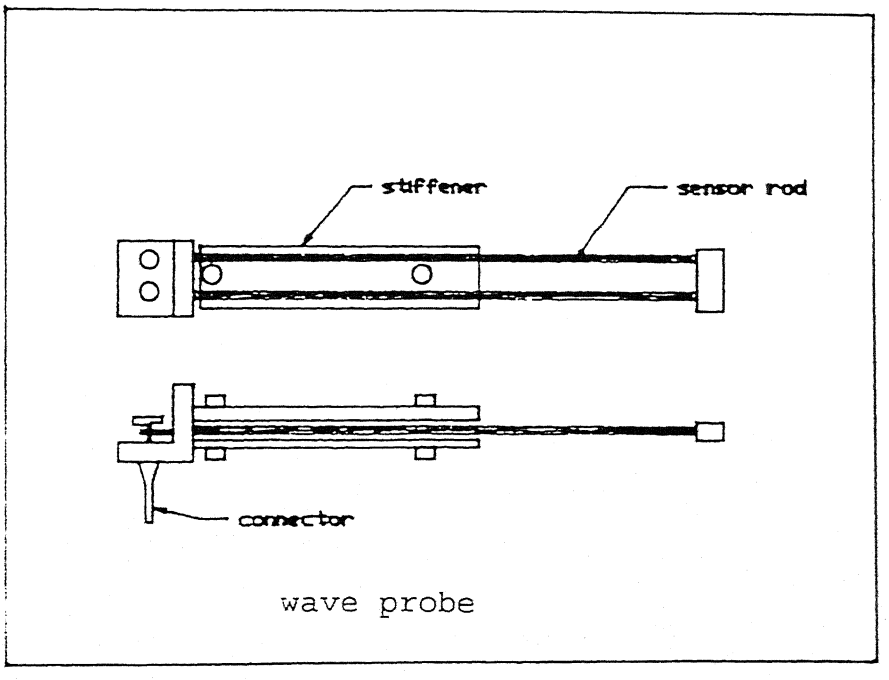

Figure 2.5 : Details of wave probe

An IBM compatible personal computer was used for data acquisition and analysis. It was 386 PC manufactured by Keonics Magnavision Computer Limited, Bangalore. A plug in card PCL712 was used for analog to digital conversion of data. Original software developed by the Department of Mechanical Engineering I.I.T. Kanpur was used for data acquisition from the HBM amplifier system. Additional software was written for acquisition of data from the wave monitor. Additional programs were written in FORTRAN 77 language for data analysis.

The plug-in-card for analogue to digital conversion of signal was PCL712 multi lab card. It was manufactured by Dynalog Micro system. It provided 16 analog input channel, out of which, 3 (three) have been used in the present. The working range of the analog input was -5V to +5V. Since the output of the HBM amplifier and also the wave monitor can vary between -10V to +10V, two equal resistances of 4.7 Kohm each are connected between the output point of the instrument and ground. The output taken from the junction of these two resistances forms the input to the analog input channel of PCL712 card.

The instrument used in the present work can also be seen on Photograph 2.1 .

2.3 Experimental Procedure

At first the transducer and probes used in the experiments were calibrated. Those calibrated are two pressure transducers, two wave probes and one water level indicator.

The pressure transducer was calibrated for static load of water column. The amplifier is adjusted to provide the output, for the working range of pressure, between 0 V to 10 V. The maximum safe static load that can be applied, with such an adjustment, was 100 cm of water. The static load between 10 cm to 80 cm, in step of 10 cm, were applied on the transducer. The output was recorded and averaged for each load. The reponse of the transducer was linear

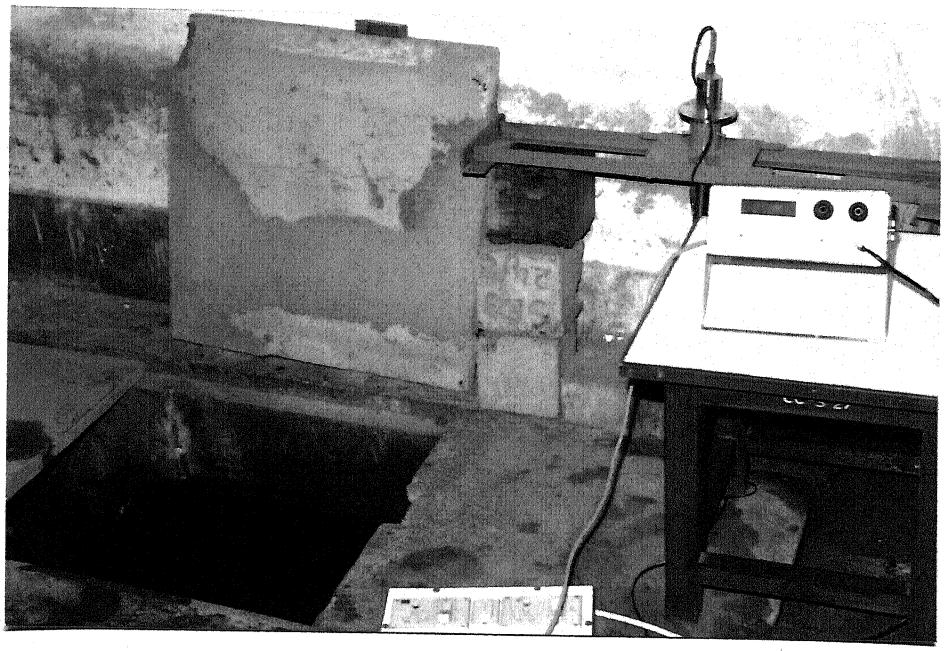

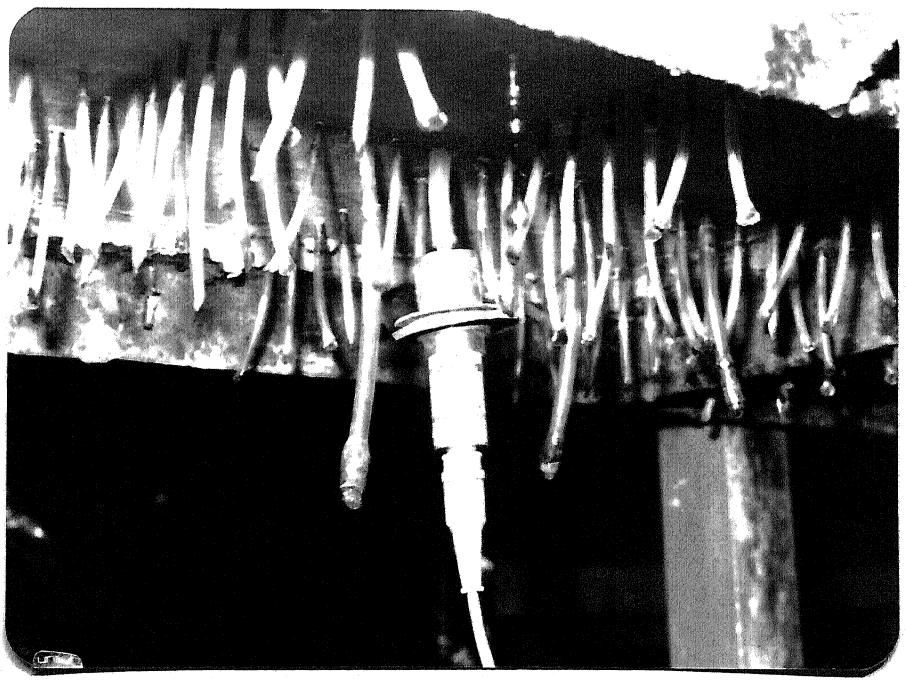

The wave gauge was calibrated by dipping it in water. Depths between 5 cm to 30 cm could be measured by the wave gauge. The probe was dipped in water from 6 cm to 24 cm, in steps of 3 cm. The output was recorded and averaged for each load. The response for one gauge was linear but for other it was nonlinear.

The water level indicator (over the weir) was calibrated in order to read the change in water level with a sensitivity of 0.1 mm.

The experiments were conducted for two Froude numbers. The experiment for each Froude number can be divided into four parts.

The first part include the sampling of data for analysis of autocorrelation and spectra for depth and pressure. The total time of measurement was 3 minutes at a sampling rate of 50 Hz. Hence 8192 discrete values of pressure and depth at 20 ms interval were recorded.

The second part of the experiment was sampling of data for analysis of cross correlation between pressure and depth. The signal was sampled at 7 (seven) points along the longitudinal axis of channel. Both pressure and depth signal at the same location were recorded simultaneously. The total time of sampling was 25 seconds. The analysis were carried out using 1024 data points.

The third part of the experiment was sampling of data for analysis of spatial correlation, probability density and general statistics for pressure fluctuation. The pressure signal was sampled at two points simultaneously. One of the points is that at which the correlation coefficient has to be determined, known as reference point. The other point was one in the vicinity of the reference point. The maximum distance between the two points, known as lag distance, was kept at 16 cm. The point other than the reference point was on the longitudinal and the transverse lines. Thus these points were on the left, right and in the longitudinal direction downstream of the reference point giving the left hand transverse spatial correlation, the right hand transverse spatial

correlation and the longitudinal spatial correlation respectively. The signal was recorded for 25 seconds. The analysis were carried out with 1024 data points. There were seven reference points in the region of the jump.

The fourth part of the experiment includes sampling of data for analysis of spatial correlation, probability density and general statistics for depth fluctuation. The details of data acquisition are similar to pressure, but only six reference points were employed in this case.

The four steps mentioned above were implemented for two Froude numbers. The Froude numbers used were 5.49 (for a weak jump) and 9.59 (for a strong jump). The results are presented in the form of tables and graphs.

2.4 Specifications

The detailed specifications of the different instruments used in the experiment are as follows :

(a) Pressure Transducer :

Type	:	P11 (inductive type)
Manufacturer	:	Hottinger Baldwin Messtechnik, Germany
Measuring range	:	0 .. 0.1 bar
Natural frequency	:	0.5 KHz
Overload limit	:	200 %
Weight	:	105 gm (approximately)
Nominal sensitivity	:	8 mV/V
Linearity deviation	:	less than ± 0.5 %
Carrier frequency	:	5 KHz
Service temperature range	:	-20 .. 100 $^{\circ}$C

(b) Signal Amplifier :

Model	:	Alpha 3000 Amplifier system
Manufacturer	:	Hottinger Baldwin Messtechnik, Germany
Transducer which can be connected	:	Strain gauge transducer (full or half bridge) and inductive type transducer
Number of channels	:	3 (three)
Frequency limit	:	Switchable low frequency (100 Hz) to high frequency (1000 Hz)
Carrier frequency	:	5 KHz ± 0.5 %
Output voltage range	:	+10 .. -10 V
Level indicator	:	Red modulation LED lights up when output voltage exceeds ± 10 V
Display interface	:	CMS32
Computer interface	:	RS 232-C and IEEE 488-78
Power required	:	220 V ± 10 % , 48 .. 62 Hz
Service temperature range	:	-20 .. 60 °C

(c) Wave Gauge :

Type	:	Capacitance
Manufacturer	:	Armfield, U.K.
Output voltage range	:	-10 .. 10 V
Power required	:	230 V AC

(d) Water Level Indicator :

Type	:	Capacitance
Manufacturer	:	Engineering Models and Equipment, Roorkee
Least count	:	0.1 mm
Power required	:	230 V

(e) Storage Oscilloscope :

Model	:	HP 54501A, 100 MHz, Digitizing oscilloscope
Manufacturer	:	Hewlett Packard
Number of input channels	:	4 (four)
Input coupling	:	AC, DC
Vertical sensitivity	:	Maximum 5 V/div Minimum 5 mV/div
Vertical gain accuracy	:	± 1.5 %
Time base range	:	Maximum 5 sec/div Minimum 2 ms/div
Time base accuracy	:	0.005 %
Maximum sampling rate	:	10 Msa/sec

(f) Personal Computer :

Type	:	IBM PC/AT 386
Manufacturer	:	Keonics Magnavision Computer Limited, Banglore
Hardware details	:	80386 CPU, 80387 co-processor and 4 MB ram
Add on card	:	PCL712 multi lab card

(g) Analogue-Digital I/O Card :

Type	:	PCL712 multi lab card
Manufacturer	:	Dynalog Micro System (DMS), Bombay
Digitization	:	12 bit
Number of channels	:	16 (3 are only used)
Range of analogue input	:	-5 .. 5 V

CHAPTER - 3

DATA ANALYSIS

3.1 Introduction

Hydraulic jump is a zone of intense turbulence. A definition sketch of hydraulic jump is given in Figure 3.1 . Mathematically, turbulent fluctuation in such a flow can be considered as stochastic, steady and ergodic process. Due to random nature of the process, description by means of analytical explicit functions is not possible. Studies on fluctuating quantities is completed only when statistical measurements are carried out. General statistical description of fluctuating quantities includes probability density function, correlation analysis and spectra. These three functions describe the nature of fluctuations in different ways. Parameters, such as, length and time scale of fluctuations can be determined from these functions.

3.2 Statistics of Fluctuation

3.2.1 Central Tendency and Dispersion

The simplest quantities that can be calculated from the record of fluctuating signal are the mean, RMS value, standard deviations skewness and kurtosis. The relationship between the signal X(t) and above mentioned quantities are as follows :

Mean : $$\bar{X} = \lim_{T \to \infty} \frac{1}{T} \int_0^T X(t)\, dt \qquad 3.1$$

RMS value : $$\bar{X}^2_{RMS} = \lim_{T \to \infty} \frac{1}{T} \int_0^T X^2(t)\, dt \qquad 3.2$$

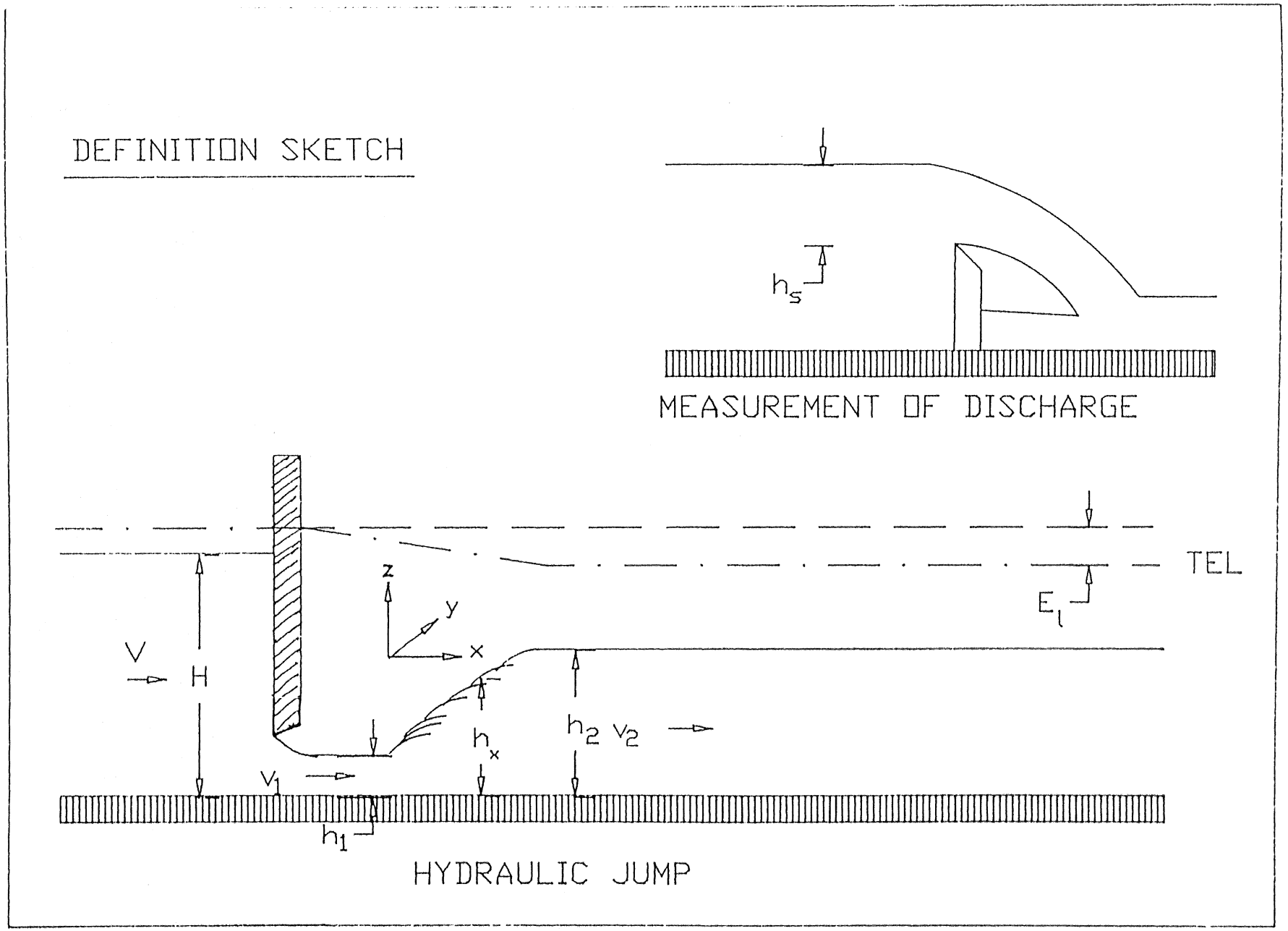

Figure 3.1 : Definition sketch of hydraulic jump

Standard deviation : $$\sigma^2 = \lim_{T \to \infty} \frac{1}{T} \int_0^T (X(t) - \bar{X})^2 dt \quad 3.3$$

Skewness : $$X_{3m}^3 = \lim_{T \to \infty} \frac{1}{T} \int_0^T (X(t) - \bar{X})^3 dt \quad 3.4$$

Kurtosis : $$X_{4m}^4 = \lim_{T \to \infty} \frac{1}{T} \int_0^T (X(t) - \bar{X})^4 dt \quad 3.5$$

The above mentioned values can be calculated in terms of probability density function and will be discussed later.

Mean and RMS value of any fluctuating signal is a single value representation of signal. Other quantities are measurement of dispersion of instantaneous value about the mean. Standard deviation is measurement of scatter of quantity about the mean. The skewness or the third moment of PDF is measurement of extent of symetricity of the quantity. The value of skewness is zero for a Gaussian signal. The kurtosis or fourth moment of PDF is the measurement of concentration of quantity about the mean. The value of kurtosis is 3 for a Gaussian signal.

3.2.2 Probability Density Function

The probability density $B_u(u)$ of any signal X(t) is indicative of the fraction of time the value of signal remains in an infinitesimal interval about u. Suppose the signal X(t) remains between u to u-du for a time t_u in the total time of record T. Then,

$$B_u(u) = \lim_{\substack{T \to \infty \\ du \to 0}} \frac{1}{T \cdot du} t_u \qquad 3.6$$

So the following properties about B_u is obvious, as,

$$B_u(u) \geq 0 \qquad 3.7a$$

$$\int_{-\infty}^{\infty} B_u(u)\, du = 1 \qquad 3.7b$$

The probability density function (PDF), $B_u(u)$, is a function with respect to u.

The different statistical quantities discussed in Section 3.2.1 are given in term of B_u as follows :

Mean $$\bar{X} = \int_{-\infty}^{\infty} B_u(u) \cdot u \, du \qquad 3.8$$

RMS value $$X_{RMS} = \int_{-\infty}^{\infty} B_u(u) \cdot u^2 \, du \qquad 3.9$$

Now with the $B'_u(u)$, the PDF of deviation from the mean , i.e., $X'(t)$ given by,

$$X'(t) = X(t) - \bar{X} \qquad 3.10$$

The other quantities mentioned in Section 3.2.1 are as follows :

Standard deviation $$\sigma^2 = \int_{-\infty}^{\infty} B'_u(u) \cdot u^2 \, du \qquad 3.11$$

Skewness $$X_{3m}^{3} = \int_{-\infty}^{\infty} B'_u(u) \cdot u^3 \, du \qquad 3.12$$

Kurtosis $$X_{4m}^{4} = \int_{-\infty}^{\infty} B'_u(u) \cdot u^4 \, du \qquad 3.13$$

The other quantities which are not discussed earlier, but are relevant to the present analysis are statistical maximum and minimum value. They are defined in terms of B_u as follows.

(a) Statistical Maximum Value :

This is a single value representing the data point having value near the upper limit. Consider the PDF shown in Figure 3.2 . Mathematically, the statistical maximum value is given by,

$$X_{max} = \frac{\int_{p'}^{\infty} B_u(u) \cdot u \, du}{\int_{p'}^{\infty} B_u(u) \cdot du} \qquad 3.14$$

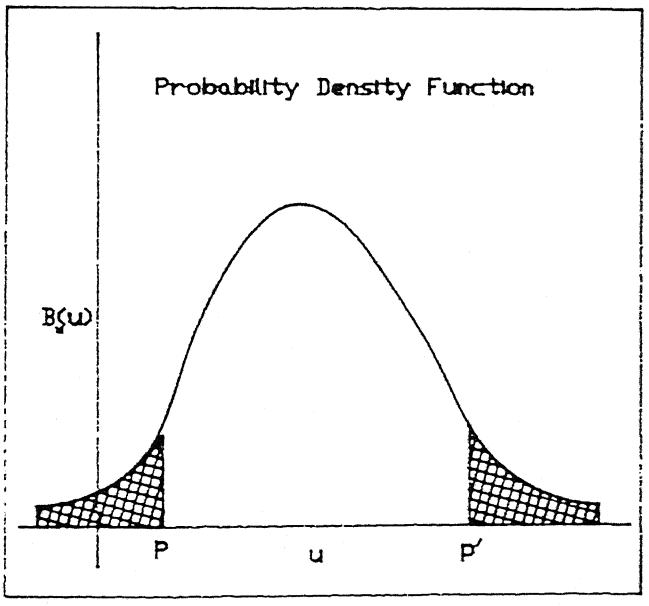

Figure 3.2 : Probability density function

The point P' is such that,

$$\int_{P'}^{\infty} B_u(u)\ du \;=\; 0.1 \int_{-\infty}^{\infty} B_u(u)\ du = 0.1 \qquad 3.15$$

(b) Statistical Minimum Value :

This is defined in a similar manner as minimum value that it represents the data point having value near the lower limit. Mathematically, the minimum value is given by,

$$X_{min} = \frac{\int_{-\infty}^{P} B_u(u)\cdot u\ du}{\int_{-\infty}^{P} B_u(u)\ du} \qquad 3.16$$

Here also, the point P is such that,

$$\int_{-\infty}^{P} B_u(u)\ du \;=\; 0.1 \int_{-\infty}^{\infty} B_u(u)\ du \;=\; 0.1 \qquad 3.17$$

In the present thesis the mean and RMS value are calculated using Equation 3.1 and 3.2, respectively. The standard deviation, skewness and kurtosis value are calculated using Equation 3.11, 3.12 and 3.13, respectively. The maximum and minimum value are calculated using Equation 3.14 and 3.16, respectively. The integration in all the cases is done using Simpson's one third rule.

One important aspect regarding the PDF of any turbulent fluctuating signal is that it tends to follow the shape of PDF of a Gaussian signal given by,

$$B_u(u) = \frac{1}{\sqrt{2\cdot\pi}\ \sigma}\ e^{-u^2/\ 2\cdot\sigma^2} \qquad 3.18$$

In the present thesis the PDF of actual signal is compared with the PDF of a Gaussian signal, having same standard deviation value, to confirm the trend.

3.2.3 Spatial Correlation

The correlation between same fluctuating signal recorded at two different points in the flow field is very important and useful in the study of turbulent flow. These are used in the study of spatial structure of turbulence in the field of flow. It helps in finding out the distance over which the fluctuations are interrelated.

The correlation coefficient for a pair of points A and B separated by a distance α is given by,

$$R(\alpha) = \lim_{T \to \infty} \frac{1}{T \cdot \sigma_A \cdot \sigma_B} \int_0^T X'_A(t) \cdot X'_B(t)\, dt \qquad 3.19$$

where $X'_A(t)$ and $X'_B(t)$ are deviation from mean calculated at points A and B and σ_A and σ_B are the standard deviation of signal measured at points A and B.

3.2.4 Temporal Correlation

Most time dependent signals arising from a turbulent flow process has some structure in time. A signal value at one time will be correlated with the signal value at later times. Similar to a space correlation coefficient, the temporal or auto correlation coefficient shows the extent of correlation that a signal will have on itself at some definite later time (known as lag time).

The auto correlation function for a signal as a function of the lag time τ is given by,

$$R(\tau) = \lim_{T\to\infty} \frac{1}{T\cdot\sigma^2} \int_0^T X'(t)\cdot X'(t+\tau)\, dt \qquad 3.20$$

where $X'(t)$ is deviation from mean calculated at the point and σ is the standard deviation of the signal.

3.2.5 Space Time Double Correlation Function

Any two dimensional signal is dependent on three basic variable x, y and t. The space time double correlation function for such a signal $X(x,y,t)$ is defined as,

$$R(x,\xi,y,\eta,\tau) = \lim_{T\to\infty} \frac{1}{T} \int_0^T X'(x,y,t)\cdot X'(x+\xi,\ y+\eta,\ t+\tau)dt \qquad 3.21$$

where $X'(x,y,t) = X(x,y,t) - \bar{X}(x,y)$ and $\bar{X}(x,y)$ is the mean value of $X(x,y,t)$.

The different correlation coefficients are special cases of the above mentioned space time double correlation function. These are as follows :

Auto correlation coefficient for $\xi=0$ and $\eta=0$, i.e.,

$$R(\tau) = R(x,0,y,0,\tau)$$

Longitudinal spatial correlation coefficient for $\eta=0$ and $\tau=0$, i.e.,

$$R(\xi) = R(x,\xi,y,0,0)$$

Transversal spatial correlation coefficient for $\xi=0$ and $\tau=0$. i.e.,

$$R(\eta) = R(x,0,y,\eta,0)$$

In the present thesis the auto correlation is calculated as

the real part of Fourier transform of the power spectrum. The other coefficient, i.e., longitudinal and transversal spatial correlation coefficient, are calculated by means of direct summation.

$$R = \frac{\frac{1}{N}\sum_{i=1}^{N} X'_{Ai} \cdot X'_{Bi}}{\sigma_A \cdot \sigma_B} \qquad 3.22$$

Here the coefficient is normalised by dividing it by the standard deviation value at respective points.

3.2.6 Power Spectrum

Power spectrum E(f) is the measure of extent of energy contribution from a infinitesimal interval of frequency about f to the total energy present in the signal.

Power spectrum of any signal can be found out by using Fourier transformation. The complex function $X^{\#}(f)$, known as the frequency spectrum of X(t), is defined as Fourier transform of X(t), i.e.,

$$X^{\#}(f) = \int_{-\infty}^{\infty} X(t) \cdot e^{-ift} dt \quad , \quad i=\sqrt{-1} \qquad 3.23$$

The power spectrum can be calculated as,

$$E(f) = [\, X^{\#}(f) \,]^2$$

In the present thesis the Fourier transformation is implemented by a Fast Fourier Transformation (FFT) algorithm.

The autocorrelation function is the real part of Fourier transform of the power spectrum.

3.2.7 Cross Correlation

The cross correlation between two signals is an important quantity which shows the extent of interrelation between them. The cross correlation coefficient between two signals X(t) and Y(t) is given by,

$$R_{XY} = \lim_{T \to \infty} \frac{1}{T \cdot \sigma_X \cdot \sigma_Y} \int_0^T X'(t) \cdot Y'(t) dt \qquad 3.25$$

Here X'(t) and Y'(t) are the deviation from mean calculated for two signals and σ_X and σ_Y are the standard deviation of the respective signal.

In the present thesis the cross correlation coefficient is calculated as direct summation of product of two signal values at same point and same time , i.e.,

$$R_{XY} = \frac{\frac{1}{N} \sum_{i=1}^{N} X_i \cdot Y_i}{\sigma_X \cdot \sigma_Y} \qquad 3.26$$

The coefficient is normalised by dividing it by the product of standard deviation value of individual signal.

3.2.8 Scales of Fluctuation

This is an important parameter in the analysis of a fluctuating signal. The correlation analysis described in the preceding sections can be summarised by calculating the scale of fluctuations. The two types of scales generally calculated are macro and micro scales. The scale can be determined in any dimension, i.e., time and space, and accordingly defined as time or length scales.

The macro scale in any dimension, say x, is defined as,

$$I_x = \int_0^\infty R(\xi)\, d\xi \qquad 3.27$$

Similarly,

$$I_y = \int_0^\infty R(\eta)\, d\eta \qquad 3.28$$

$$I_t = \int_0^\infty R(\tau)\, d\tau \qquad 3.29$$

Here R( ) is the corresponding correlation function .

The macro scale, also known as integral scale of correlation function, is the measure of distance in the corresponding direction, at which the two instantaneous values of the signal become uncorrelated. The value can be estimated by judging the first zero crossing point on the direction axis by the correlation function.

The micro scale defines the persistence of the random signal. It is a measure of the size of the smallest eddy generated in the field. The time micro scale is derived from the relation given by,

$$R(\tau) = \sigma \left[1 - \frac{\tau^2}{\lambda_t} + 0(\tau^4) \right] \qquad 3.30$$

where λ_t = time micro scale.

In the present thesis the integral scale is calculated in space and time.

3.2.9 Air Content and Apparent Unit Weight

The flow in the hydraulic jump entrains some amount of air. This air entrainment becomes less in the downstream direction. The effect of entrained air is to decrease the unit weight of the air water mixture, so that the depth of water in the jump is higher than that corresponding to pressure on floor. Assuming the hydrostatic pressure distribution in the jump one can calculate the air content at any section.

Let p_x be the pressure in cm of water at the floor and γ_m be apparent unit weight. Also let h_x be the depth of flow at the same section. Then,

$$\gamma_w p_x = \gamma_m \cdot h_x \qquad \text{(assuming the hydrostatic pressure distribution)}$$

$$\text{So,} \quad \frac{\gamma_m}{\gamma_w} = \frac{p_x}{h_x} \qquad 3.31$$

Now as the fluid in the hydraulic jump is mixture of air and water. So,

$$\gamma_m = a_c \gamma_a + (1 - a_c) \gamma_w \qquad 3.32$$

where a_c is the air content defined as the ratio of volume of air to total volume of mixture, γ_a and γ_w are unit weight of air and water respectively.

Neglecting the unit weight of air as compared to water we have,

$$\gamma_m = (1 - a_c) \gamma_w$$

$$1 - a_c = \frac{\gamma_m}{\gamma_w}$$

$$a_c = 1 - \frac{\gamma_m}{\gamma_w} = 1 - \frac{p_x}{h_x} \qquad 3.33$$

Knowing the value of p_x and h_x one can calculate the variation of γ_m and a_c along the jump.

3.3 Data Presentation

The data obtained after analysis have been presented in form of graphs and tables in this work

3.3.1 Nondimensionalisation of Parameters

In any graphical representation of data the parameters are nondimensionalised in order to remove bias due to scale of the system. The nondimensional form of different parameters are given in

Table 3.1 .

Table 3.1 : Nondimensional Parameters

Description	Symbol	Definition
Distance from the toe of jump	x^*	$\frac{x}{h_1}$
Lag distance in longitudinal direction	ξ^*	$\frac{\xi}{h_1}$
Lag distance in transverse direction	η^*	$\frac{\eta}{h_1}$
Lag time	τ^*	$\frac{\tau \cdot v_1}{h_1}$
Frequency	f^*	$\frac{f \cdot h_1}{v_1}$
Spectrum amplitude	E^*	$\frac{E}{E_{min}}$
Depth	h^*	$\frac{h}{h_2}$
Pressure	p^*	$\frac{p}{p_2}$
Integral scale	I^*	$\frac{I^*}{h_1}$

3.3.2 Probability density function

The probability density function is plotted as relative frequency vs normal variate. The normal variate 'z' is given by,

$$z = \frac{x - \bar{x}}{\sigma} \qquad 3.34$$

$\bar{x}$ = mean value of sample

σ = standard deviation of sample

3.3.3 Correlation Function

A smooth curve is fitted to data obtained by correlation analysis. In some cases of correlation analysis, the correlation coefficient is nonnegative. For such a case a curve given by Equation 3.35 is fitted.

$$y = e^{ax} \qquad 3.35$$

In Equation 3.35 , 'y' denotes the correlation coefficient and 'x' denotes the lag time or lag distance. In other cases when correlation coefficient changes sign a curve given by Equation 3.36 is fitted.

$$y = e^{ax} (\cos bx + c \cdot \sin bx) \qquad 3.36$$

In Equation 3.36, as before, 'y' denotes the correlation coefficient and 'x' denotes the lag time or lag distance.

The value of constant, i.e., a in Equation 3.35 and a, b and c in Equation 3.36, are estimated such that the sum of squares of error between the actual and fitted value is minimum (i.e., the least square procedure).

3.3.4 Power spectrum

Power spectrum is calculated as Fourier transformation of the signal. The spectrum was calculated as average of 8 consecutive run of 1024 points. The spectrum thus calculated was found to have some noise added to it. The noise is supposed to be added due to following reason :

(a) Due to A-to-D card

(b) Oscillations of water column in connecting tubes pressure transducer

The noise can be introduced in signal due to lack of resolution during digitization of data by the A-to-D card. In order to test the effect of A-to-D card error, if any, two signals (a square wave and a sine wave) were generated by a signal generator and recorded by the A-to-D card. The spectrum was calculated. The same signals were fed to a spectrum analyser and spectrum was obtained. The exact and calculated spectra are shown in Figure 3.3 . It is obvious from the figure that the spectrum as calculated from the data obtained by the A-to-D card has some noise. So it can be concluded that the noise added to the spectrum is generated by the A-to-D card. The other possibility as referred above cannot be ruled out, but it was not possible to test the existence of the same.

In order to capture the trend in the spectrum a two stage averaging was implemented to smoothen the spectrum. In first stage the Tukey Hanning filter was applied. The signal value after applying the filter is given by,

$$E_{ni}^2 = \frac{1}{4} E_{o(i-1)}^2 + \frac{1}{2} E_{oi}^2 + \frac{1}{4} E_{o(i+1)}^2 \qquad 3.37$$

where E_n = older value of amplitude,

E_o = new value after first stage of averaging.

For second stage of averaging, the whole range of frequency is divided in equal interval of 10 discrete values each. Each interval was represented by frequency and amplitude at its midpoint. The amplitude is average of amplitude in the interval. The above process is shown by block diagram in figure 3.4 .

The amplitude was nondimensionalised as discussed in Section 3.3.1 . The result was presented as plot of $\ln(E^*)$ versus $\ln(f^*)$. Smooth curve are suitable polynomial of order which has better representation.

3.3.5 Scales of Fluctuation

The integral scale was calculated analytically by integration of the best fit curve. The value at some points are misrepresented because of improper best fit due to mathematical

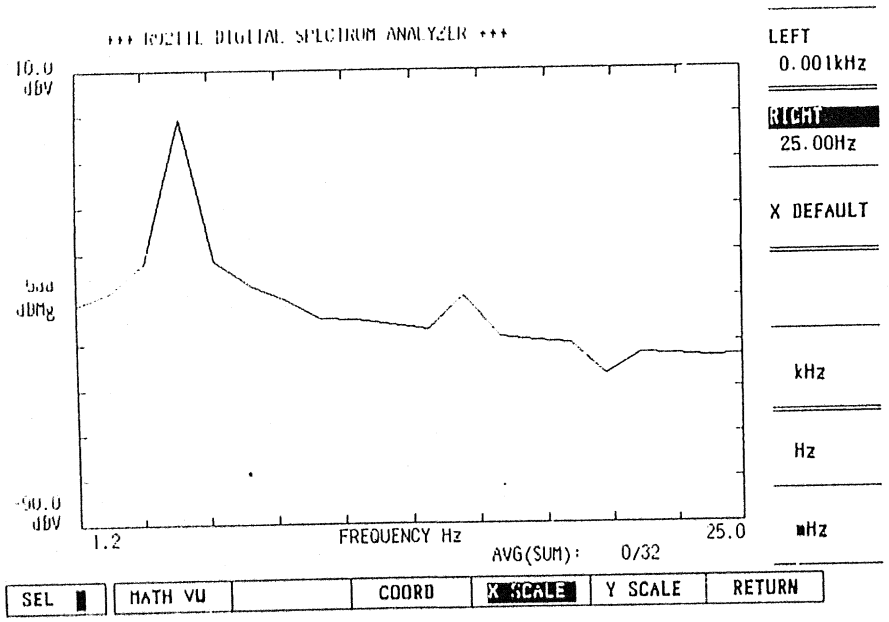

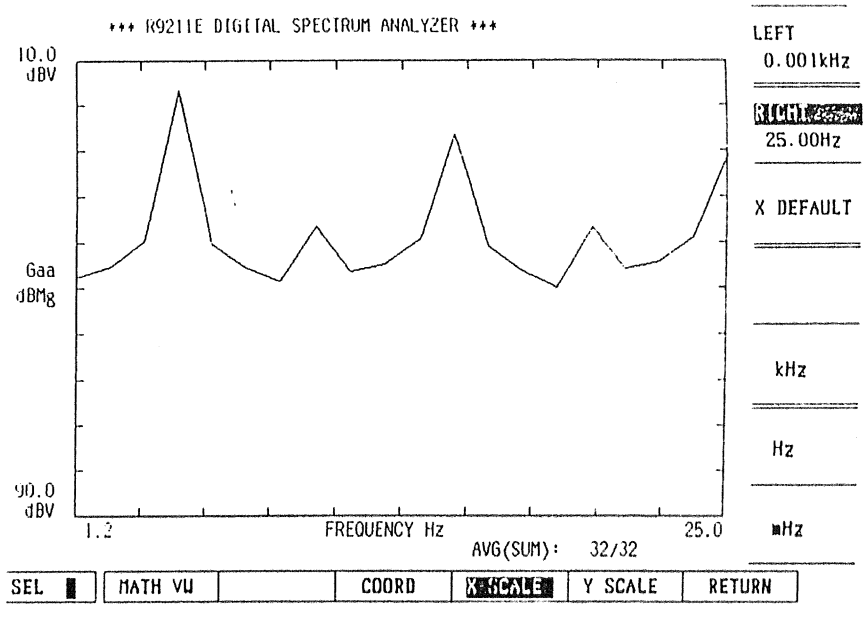

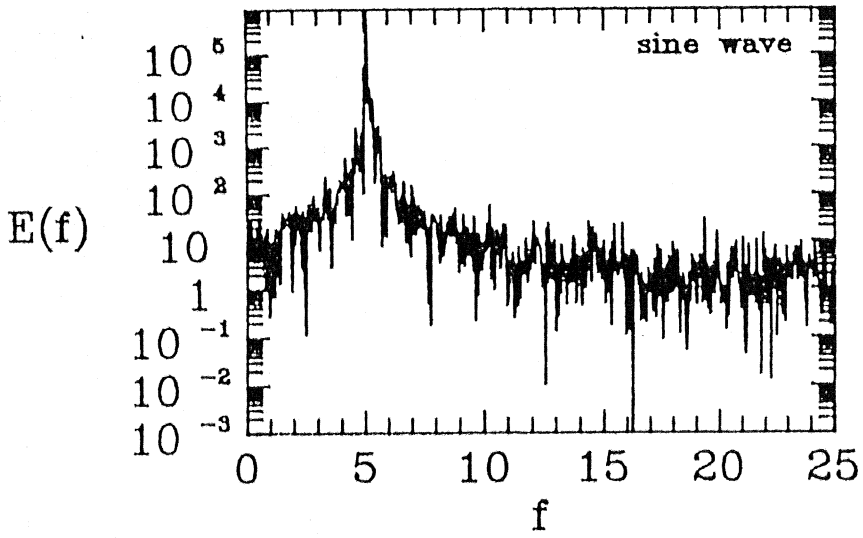

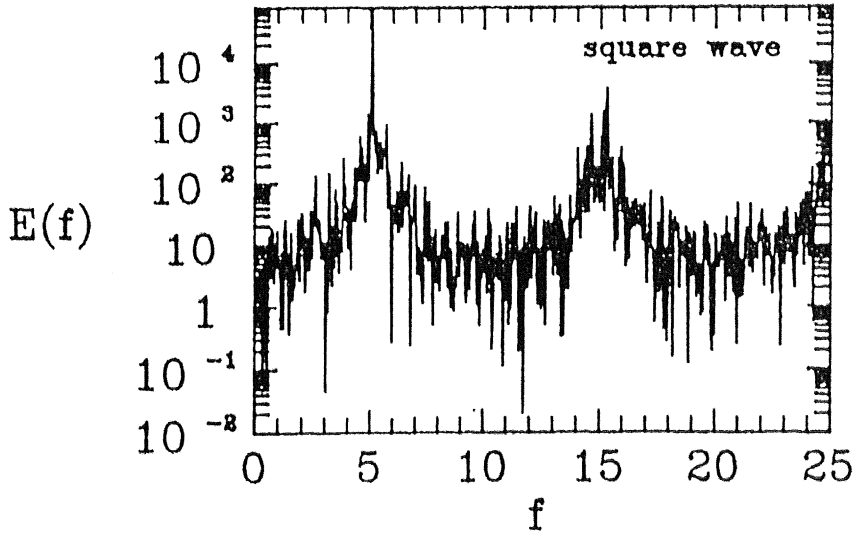

Figure 3.3 : Spectra of sine and square wave (top two is obtained by spectrum analyser and bottom two is calculated from recorded data)

misrepresented because of improper best fit due to mathematical limitation.

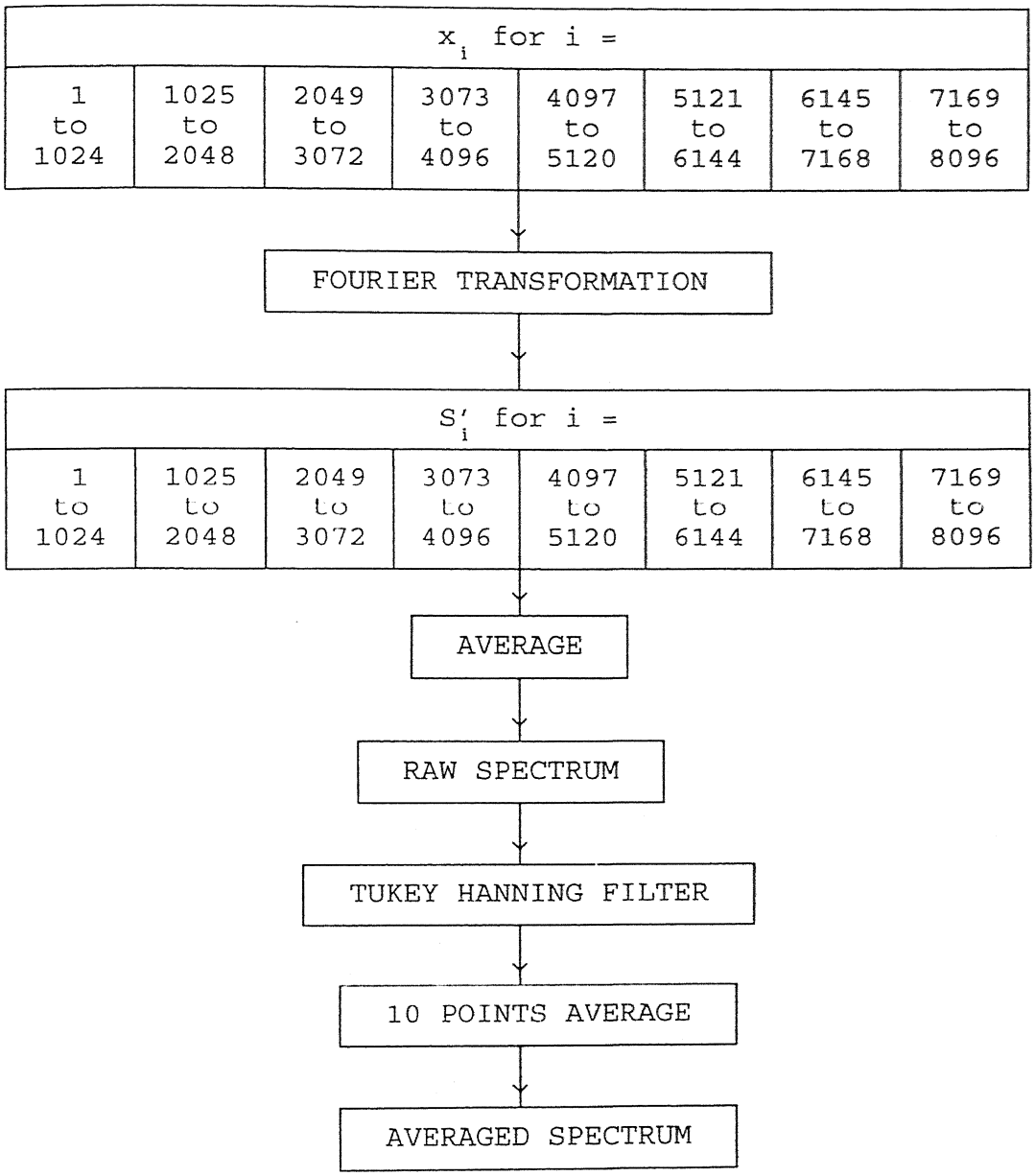

Figure 3.4 : Calculation of power spectrum

As the value of time interval between consecutive reading was 20 ms, which is comparable to the micro scale as reported in past reports. So it was meaningless to calculate its value.

CHAPTER - 4

RESULT AND DISCUSSION

4.1 Introduction

Experiments were conducted at two Froude numbers namely 5.49 and 9.59. The details of flow parameters are given in Table 4.1

Table 4.1 Details of Flow Parameters

Run	initial depth (h_1)	final depth (h_2)	initial velocity (v_1)	discharge (Q)	initial Froude number (Fr_1)
-	cm	cm	m/sec	l/sec	—
1	2.45	18.15	2.69	26.926	5.49
2	1.60	20.90	3.80	27.360	9.59

Photograph 4.1 shows the flow at two Froude numbers for which the study was done. Figure 4.1 shows the realization of digital data collected for pressure and depth at an arbitrary location and Fr = 5.49. Depth signal looks smoother than pressure because frequency response of depth gauge is less than the pressure transducer.

For the convenience of presentation four cases have been identified as follows :

Case 1 : Analysis of pressure signals p(t) for Fr = 5.49,
Case 2 : Analysis of depth signals h(t) for Fr = 5.49,
Case 3 : Analysis of pressure signals p(t) for Fr = 9.59,
Case 4 : Analysis of depth signals h(t) for Fr = 9.59.

Quantities reported are time-averaged value, probability density function, spatial correlation function, autocorrelation

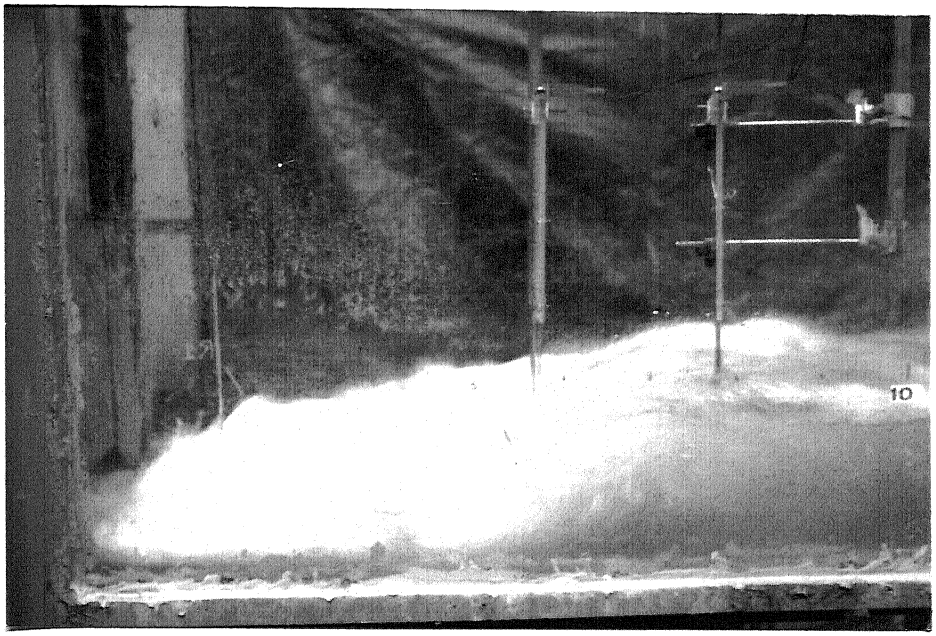

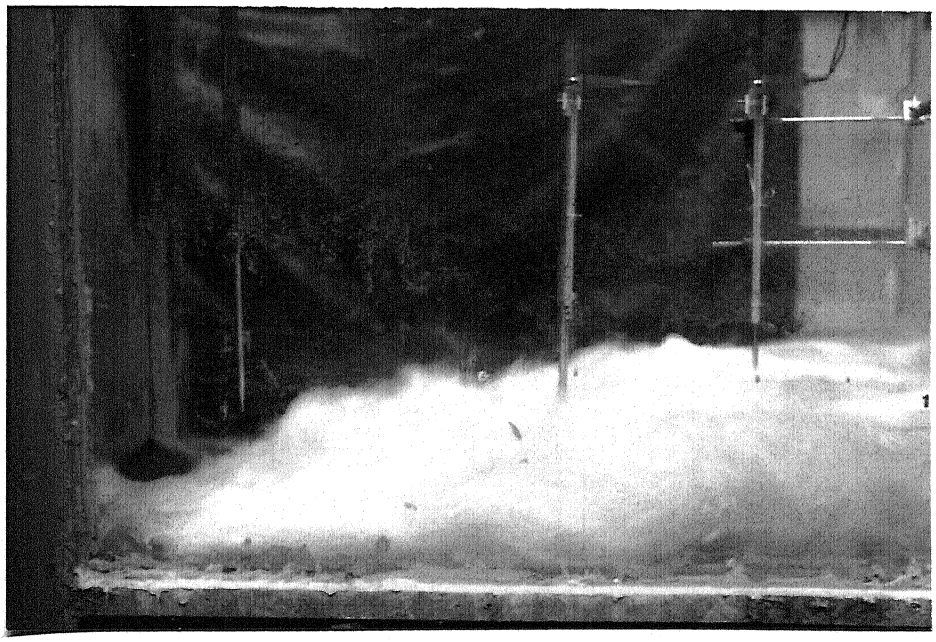

Photograph 4.1 : Hydraulic jump formed for experiments (top photograph is at Fr=5.49 and bottom photograph is at Fr=9.59)

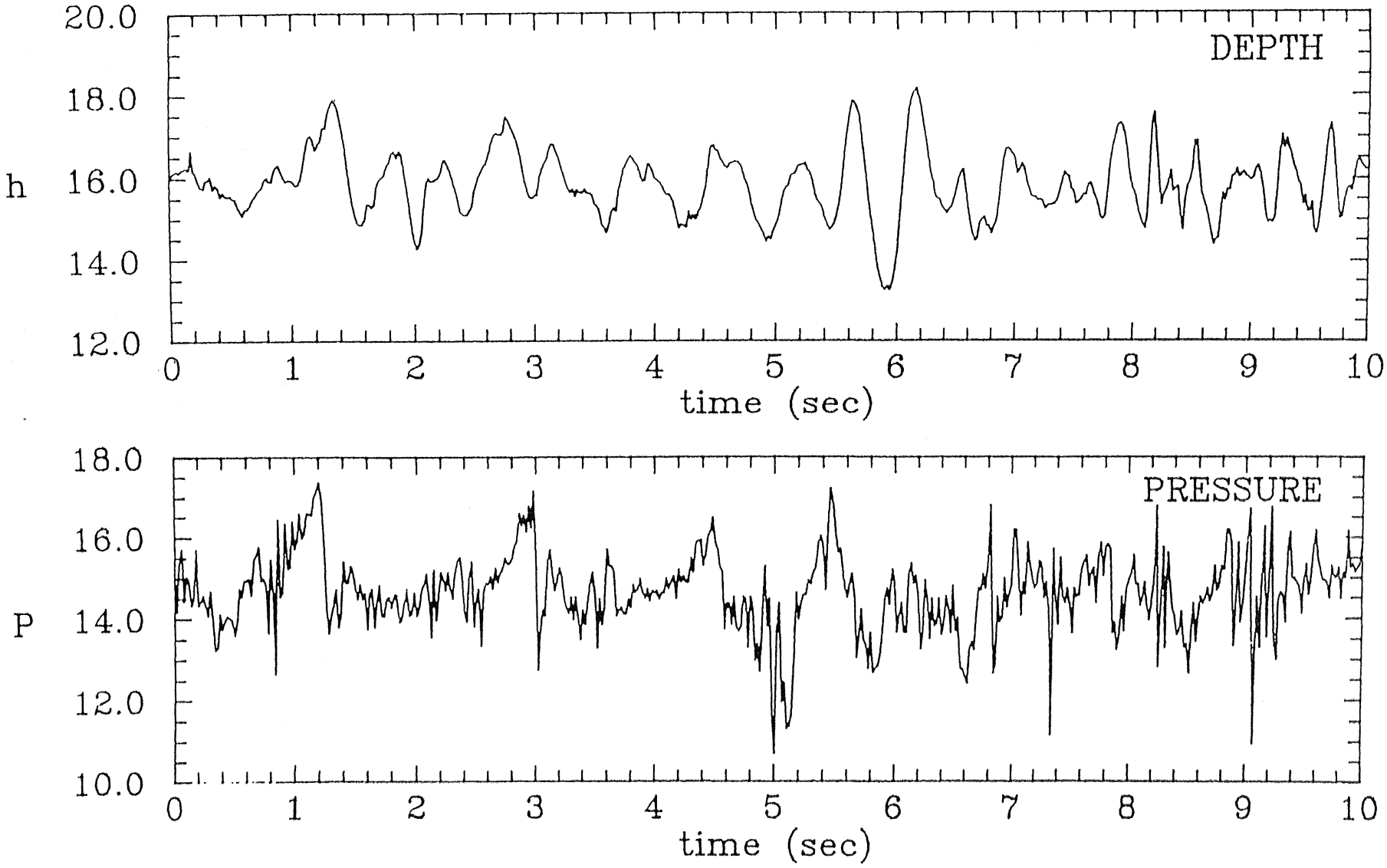

Figure 4.1 : Realization of pressure and depth data (at $x^* = 30$ and Fr = 5.49)

function, spectra, crosscorrelation coefficient, integral scale of fluctuation, air content and apparent unit weight.

4.2 Time-averaged value

Figure 4.2 shows the variation of maximum, mean and minimum value of p and h for all four cases. The smooth curves shown in the figure are second order polynomials fitted to the data points, which minimize the sum of the squares of the errors. Figure 4.3 shows the variation of the mean values of p and h (on the same scale). The circles are the manually determined values. It is obvious from the graph that the fluctuations in p and h decrease with distance from the toe of the jump. Near the toe of the jump the measured depth is greater as compared to pressure. This shows the effect of air entrainment in the jump. The entrained air decreases the unit weight of the air-water mixture. Away from the toe, the pressure and depth tend to become equal due to reduction of air entrainment. The details of air entrainment are discussed later in this chapter.

Figure 4.4 shows the variation of standard deviation, skewness and kurtosis with distance from the toe of the jump for all the four cases. The dashed line in the graph are values corresponding to a Gaussian signal. The value of skewness and kurtosis for both signals are very close to the value corresponding to the Gaussian signal. In all cases one can observe that the skewness is positive near the toe and decreases to become negative at larger distances. This depicts that the positive fluctuation (corresponding to the upward movement)is more probable as compared to negative fluctuation in the region near the toe of the jump and the negative fluctuation is more probable than the positive in the region far away. It can also be observed that the points where the skewness curves cross zero are close for both pressure and depth signals for a given Froude number. The standard deviation decreases with distance from the toe of the jump in all cases. This is an expected result because turbulence decays by viscous dissipation in the absence of mean shear. The normalised standard deviation of pressure falls more rapidly than that of the depth signal.

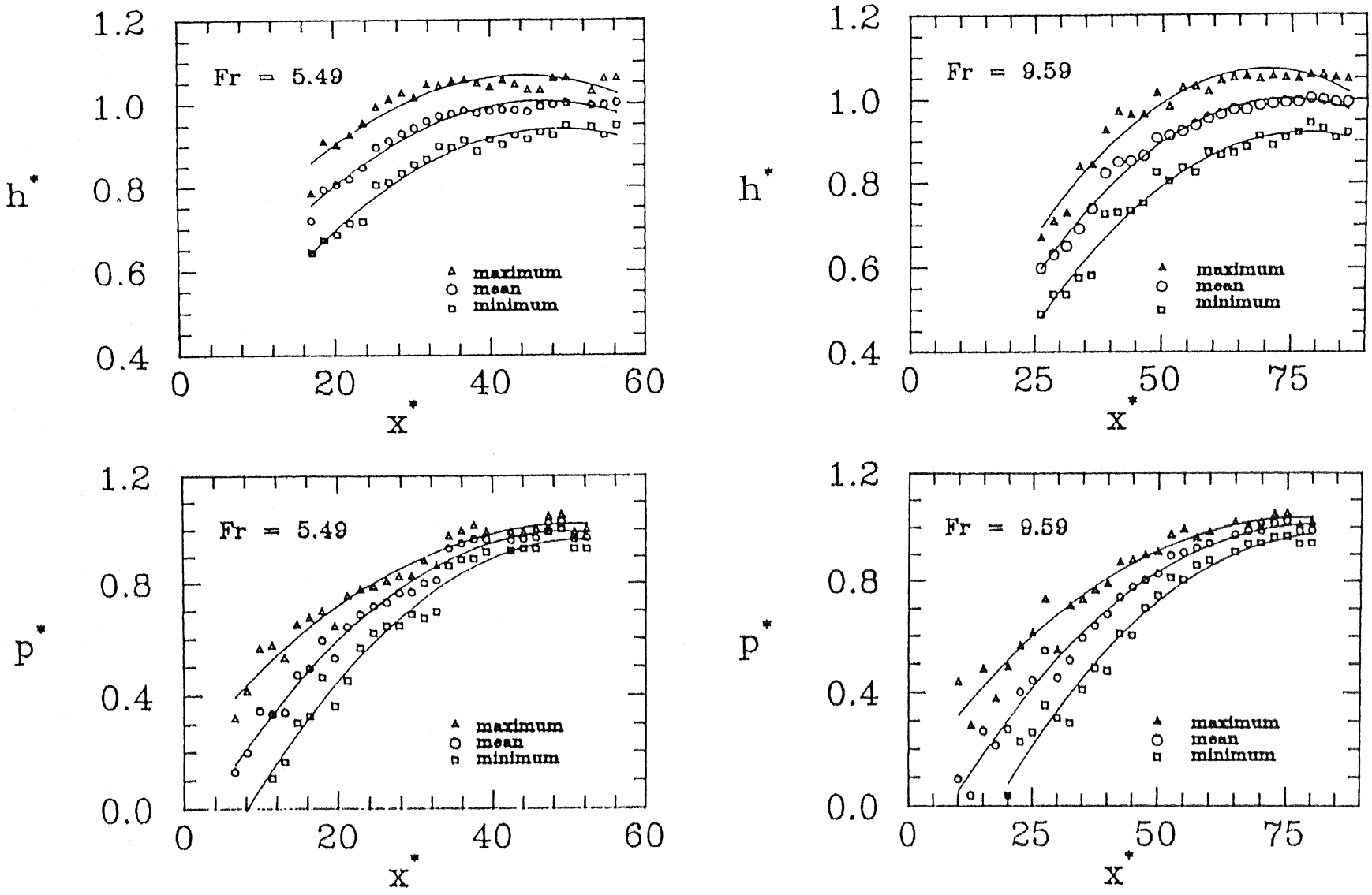

Figure 4.2 : Variation of maximum, mean, and minimum value of p^* & h^* with distance at Fr = 5.49 and Fr = 9.59

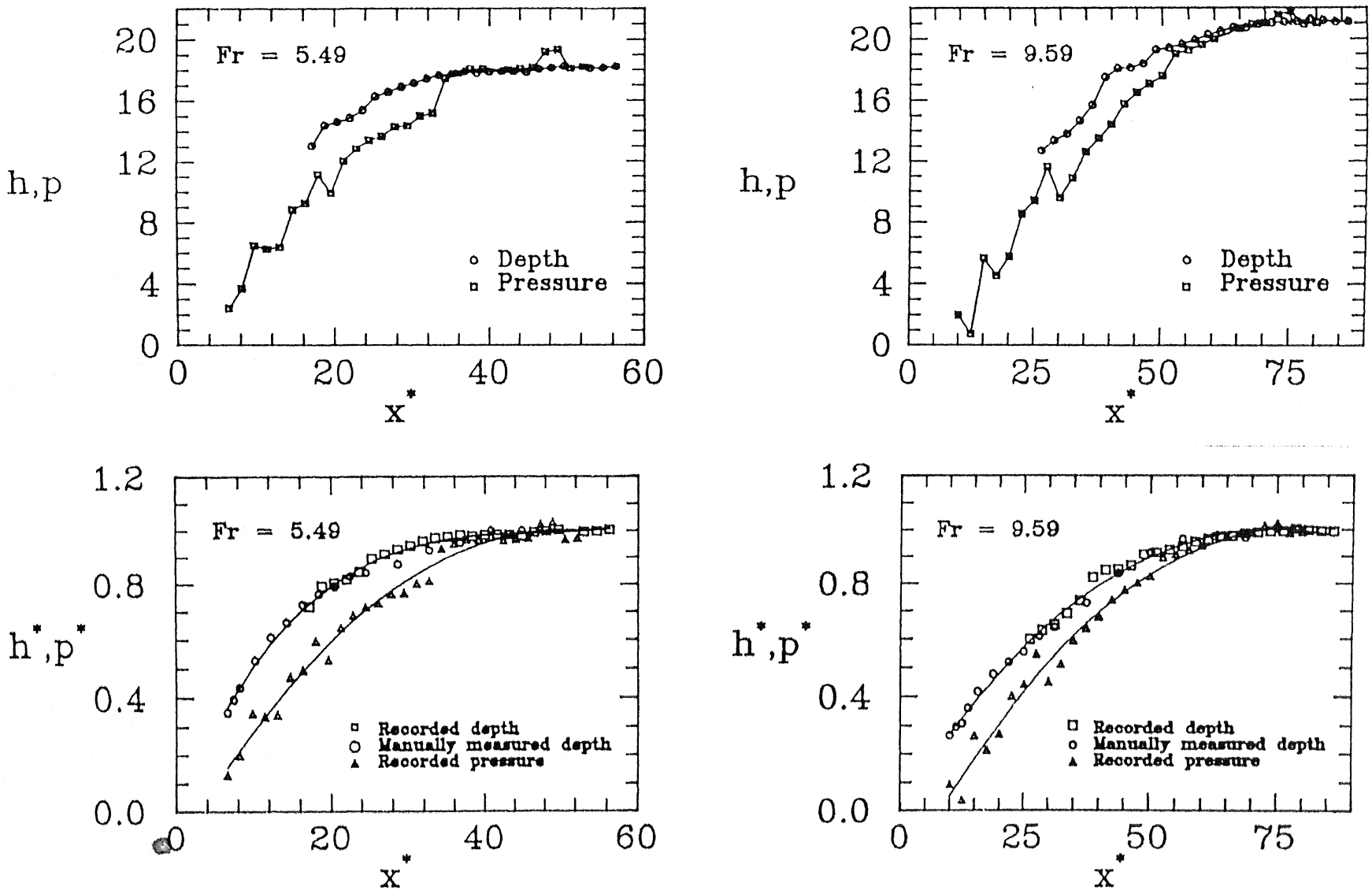

Figure 4.3 : Variation of mean value of p & h with distance at Fr = 4.59 & 9.59 (top two shows dimensional form and bottom two shows nondimensional form)

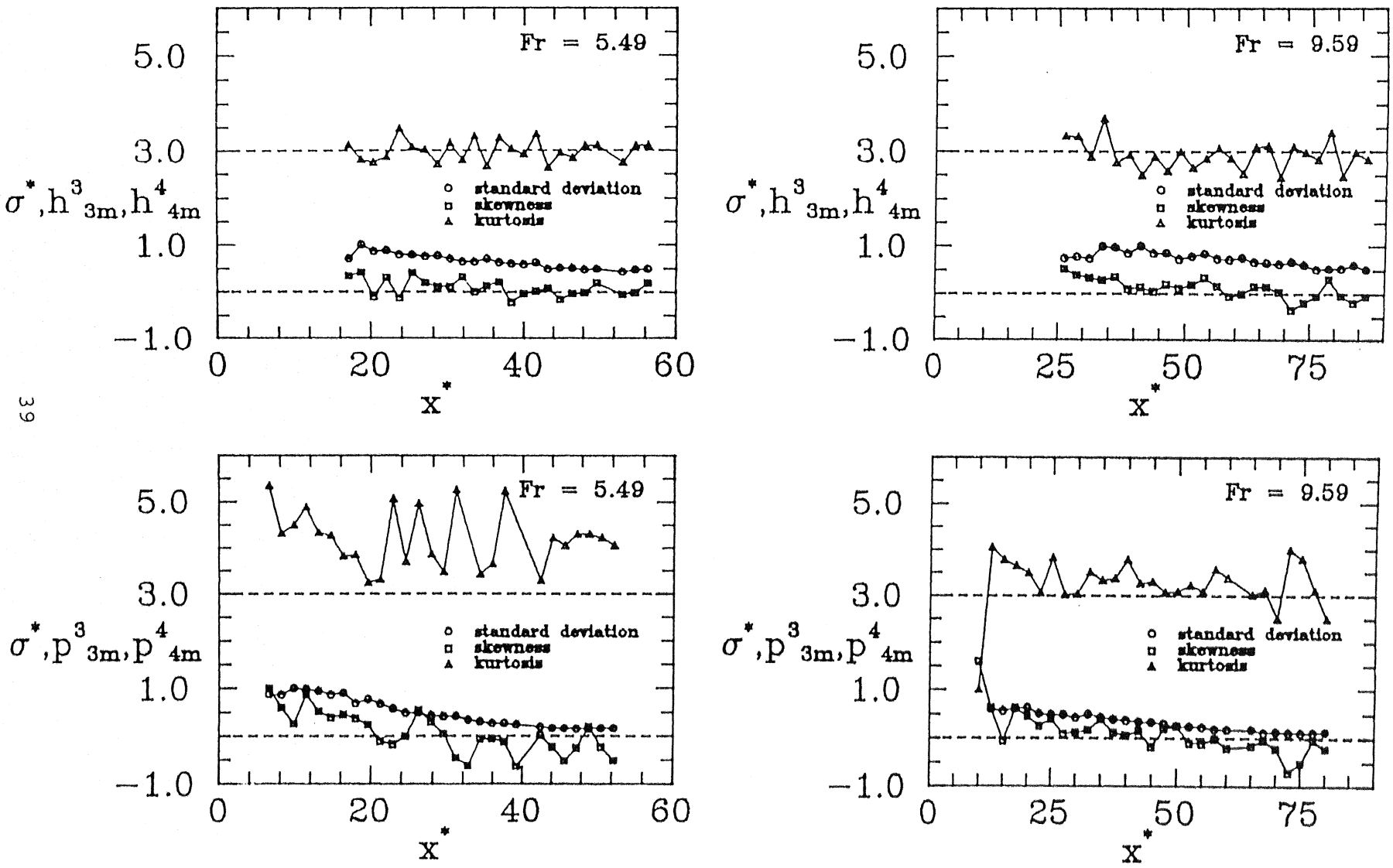

Figure 4.4 : Variation of nondimensional standard deviation, skewness and kurtosis of pressure and depth signal at Fr =5.49 & 9.59

4.3 Probability Density Function

The probability density function for the four cases referred above are respectively shown in Figures 4.5 to 4.8. The dashed curve in the plot is the PDF for a Gaussian signal with a standard deviation equal to that of the signal. The analysis for these graphs has been performed on a sample space of 1024 points. The PDFs for the pressure signal are reported at 8 x-locations, while for depth it is reported at 7 x-locations within the jump. From the figure one can observe that the PDF of the signal collected experimentally matches well with that of a Gaussian signal. The match is closer for the depth signal than that of pressure signal.

4.4 Spatial Correlation

The normalised spatial correlation function is shown in graph in Figures 4.9 - 4.20. The spatial correlation is computed using a sample space of 1024 points. A portion of the curve is shown by a dashed line. This represents the extrapolated range for which experimental data is not available, but the function is expected to follow this trend. The result for pressure is shown at 7 different locations,while for depth it is shown at 6 locations in the region of jump.

By observing the Figures 4.9 -4.12 it is clear that in all cases, the spatial longitudinal correlation increases as the distance from the toe increases. The depth signal data is more correlated as compared to the pressure signal at a given point.

The spatial correlations for left side and the right side (Figure 4.13 - 4.20) are found to be almost identical. This indicates that the assumption of symmetricity is valid and the phenomena can be considered to be one dimensional. Here also the correlation for depth signal is greater as compared to the pressure signal. In the region near the toe of the jump the transverse correlation is greater as compared to longitudinal correlation for

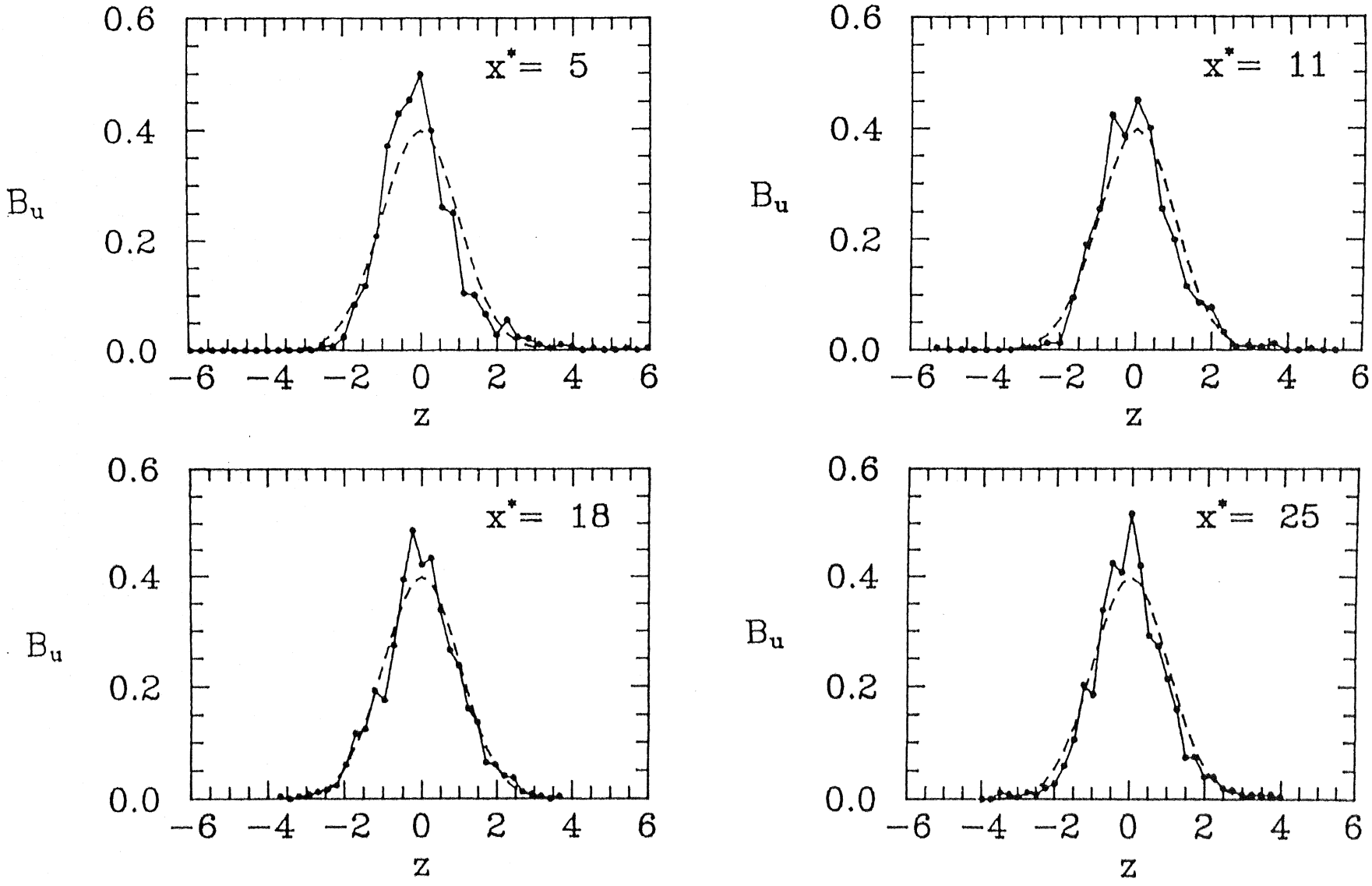

Figure 4.5a : PDF of pressure signal at x^* = 5, 11, 18 & 25 and Fr = 5.49

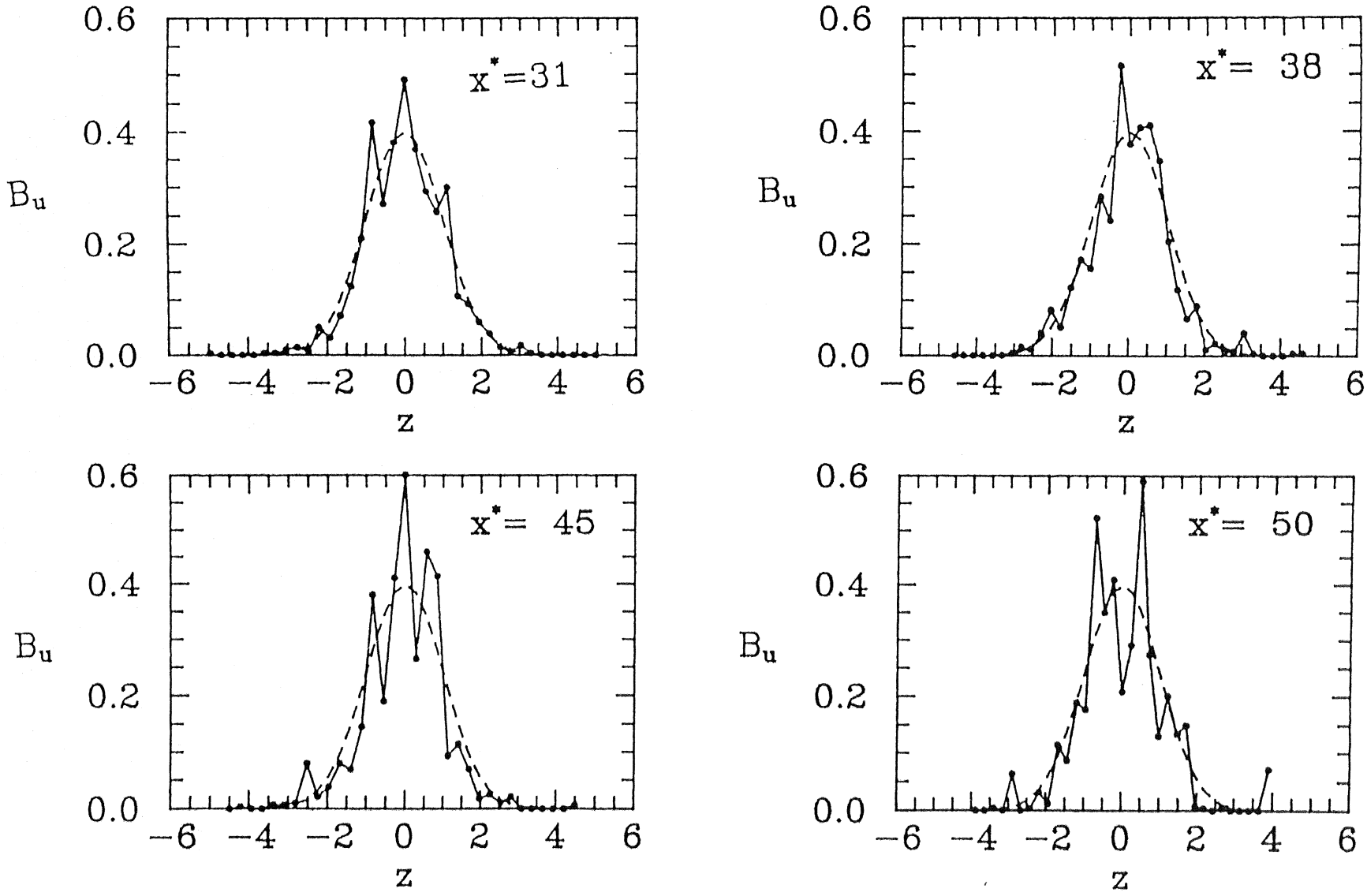

Figure 4.5b : PDF of pressure signal at x^* = 31, 38, 45 & 50 and Fr = 5.49

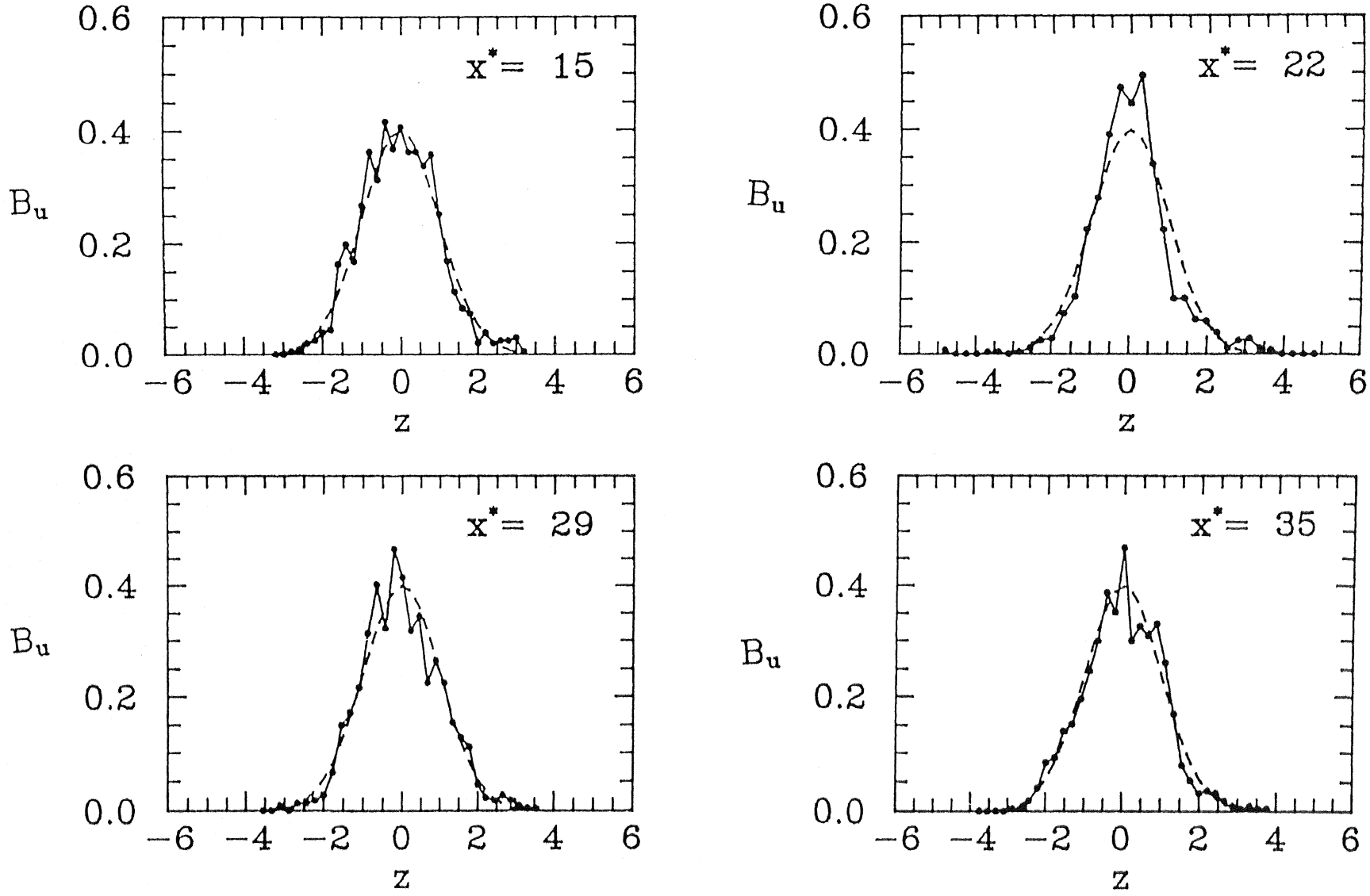

Figure 4.6a : PDF of depth signal at x^* = 15, 22, 29 & 35 and Fr = 5.49

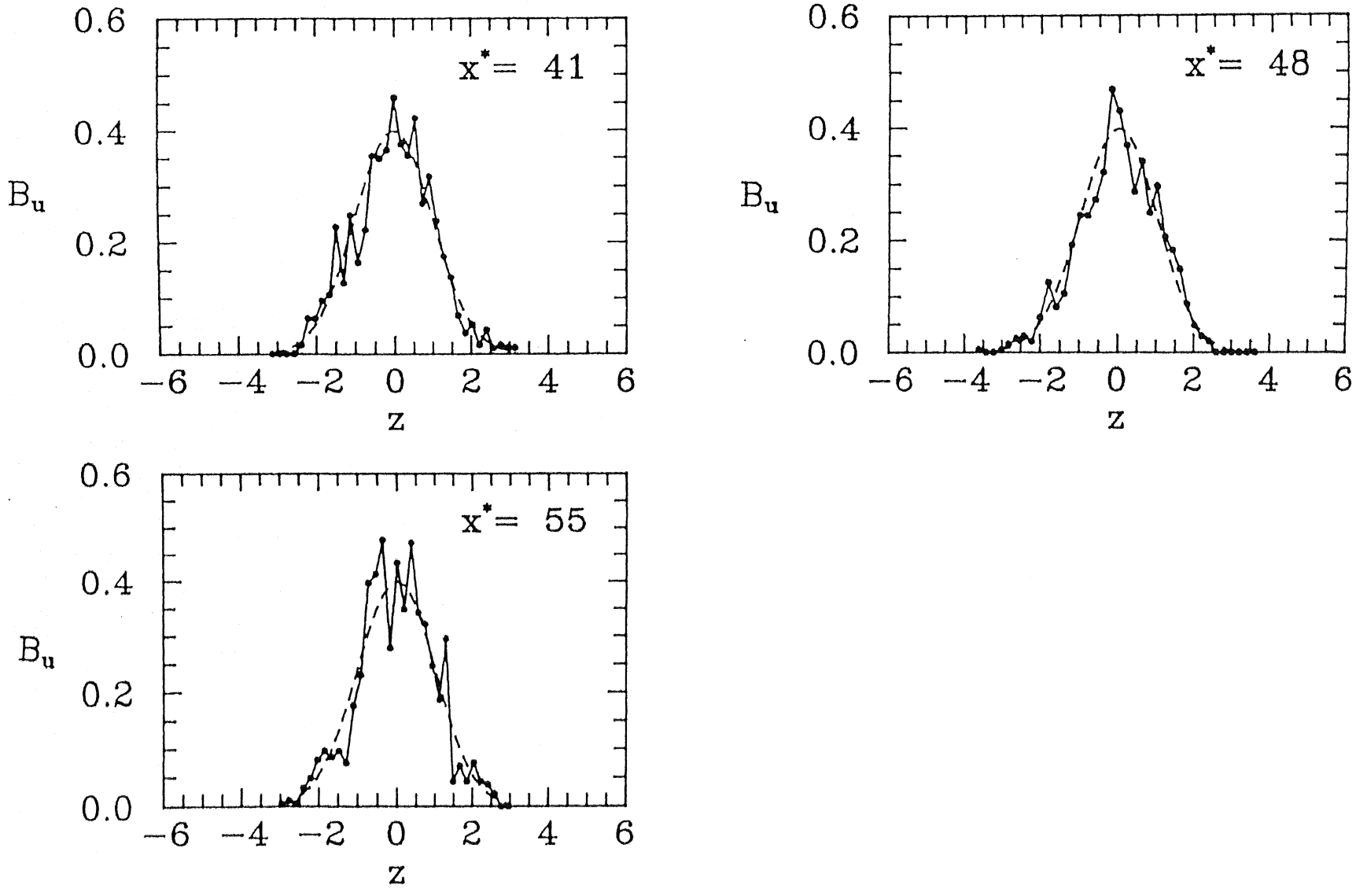

Figure 4.6b : PDF of depth signal at x^* = 41, 48, & 55 and Fr = 5.49

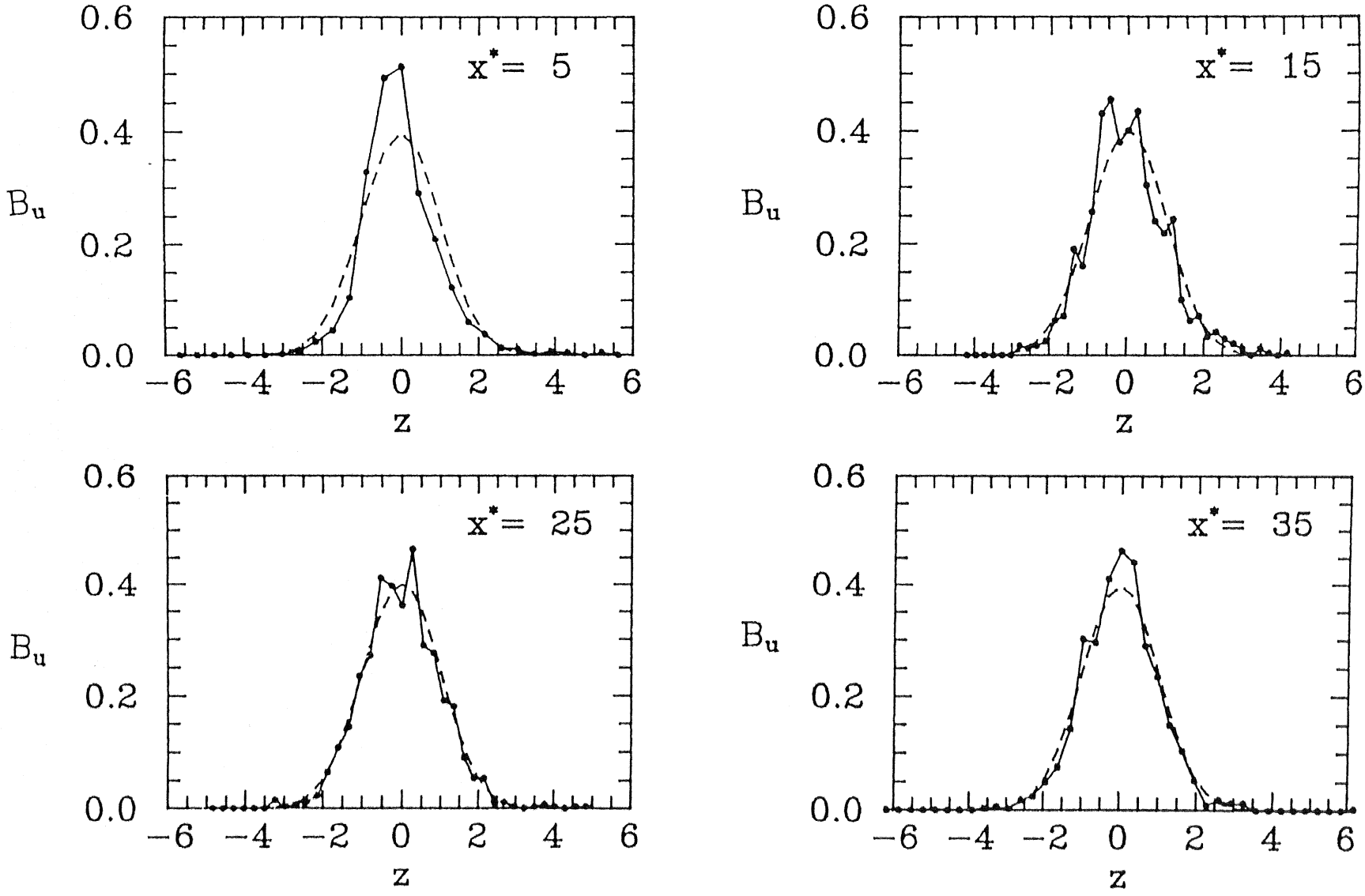

Figure 4.7a : PDF of pressure signal at x^* = 5, 15, 25 & 35 and Fr = 9.59

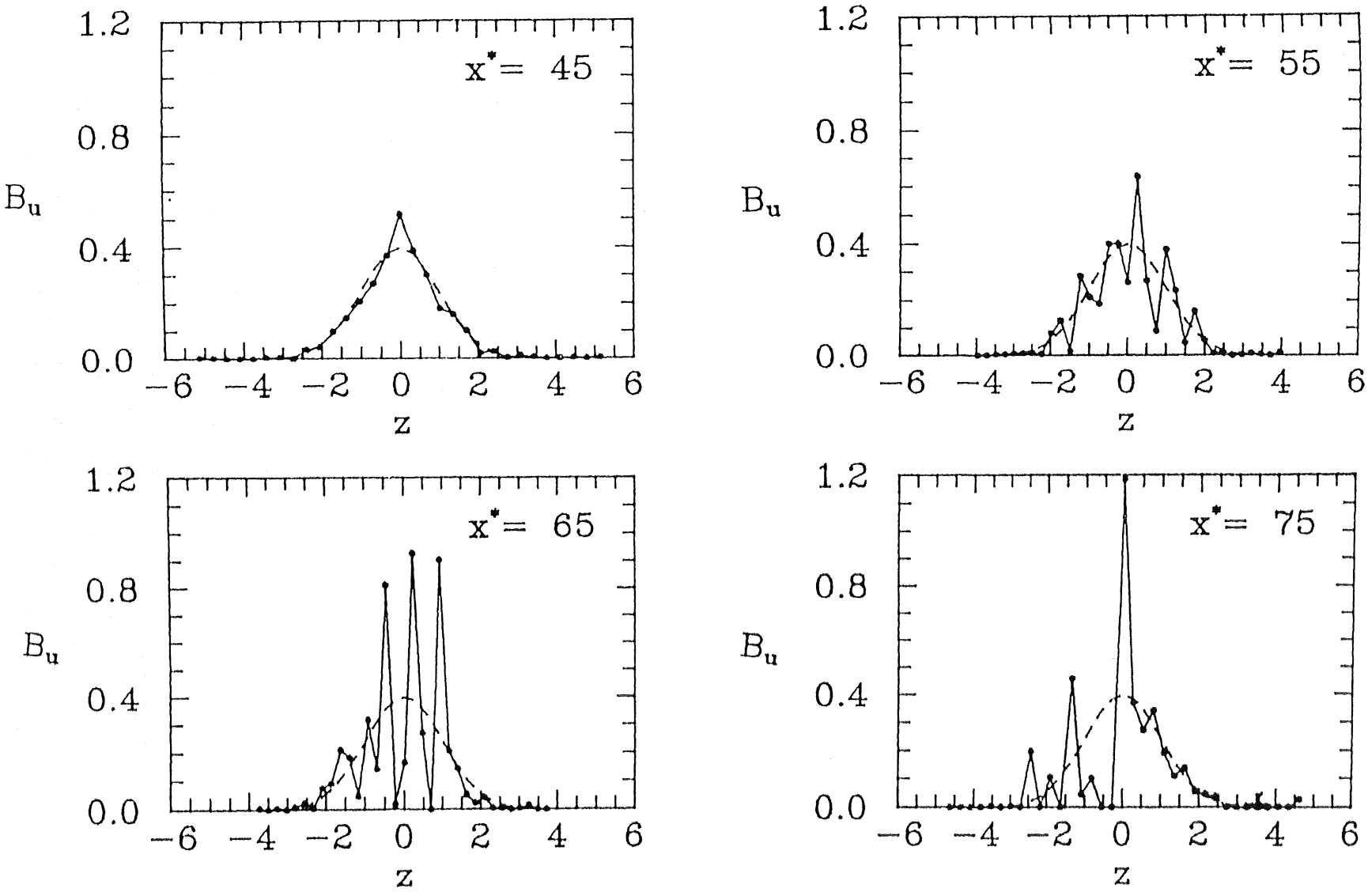

Figure 4.7b : PDF of pressure signal at x^* = 45, 55, 65 & 75 and Fr = 9.59

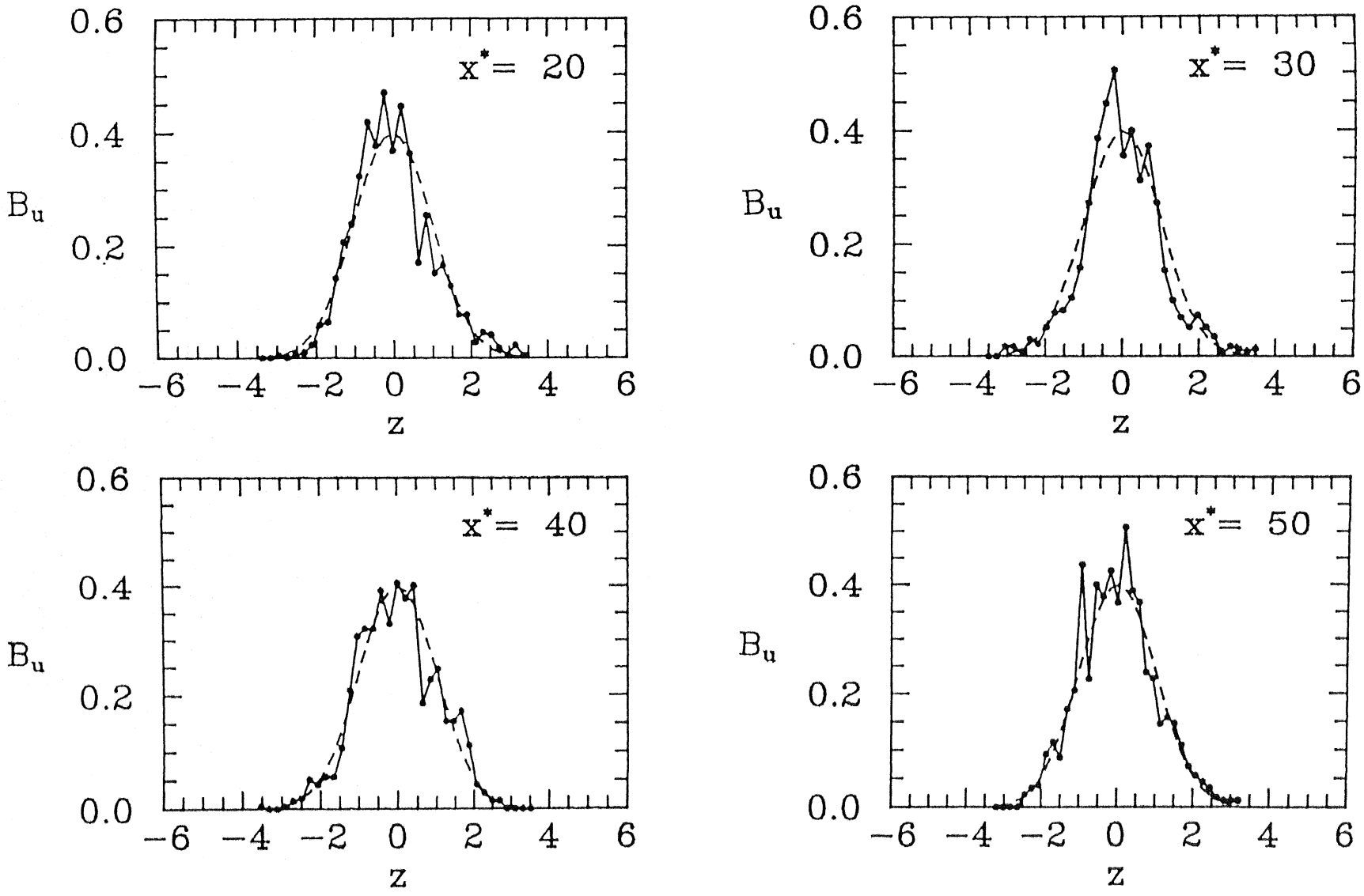

Figure 4.8a : PDF of depth signal at x^* = 20, 30, 40 & 50 and Fr = 9.59

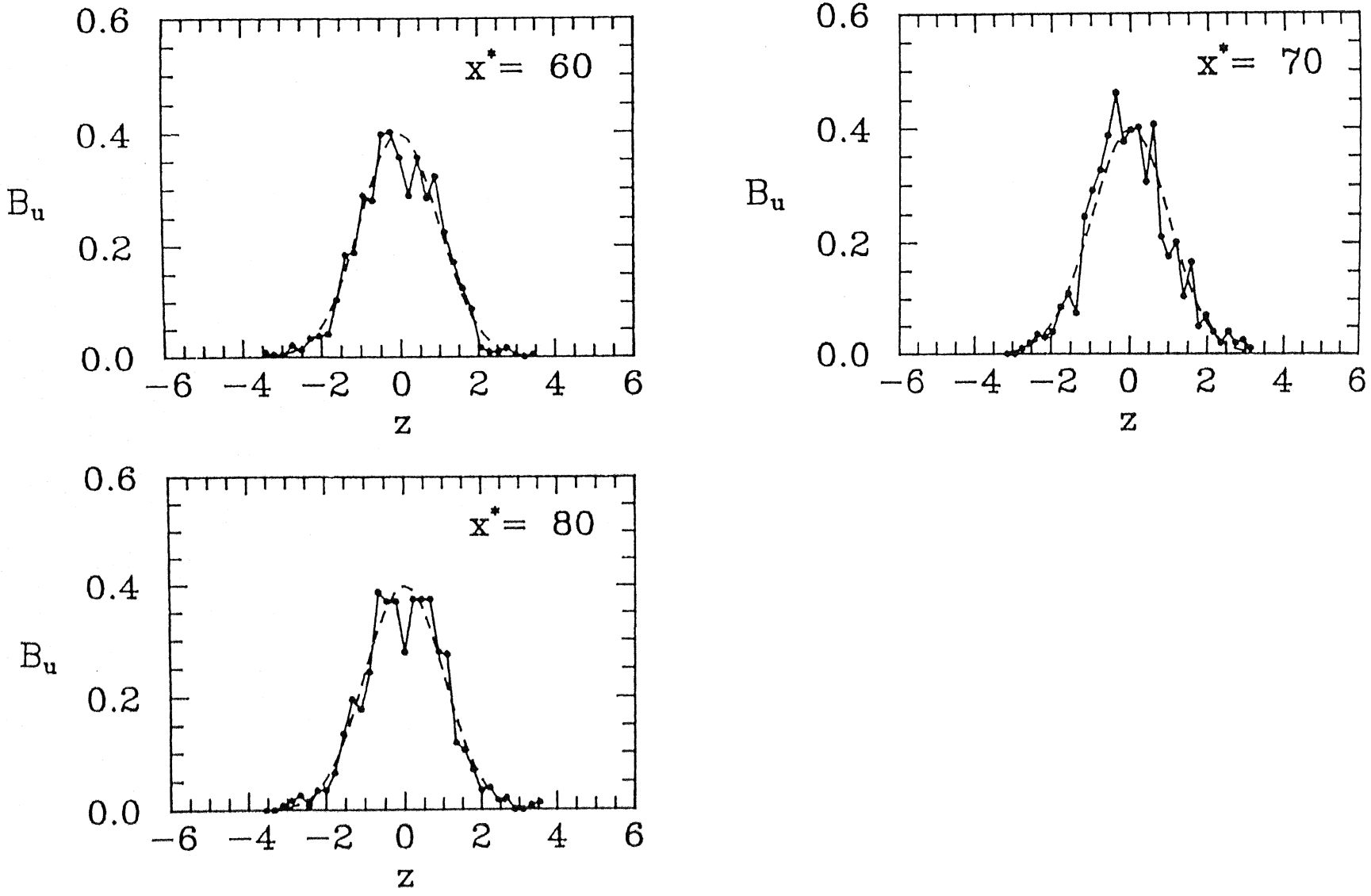

Figure 4.8b : PDF of depth signal at x^* = 60, 70, & 80 and Fr = 9.59

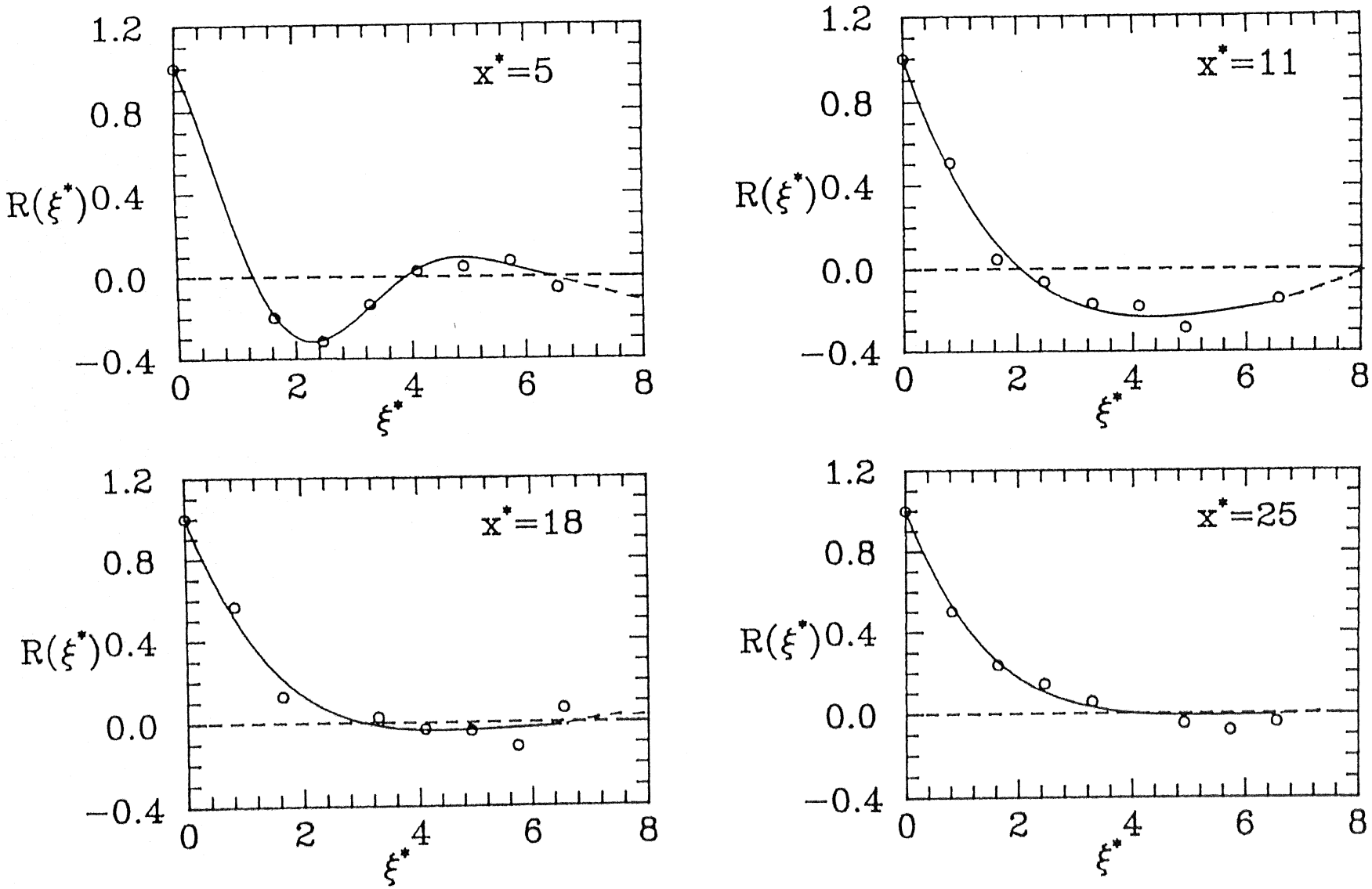

Figure 4.9a : Normalised longitudinal spatial correlation function of pressure signal at x^*= 5, 11, 18 & 25 and Fr = 5.49

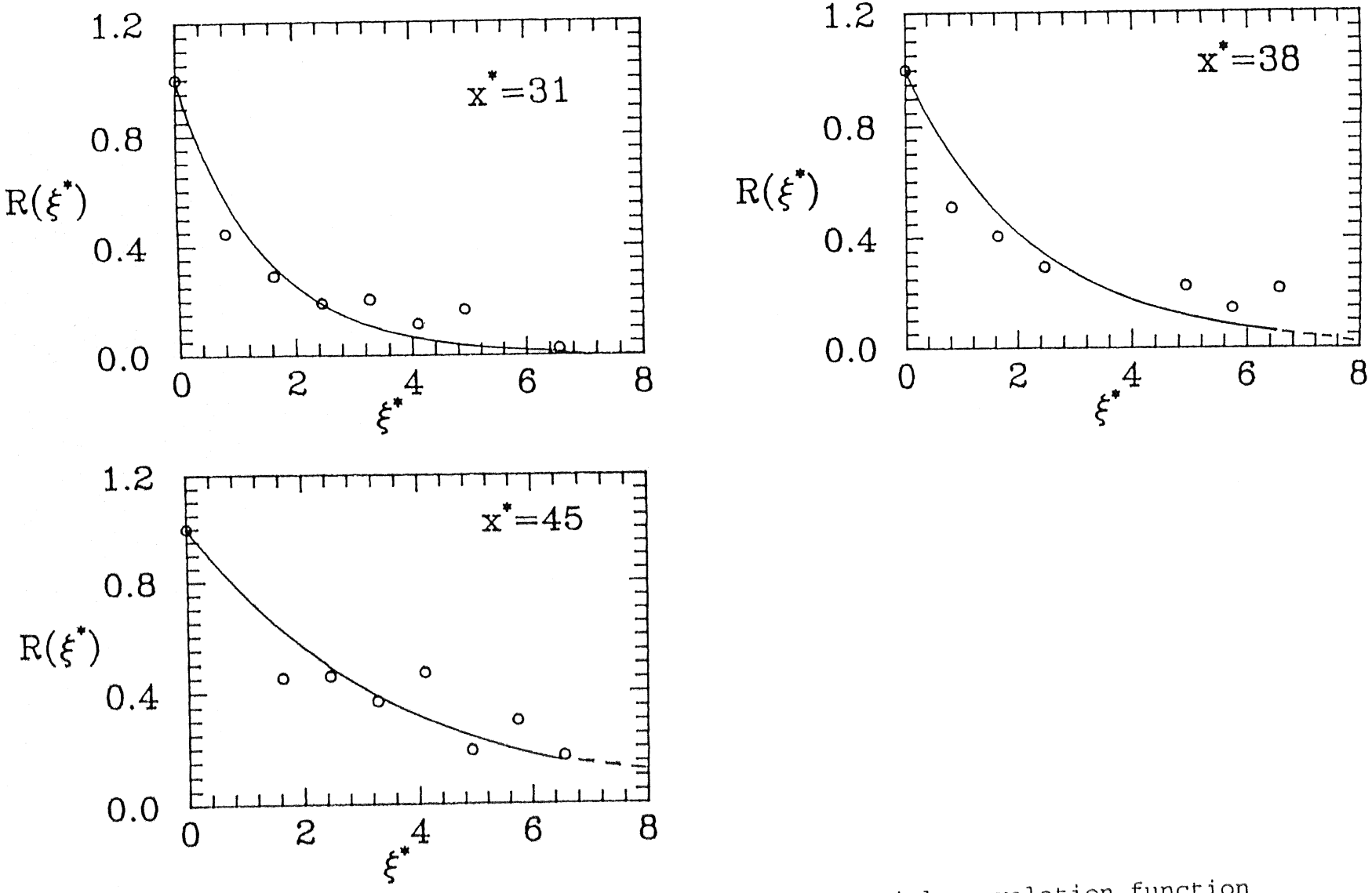

Figure 4.9b : Normalised longitudinal spatial correlation function of pressure signal at x^* = 31, 38 & 45 and Fr = 5.49

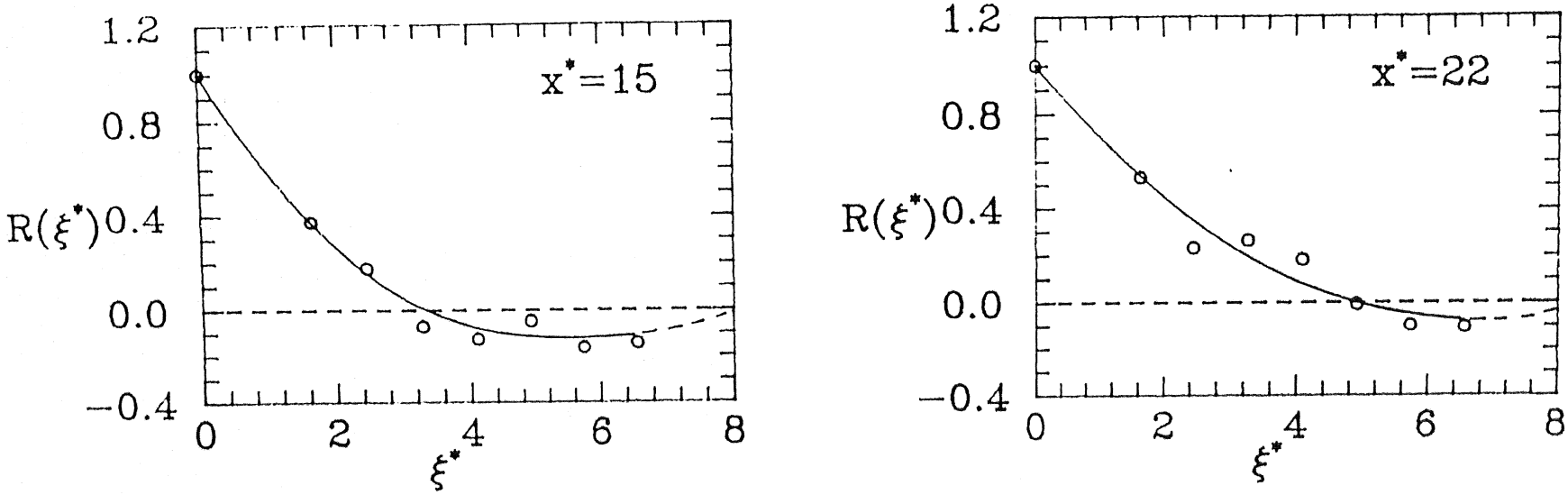

Figure 4.10a : Normalised longitudinal spatial correlation function of depth signal at x^*= 15 & 22 and Fr = 5.49

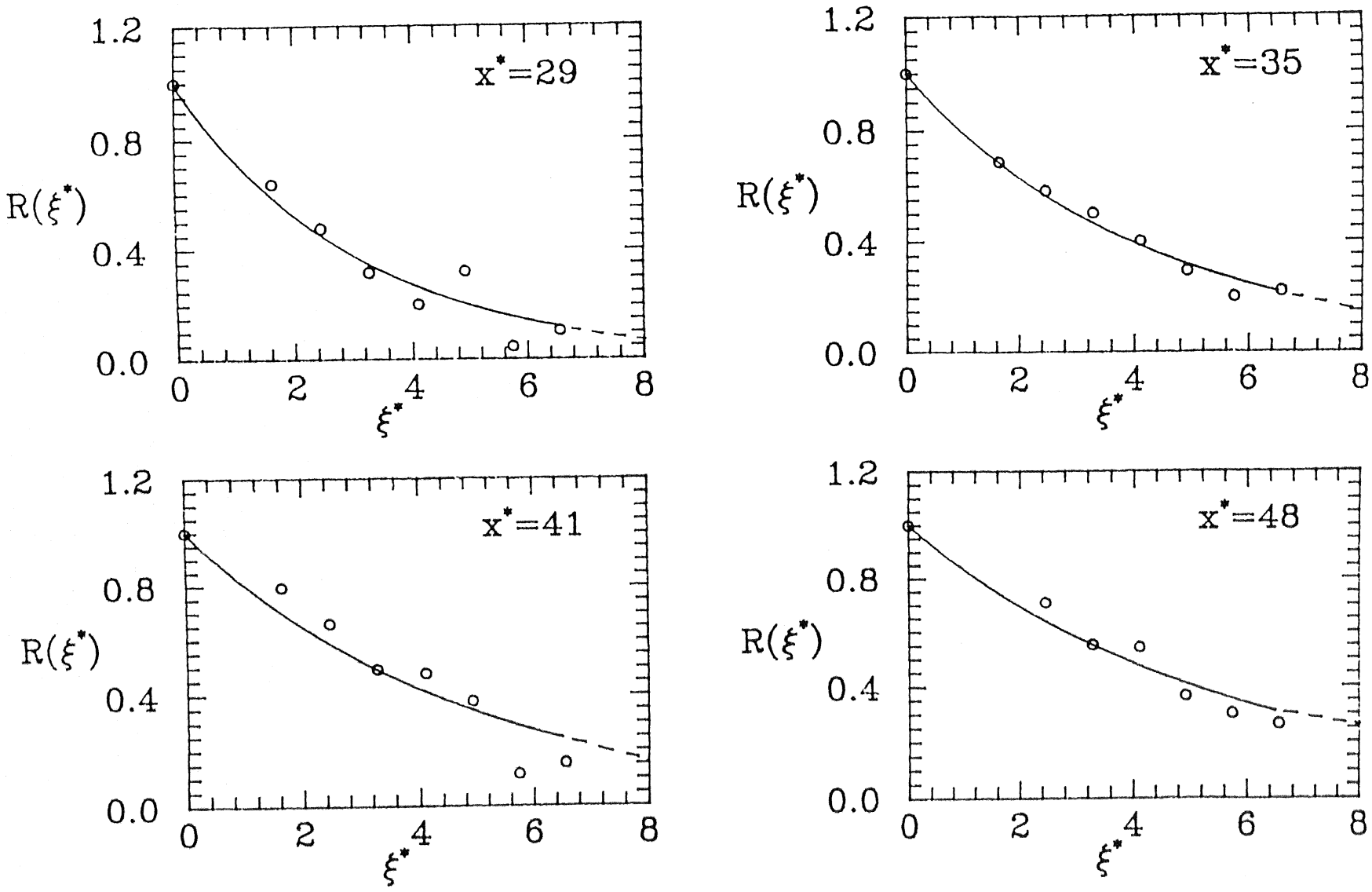

Figure 4.10b : Normalised longitudinal spatial correlation function of depth signal at x^*= 29, 35, 41 & 48 and Fr = 5.49

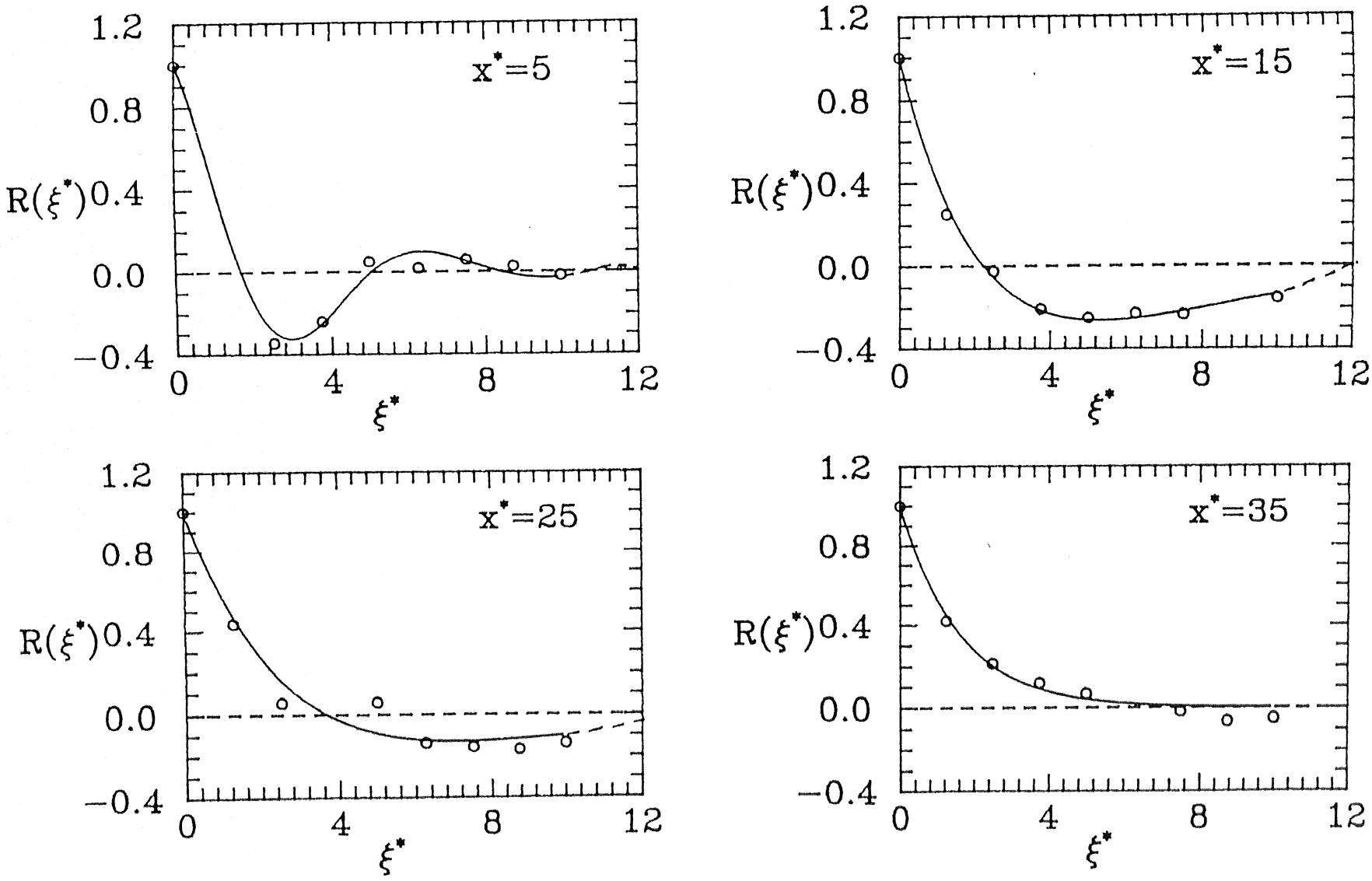

Figure 4.11a : Normalised longitudinal spatial correlation function of pressure signal at x^*= 5, 15, 25 & 35 and Fr = 9.59

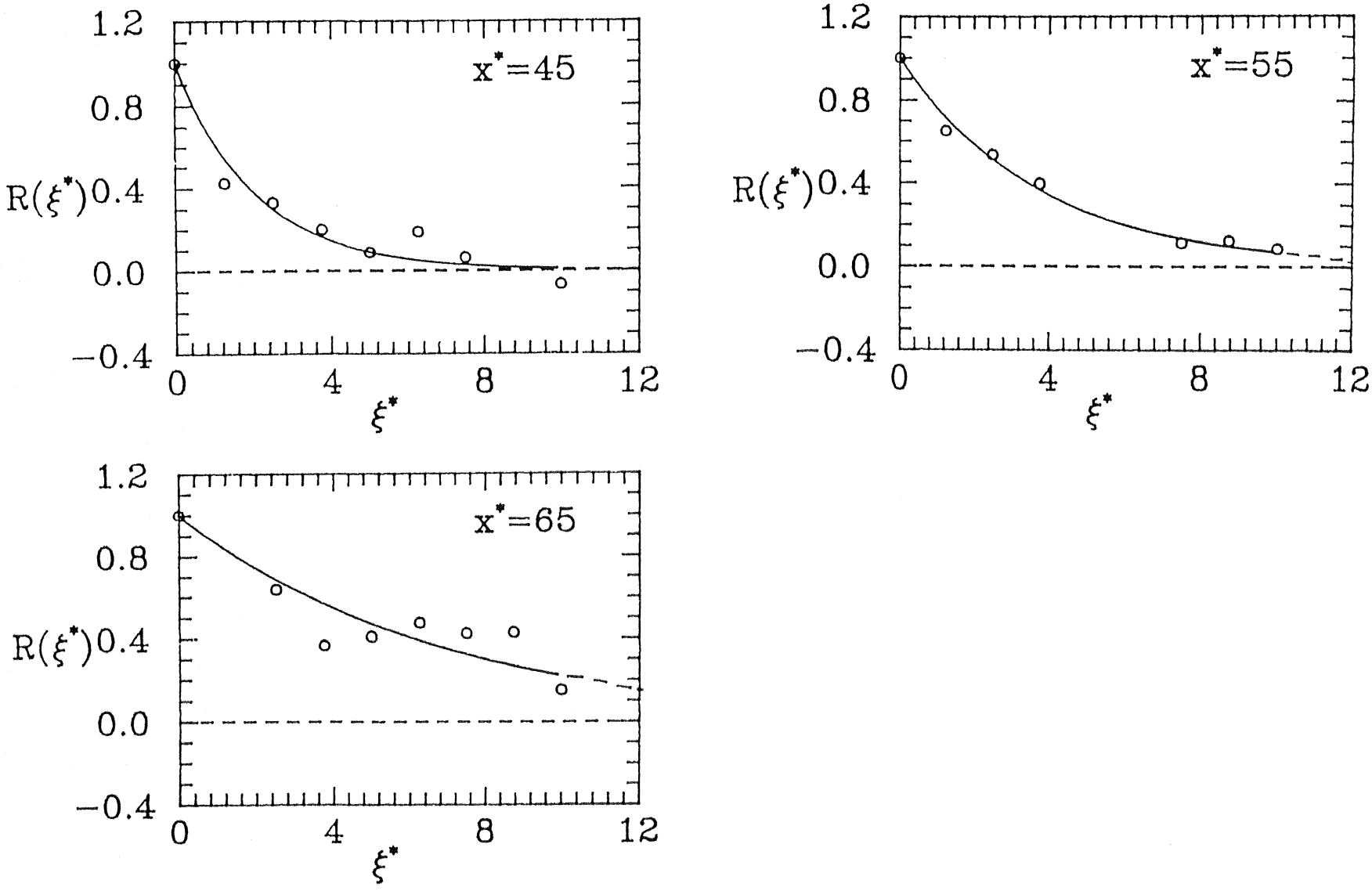

Figure 4.11b : Normalised longitudinal spatial correlation function of pressure signal at x^* = 45, 55 & 65 and Fr = 9.59

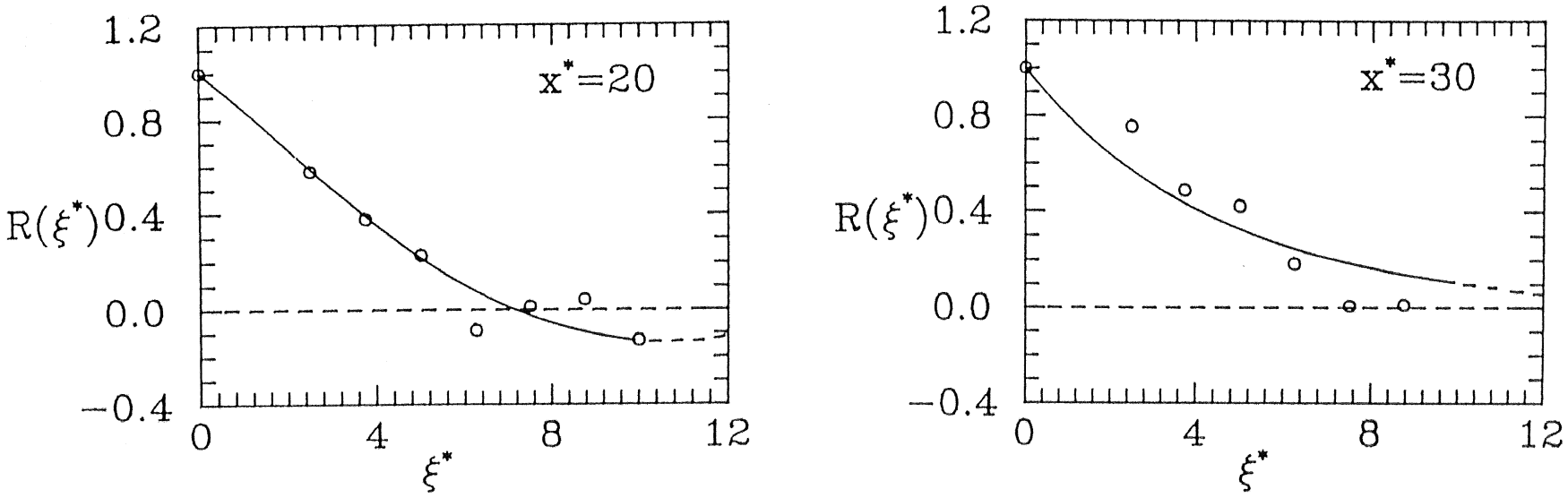

Figure 4.12a : Normalised longitudinal spatial correlation function of depth signal at x^*= 20 & 30 and Fr = 9.59

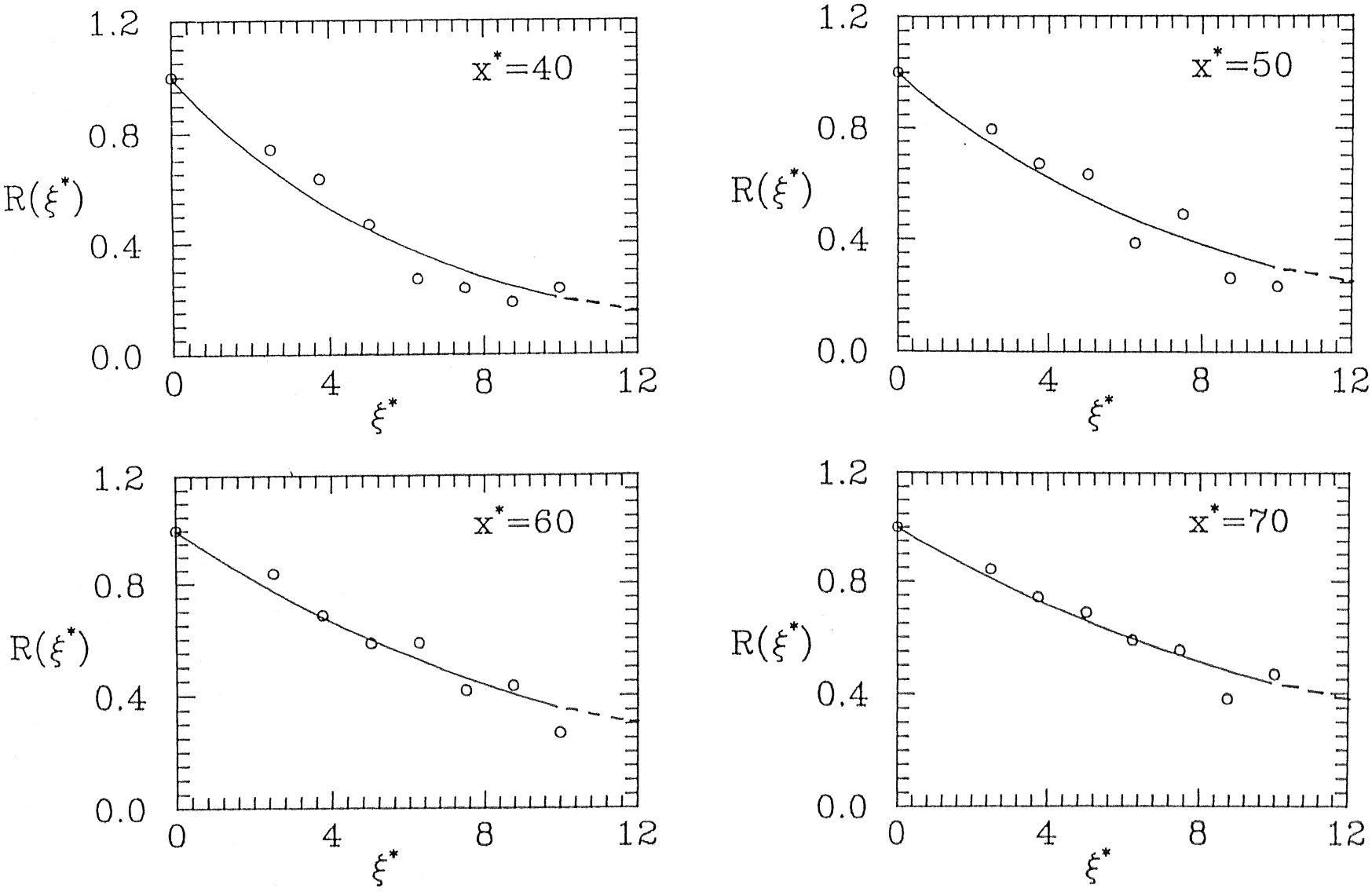

Figure 4.12b : Normalised longitudinal spatial correlation function of depth signal at x^* = 40, 50, 60 & 70 and Fr = 9.59

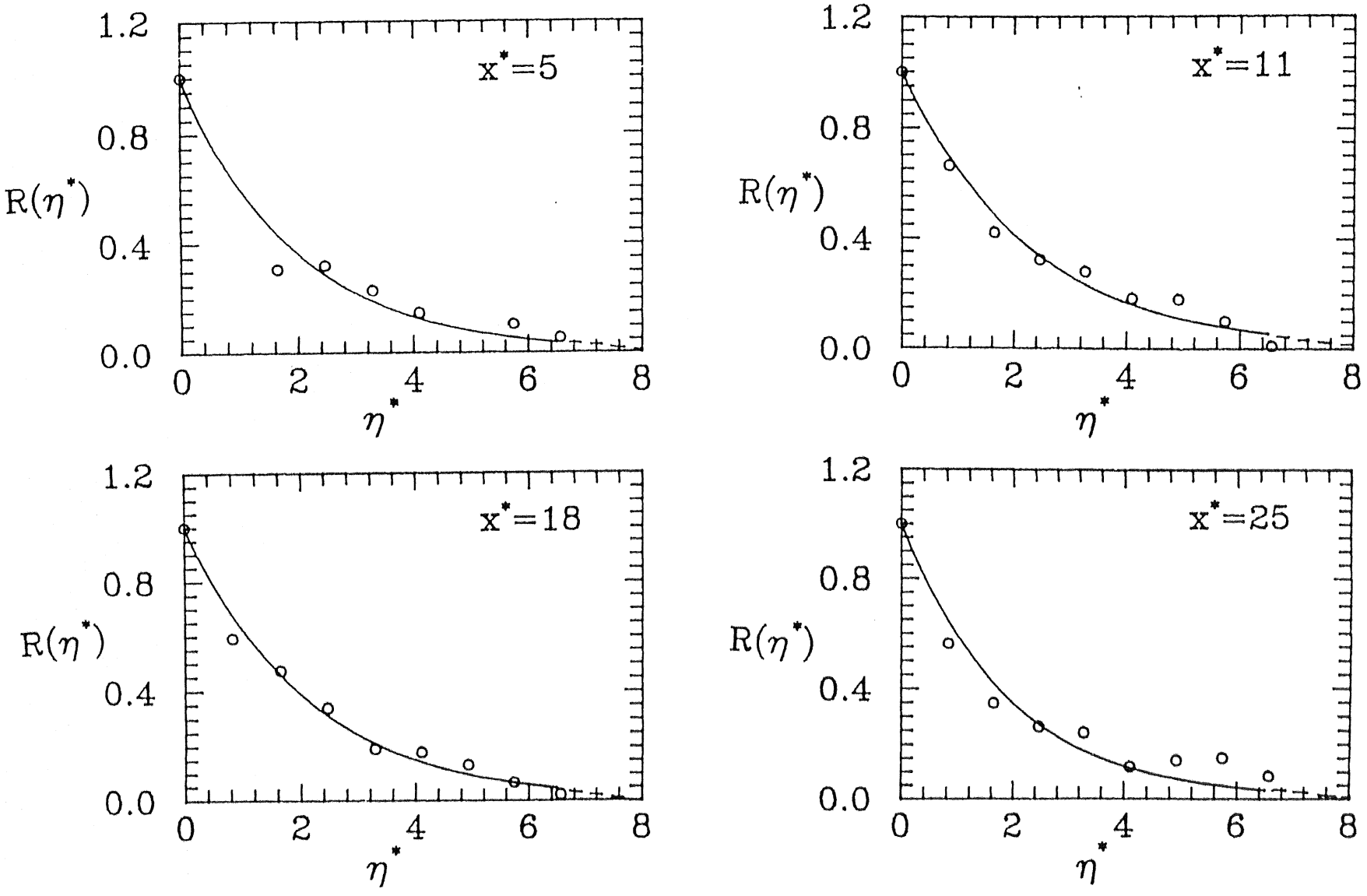

Figure 4.13a : Normalised transverse right side spatial correlation function of pressure signal at x^*= 5, 11, 18 & 25 and

Fr = 5.49

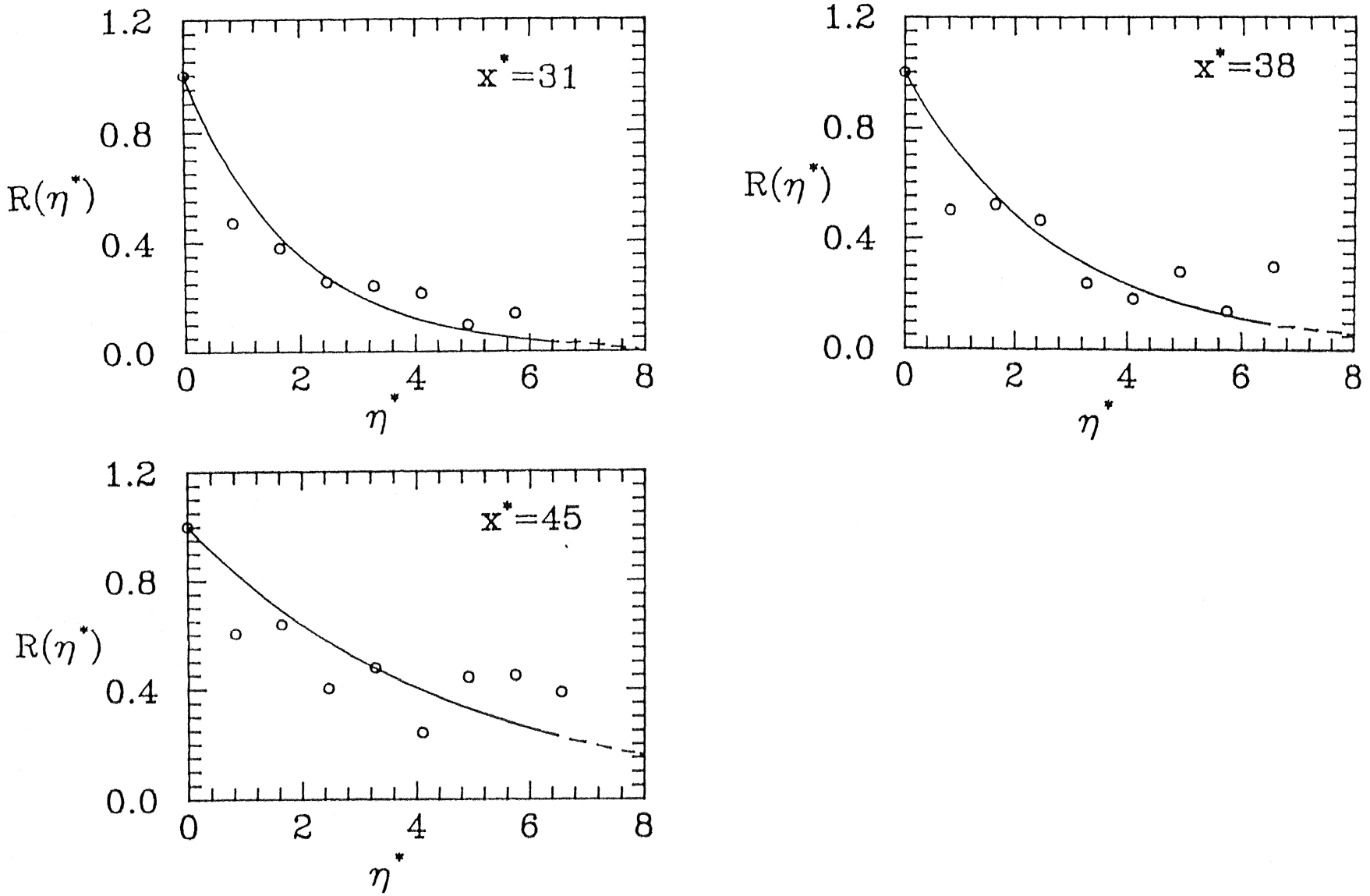

Figure 4.13b : Normalised transverse right side spatial correlation function of pressure signal at x^* = 31, 38 & 45 and Fr = 5.49

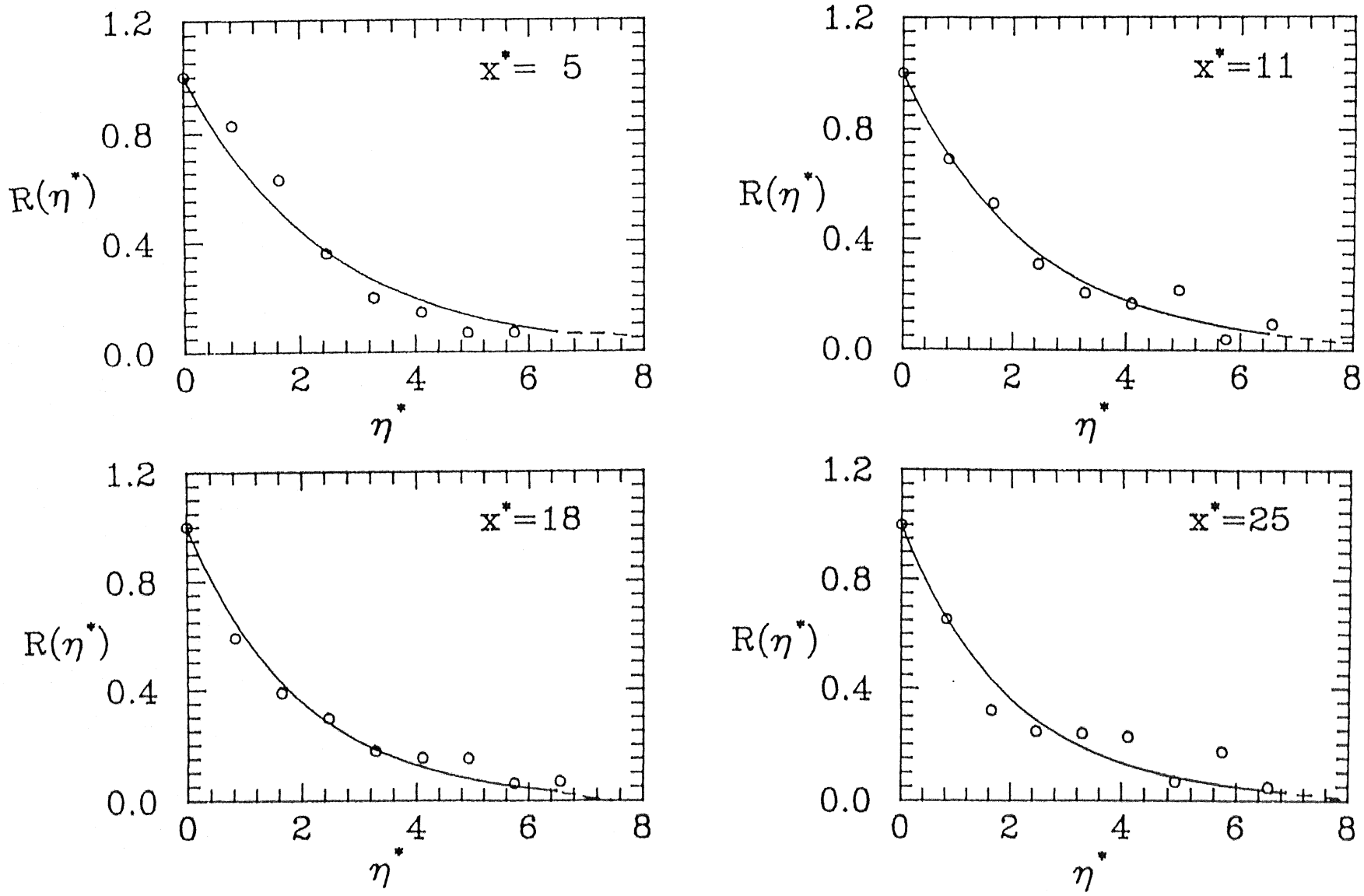

Figure 4.14a : Normalised transverse left side spatial correlation function of pressure signal at x^* = 5, 11, 18 & 25 and Fr = 5.49

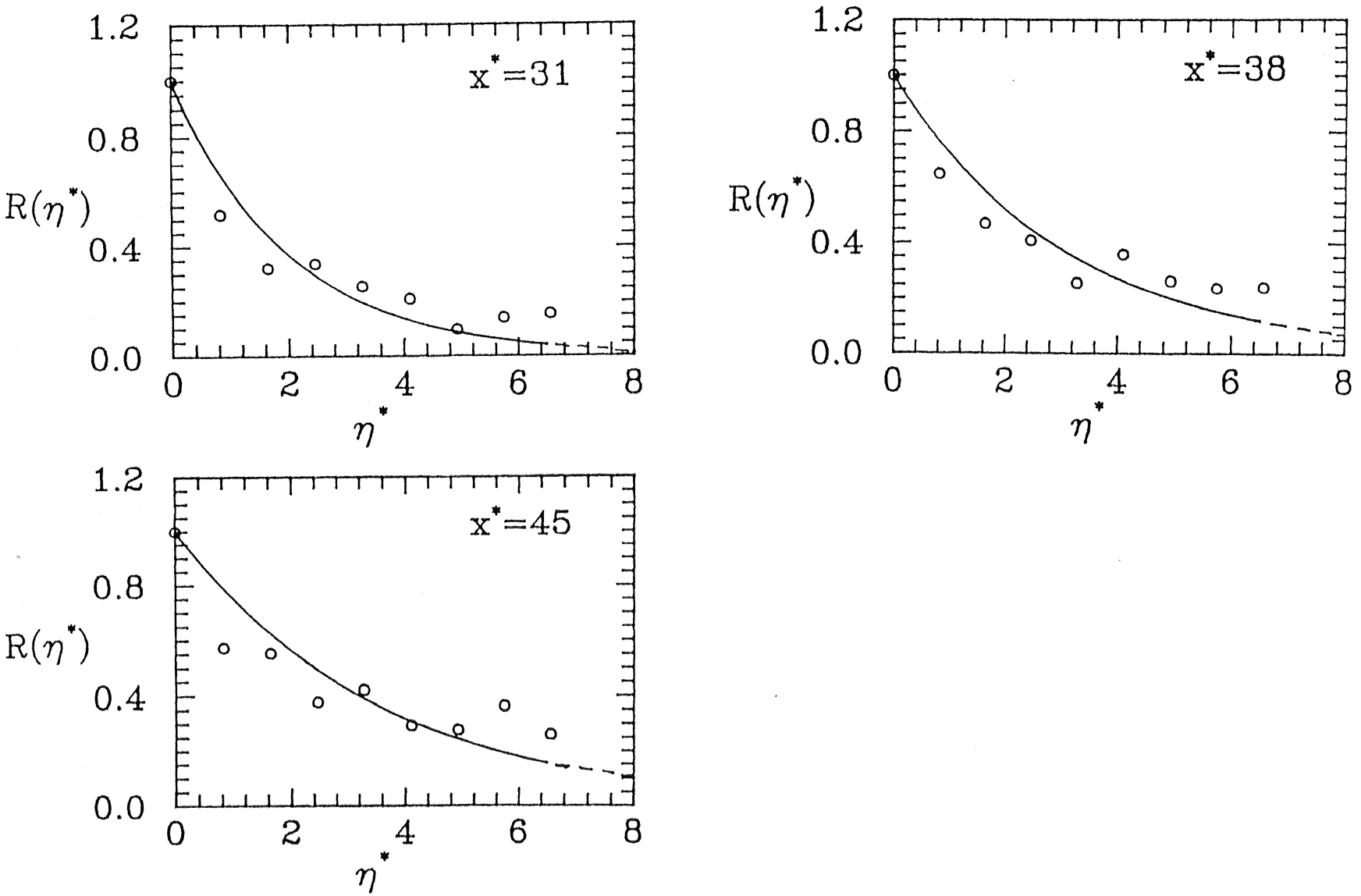

Figure 4.14b : Normalised transverse left side spatial correlation function of pressure signal at x^* = 31, 38 & 45 and

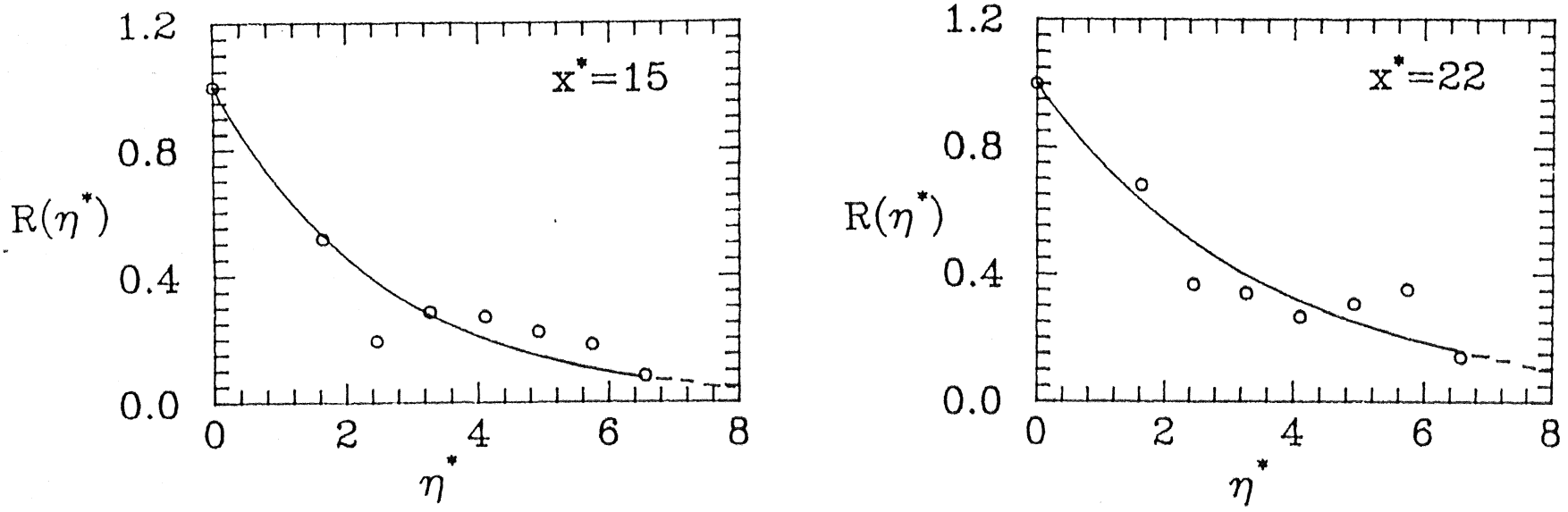

Figure 4.15a : Normalised transverse right side spatial correlation function of depth signal at x^*= 15 & 22 and Fr = 5.49

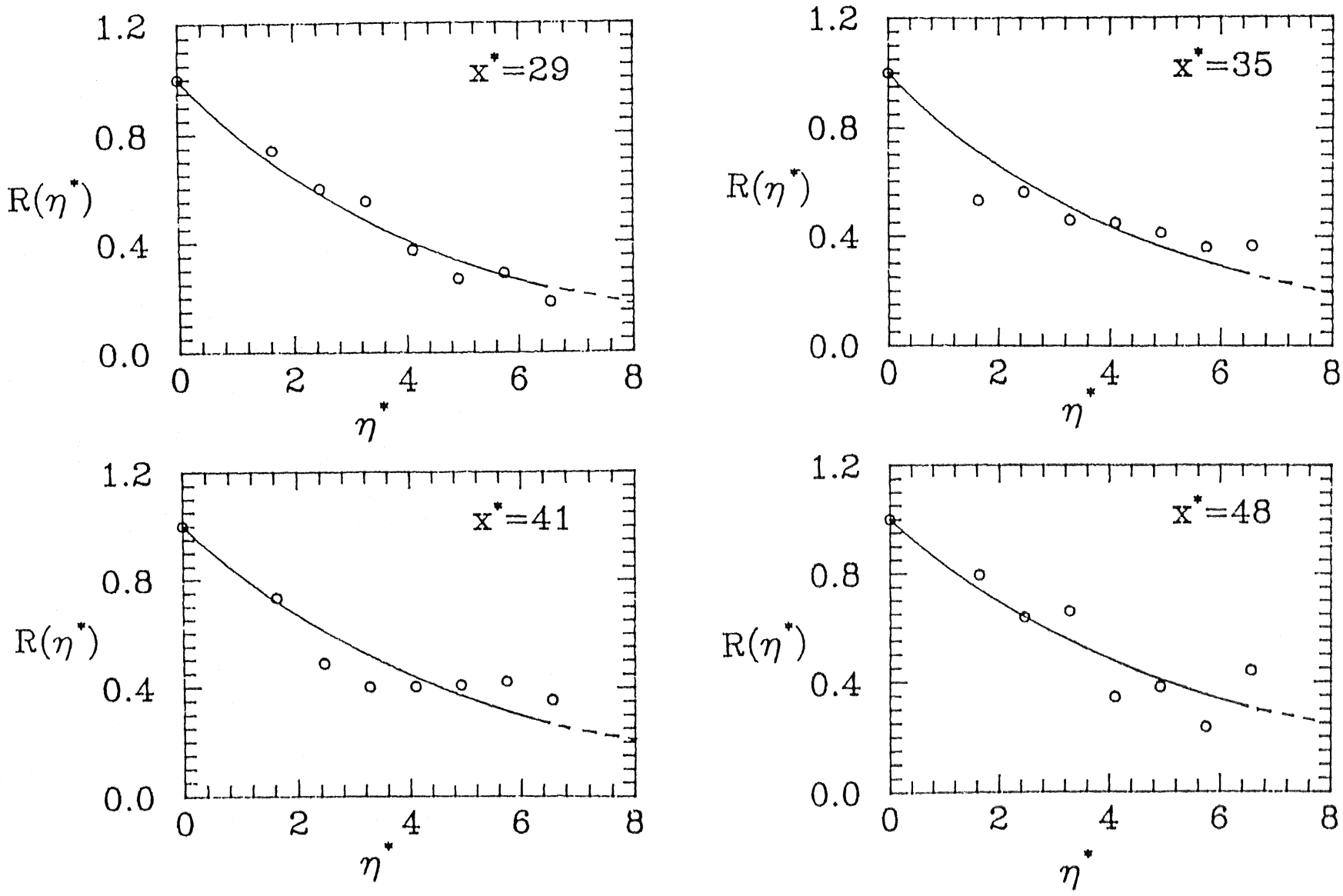

Figure 4.15b : Normalised transverse right side spatial correlation function of depth signal at x^*= 29, 35, 41 & 48 and Fr = 5.49

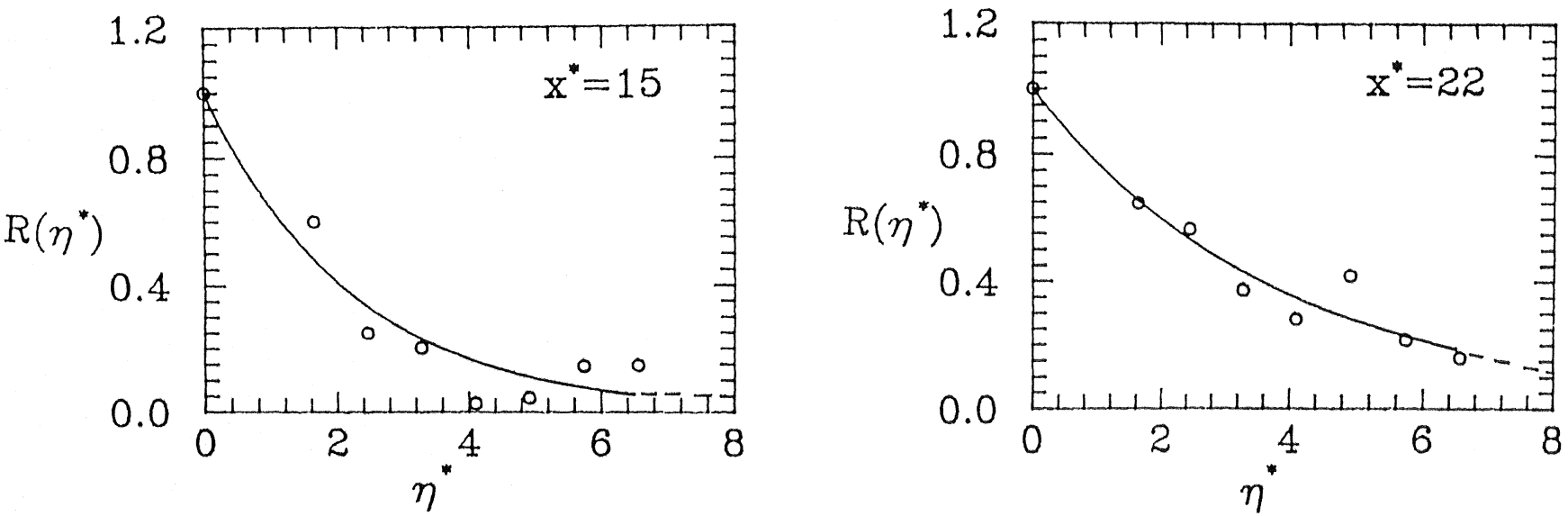

Figure 4.16a : Normalised transverse left side spatial correlation function of depth signal at x^*= 15 & 22 and Fr = 5.49

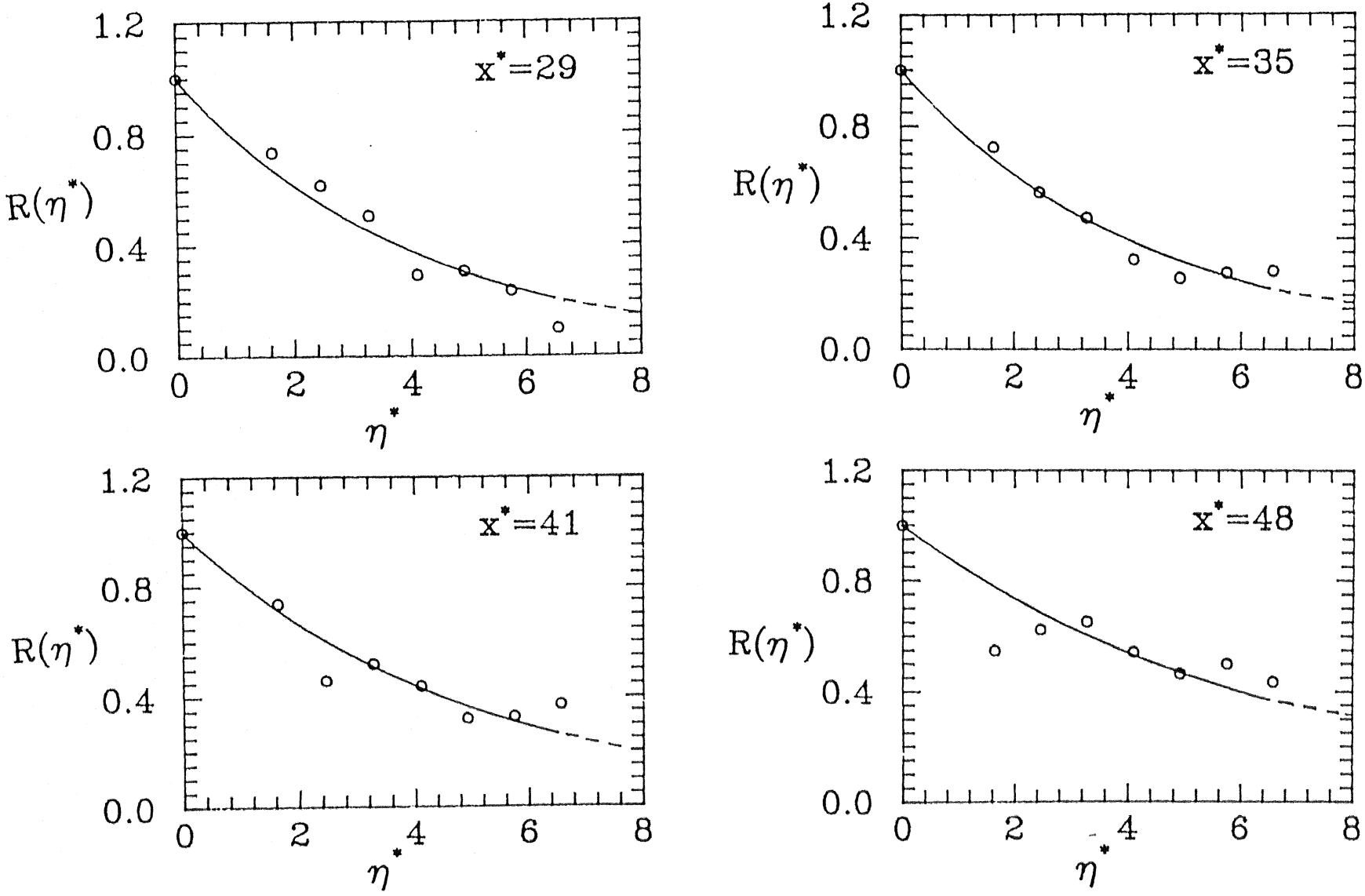

Figure 4.16b : Normalised transverse left side spatial correlation function of depth signal at x^*= 29, 35, 41 & 48 and Fr = 5.49

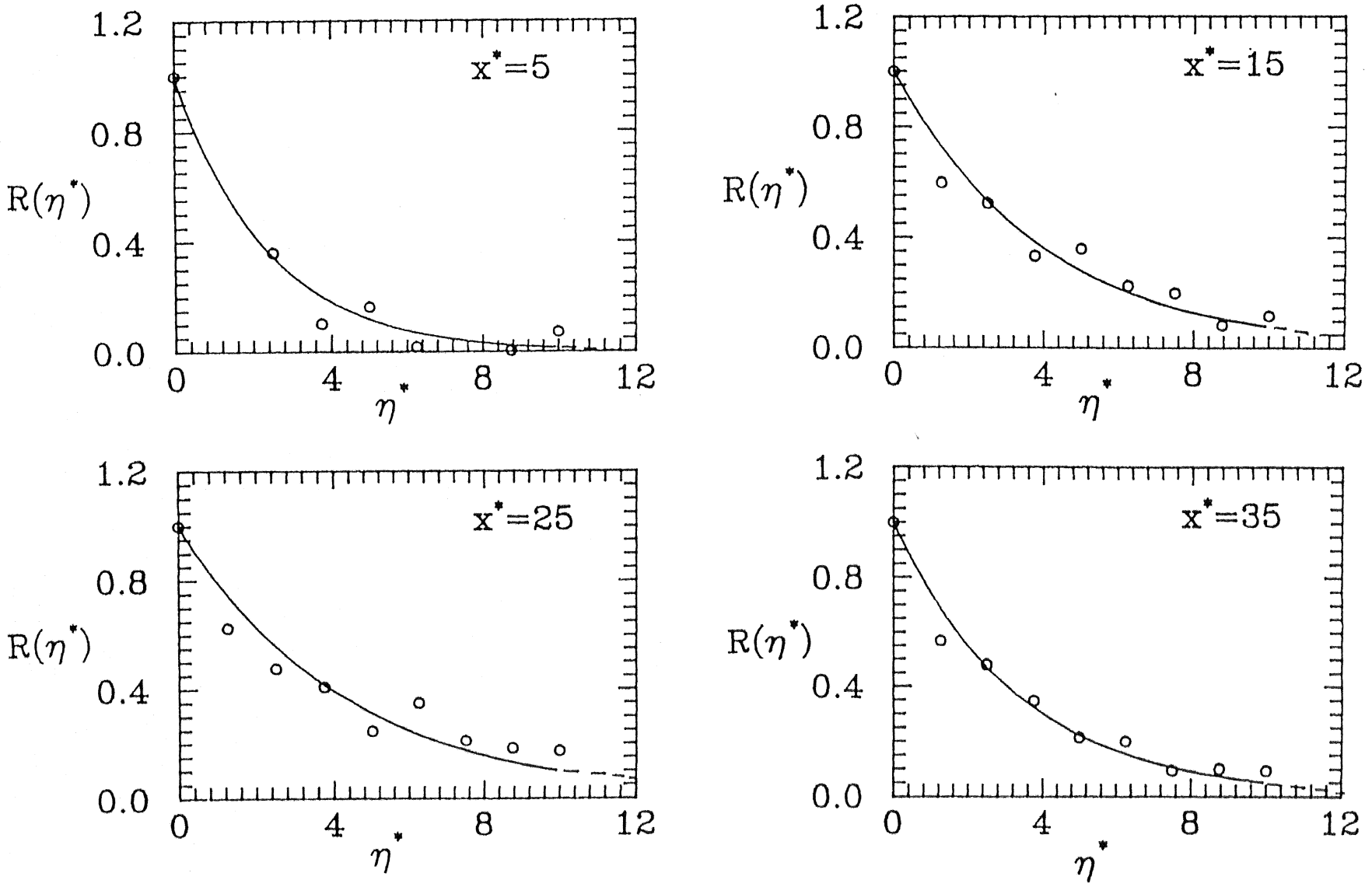

Figure 4.17a : Normalised transverse right side spatial correlation function of pressure signal at x^*= 5, 15, 25 & 35 and Fr = 9.59

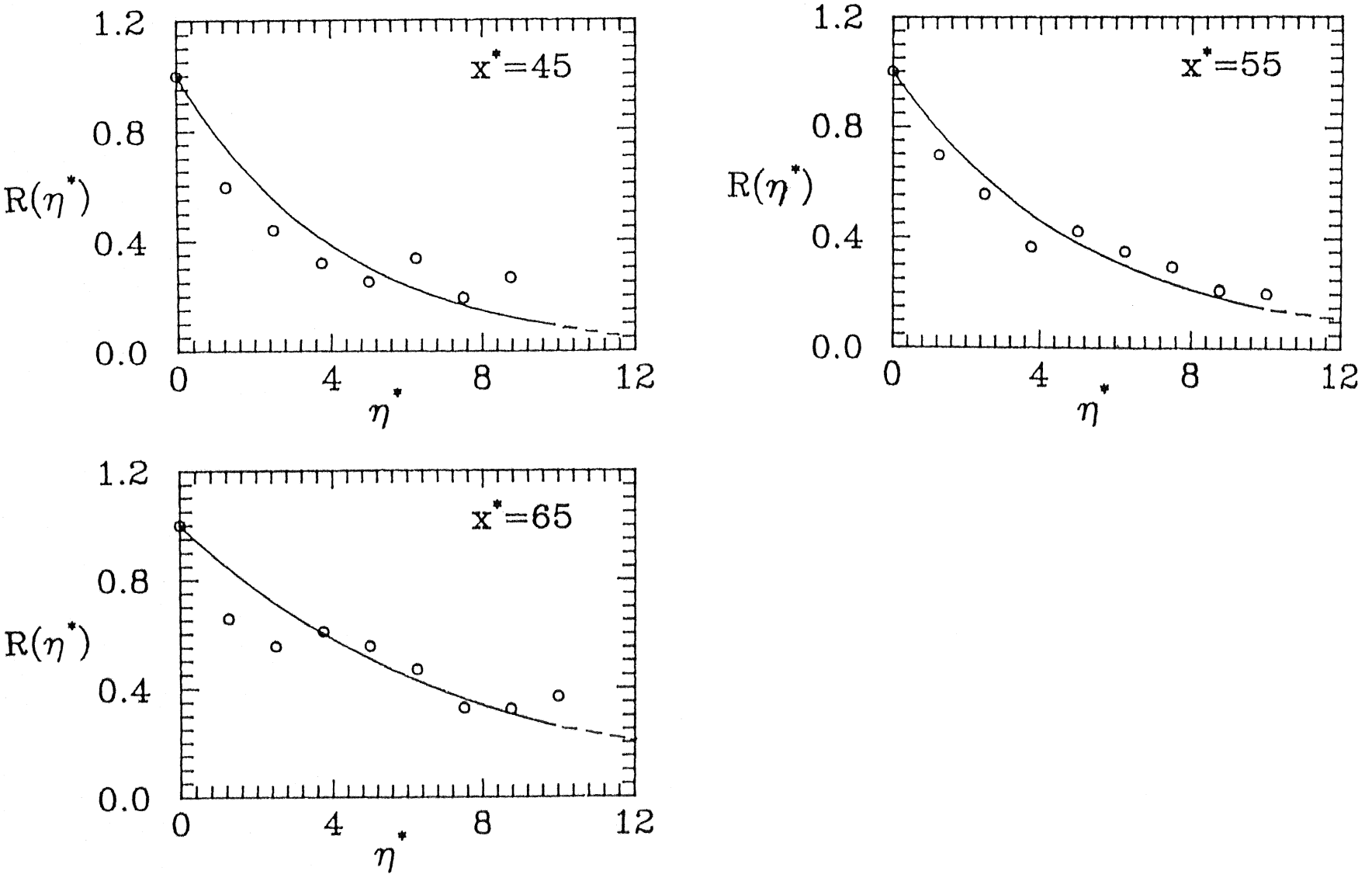

Figure 4.17b : Normalised transverse right side spatial correlation function of pressure signal at x^* = 45, 55 & 65 and Fr = 9.59

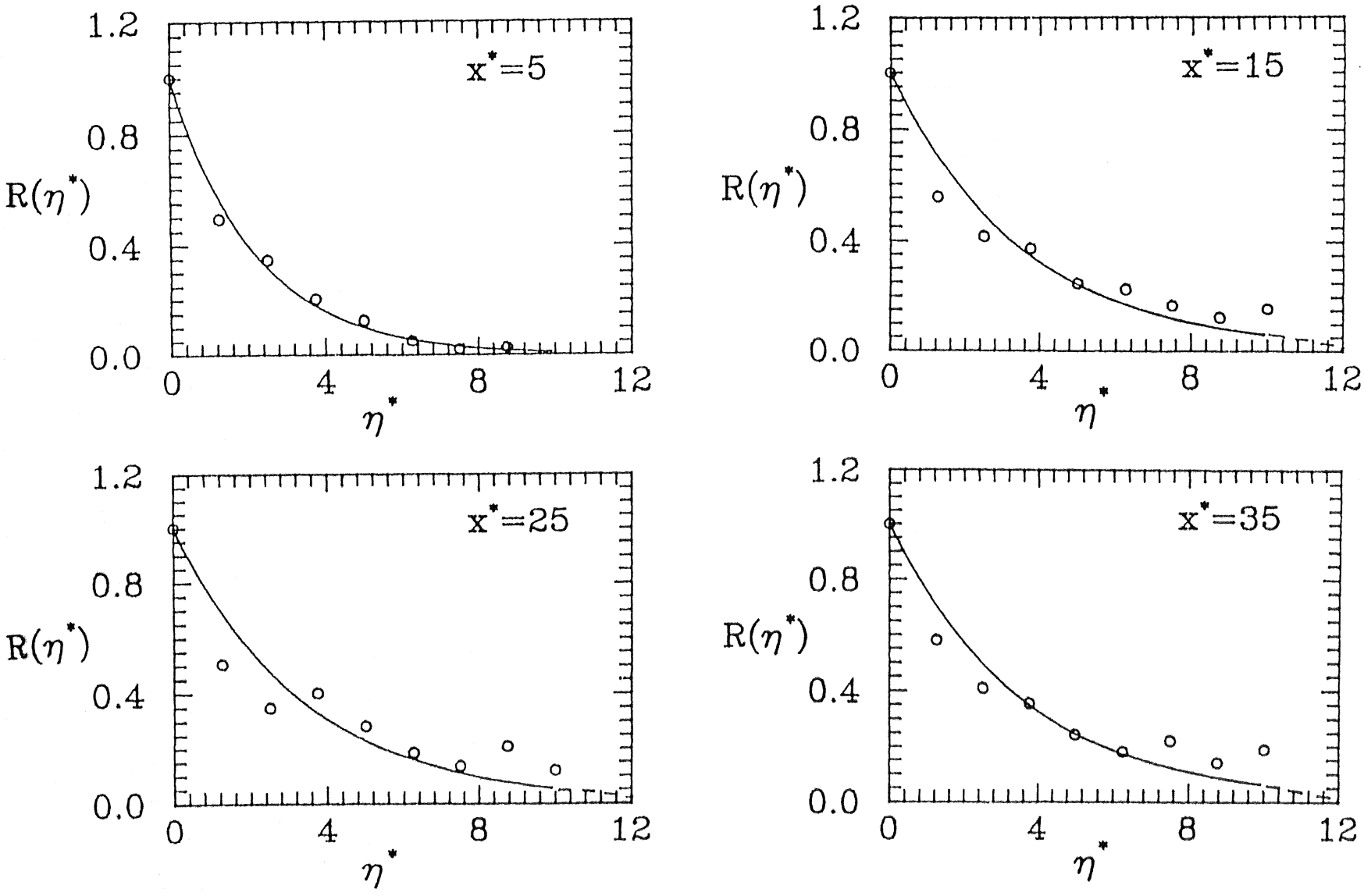

Figure 4.18a : Normalised transverse left side spatial correlation function of pressure signal at x^*= 5, 15, 25 & 35 and Fr = 9.59

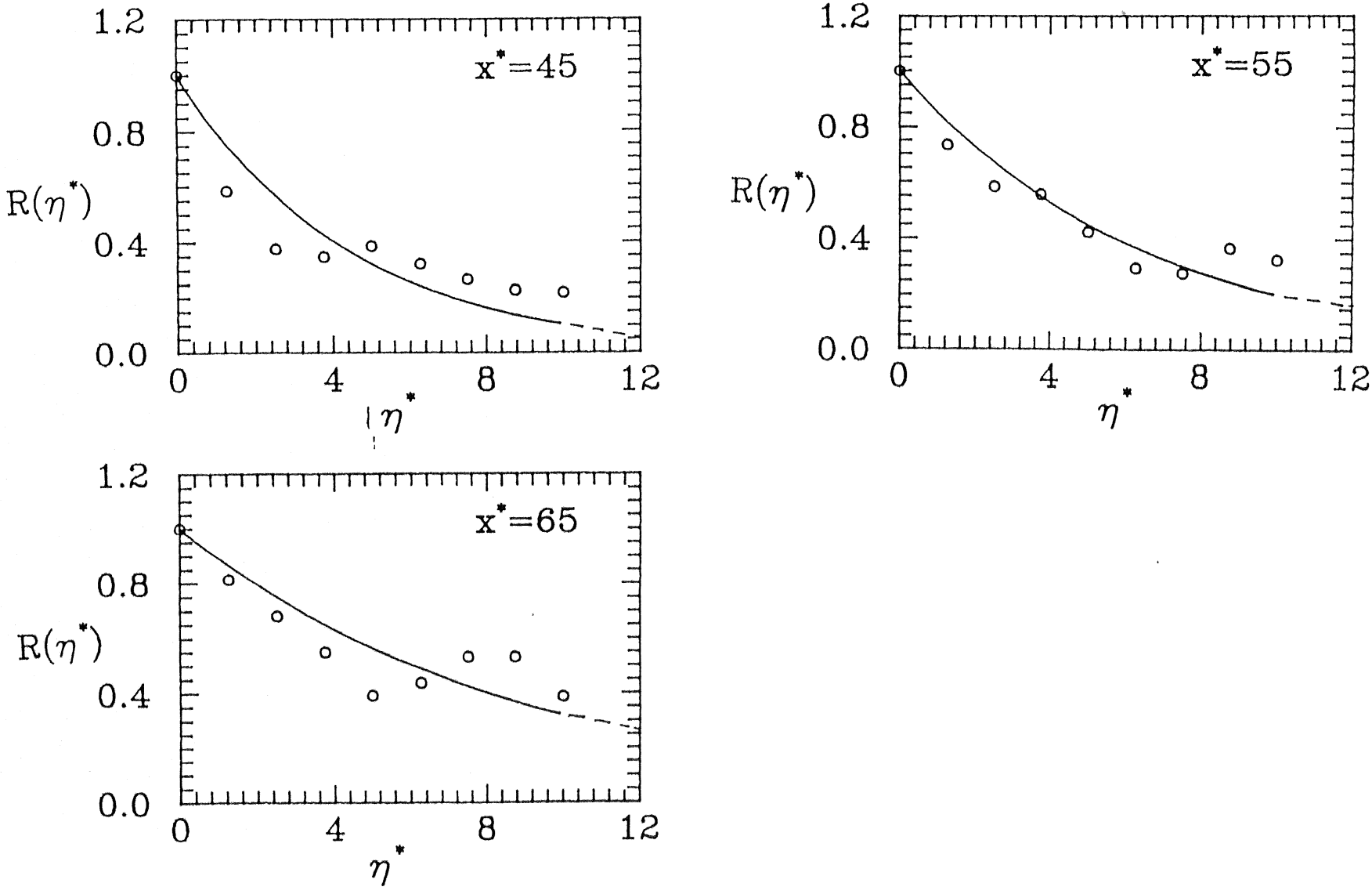

Figure 4.18b : Normalised transverse left side spatial correlation function of pressure signal at x^* = 45, 55 & 65 and Fr = 9.59

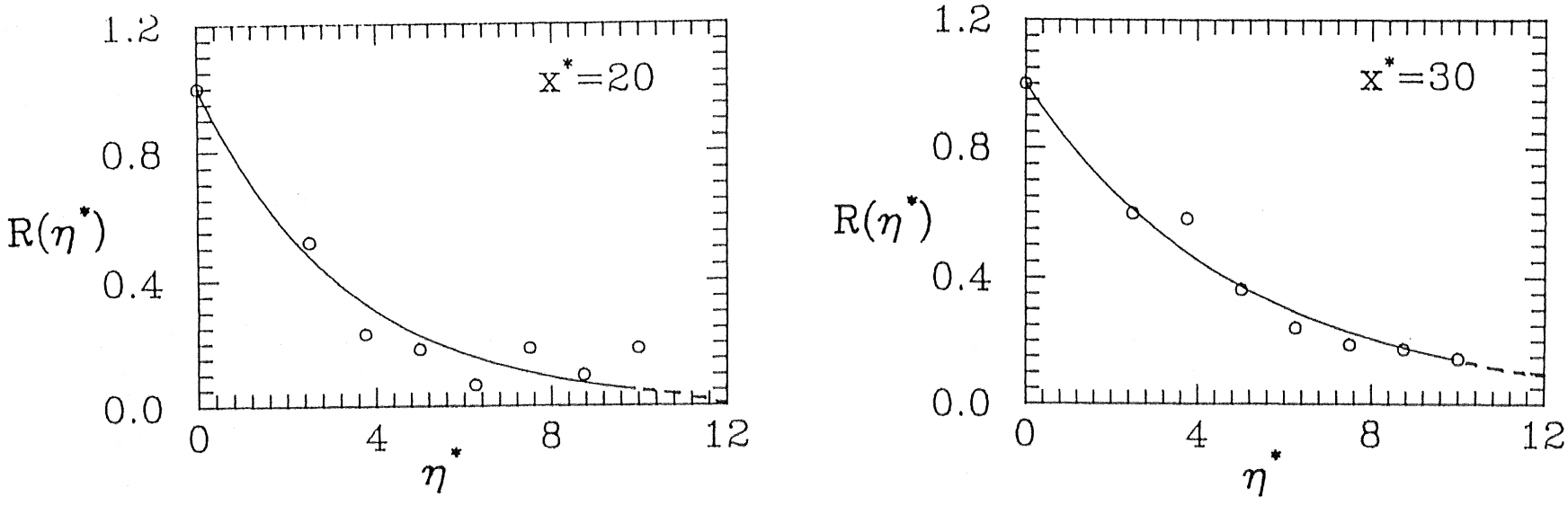

Figure 4.19a : Normalised transverse right side spatial correlation function of depth signal at x^*= 20 & 30 and Fr = 9.59

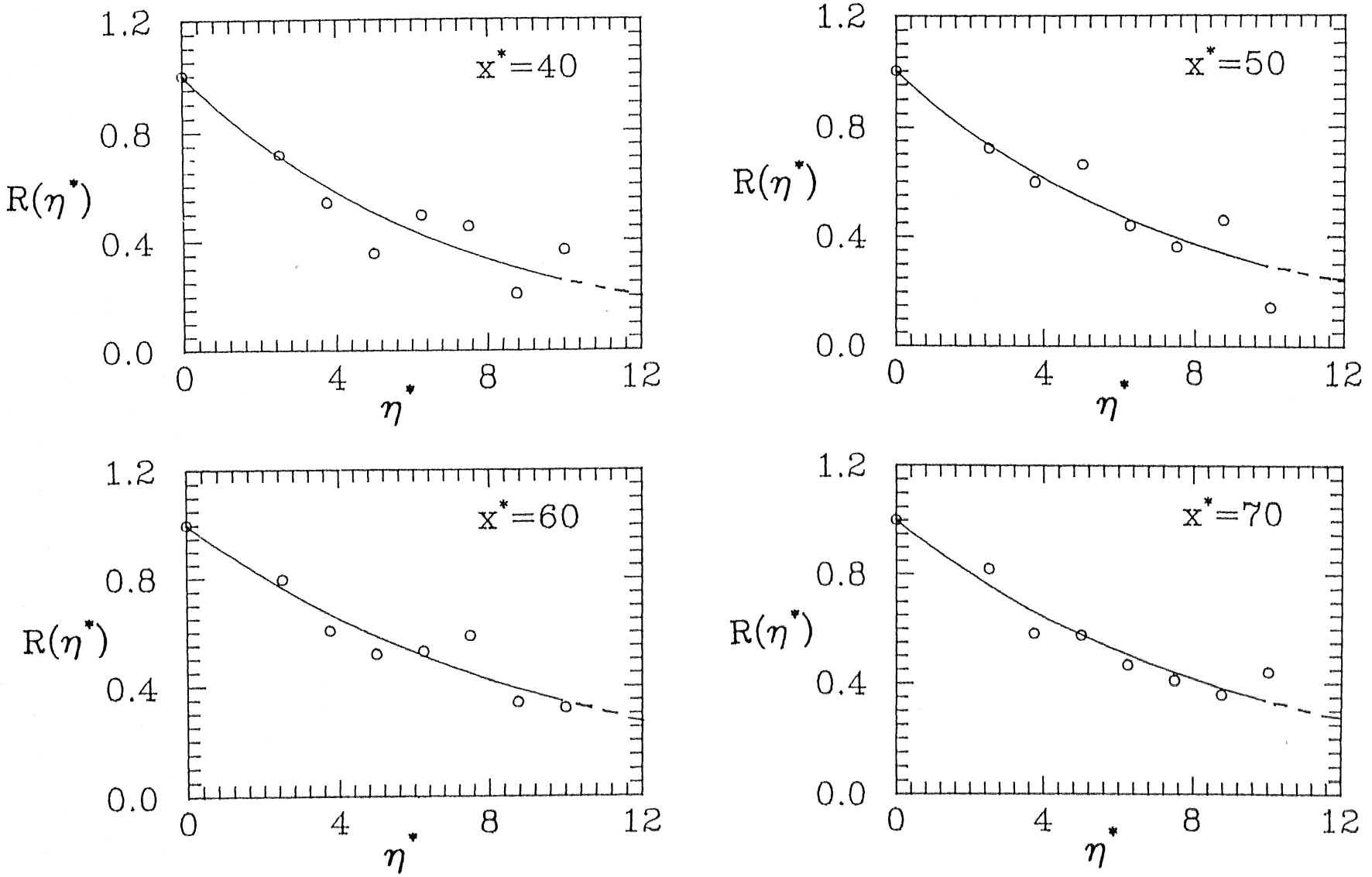

Figure 4.19b : Normalised transverse right side spatial correlation function of depth signal at x^* = 40, 50, 60 & 70 and Fr = 9.59

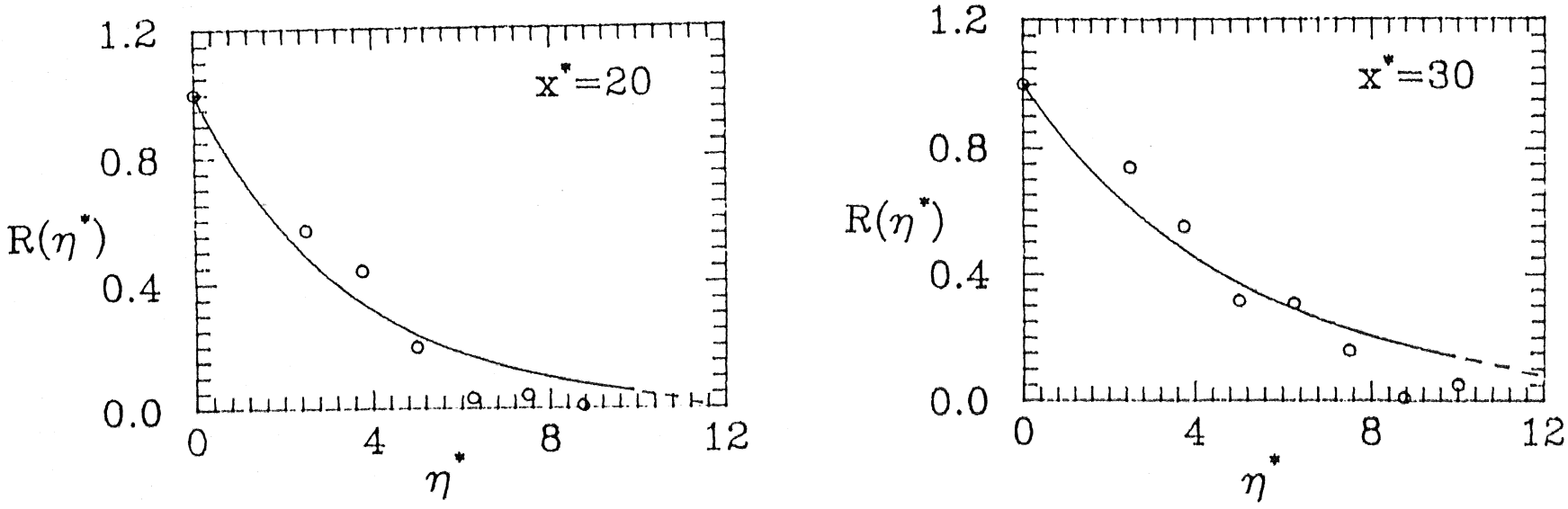

Figure 4.20a : Normalised transverse left side spatial correlation function of depth signal at x^* = 20 & 30 and Fr = 9.59

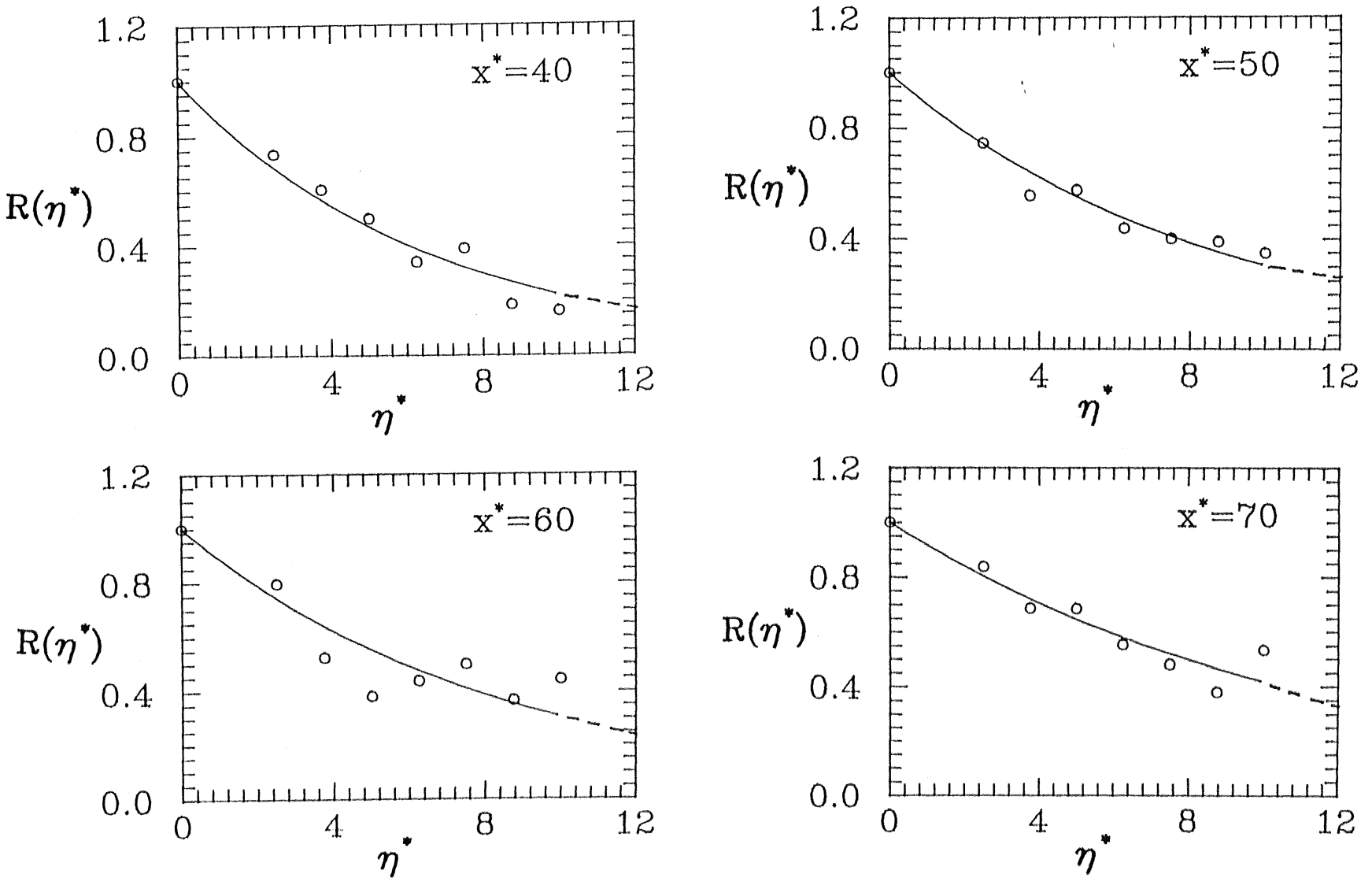

Figure 4.20b : Normalised transverse left side spatial correlation function of depth signal at x^*= 40, 50, 60 & 70 and Fr = 9.59

both signals. It confirms the expectation that the fluctuations in pressure and depth are anisotropic in nature. In the region far away from the toe the correlations in either direction are nearly equal and this trend is seen for both signals. One can say that the fluctuation becomes isotropic as it goes further downstream. This result is strengthened by calculating the integral scales in a later section.

A possible explanation for the transverse correlation length scale being initially greater than the longitudinal correlation length scale is the following. The transverse scale is initially determined by the spacing between the flume walls while the longitudinal scale is initially related to the mechanism which produces turbulence. For a hydraulic jump, turbulence is initiated by the instability of interfacial shear between air and water and hence by the associated mixing layer. The mixing layer thickness is small at high fluid velocities,then serves to act as a measure of the longitudinal length scale. As a result of extensive mixing at the air water interface, the shear practically vanishes and turbulence decays downstream. The decay is more prominent in the transverse fluctuation which are initially larger, a manifestation of the 'return-to-isotropy' principle and turbulence approaches the isotropic state. At larger distances downstream, the longitudinal length scale increases monotonically in the absence of a characteristic dimension in the flow direction.

4.5 Autocorrelation

The autocorrelation function is obtained as the real part of the Fourier transform of the spectral amplitude. Figures 4.21 - 4.24 show the autocorrelation for the four cases referred earlier. The results are shown for 8 different locations, for pressure and depth signal within the region of jump.

The autocorrelation function can be understood keeping in view the limiting cases of certain benchmark signals. These cases are : white noise, Gaussian signal and sinusoidal signal. The

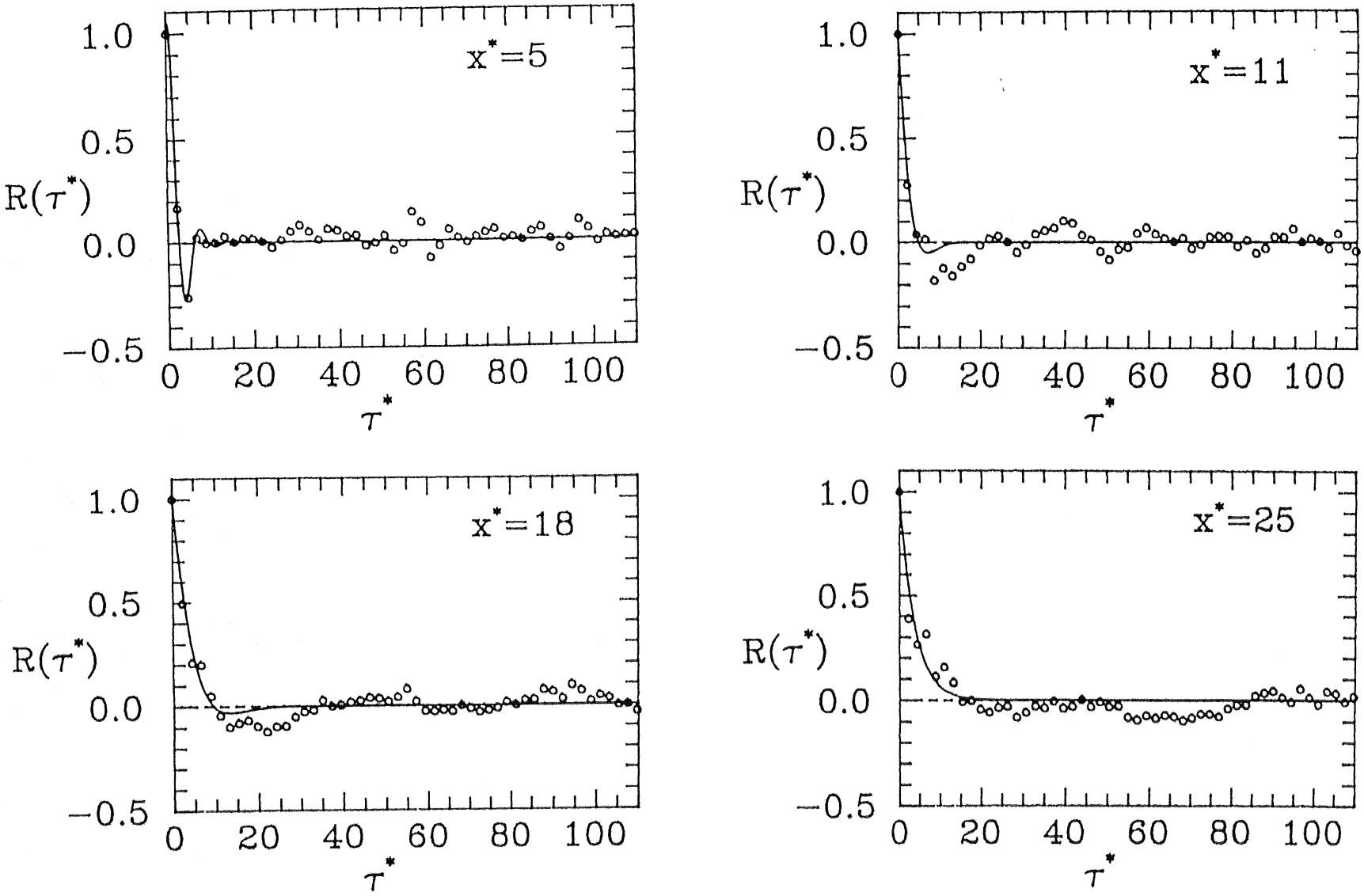

Figure 4.21a : Normalised autocorrelation function of pressure signal at x^* = 5, 11, 18 & 25 and Fr = 5.49

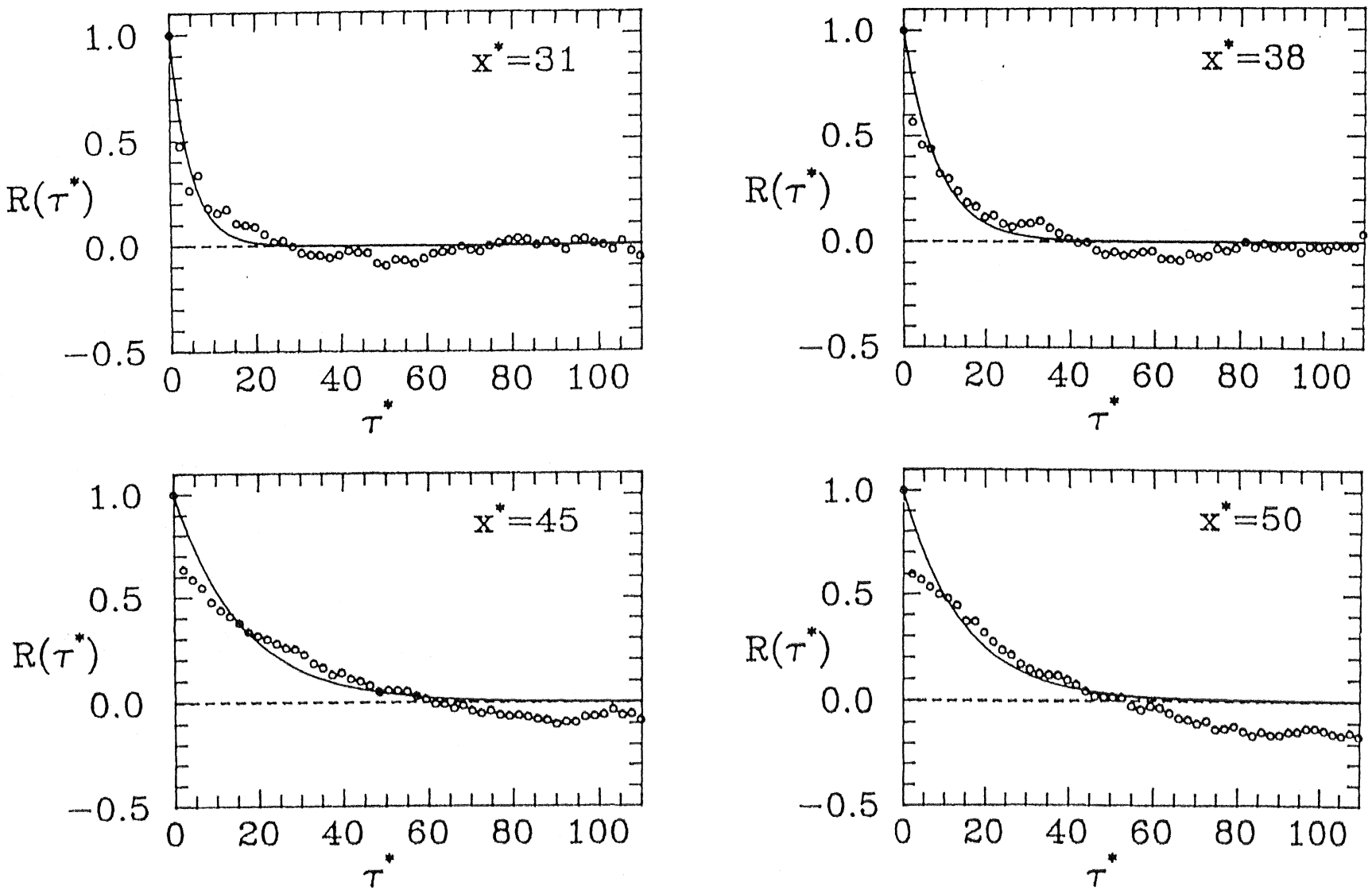

Figure 4.21b : Normalised autocorrelation function of pressure signal at x^* = 31, 38, 45 & 50 and Fr = 5.49

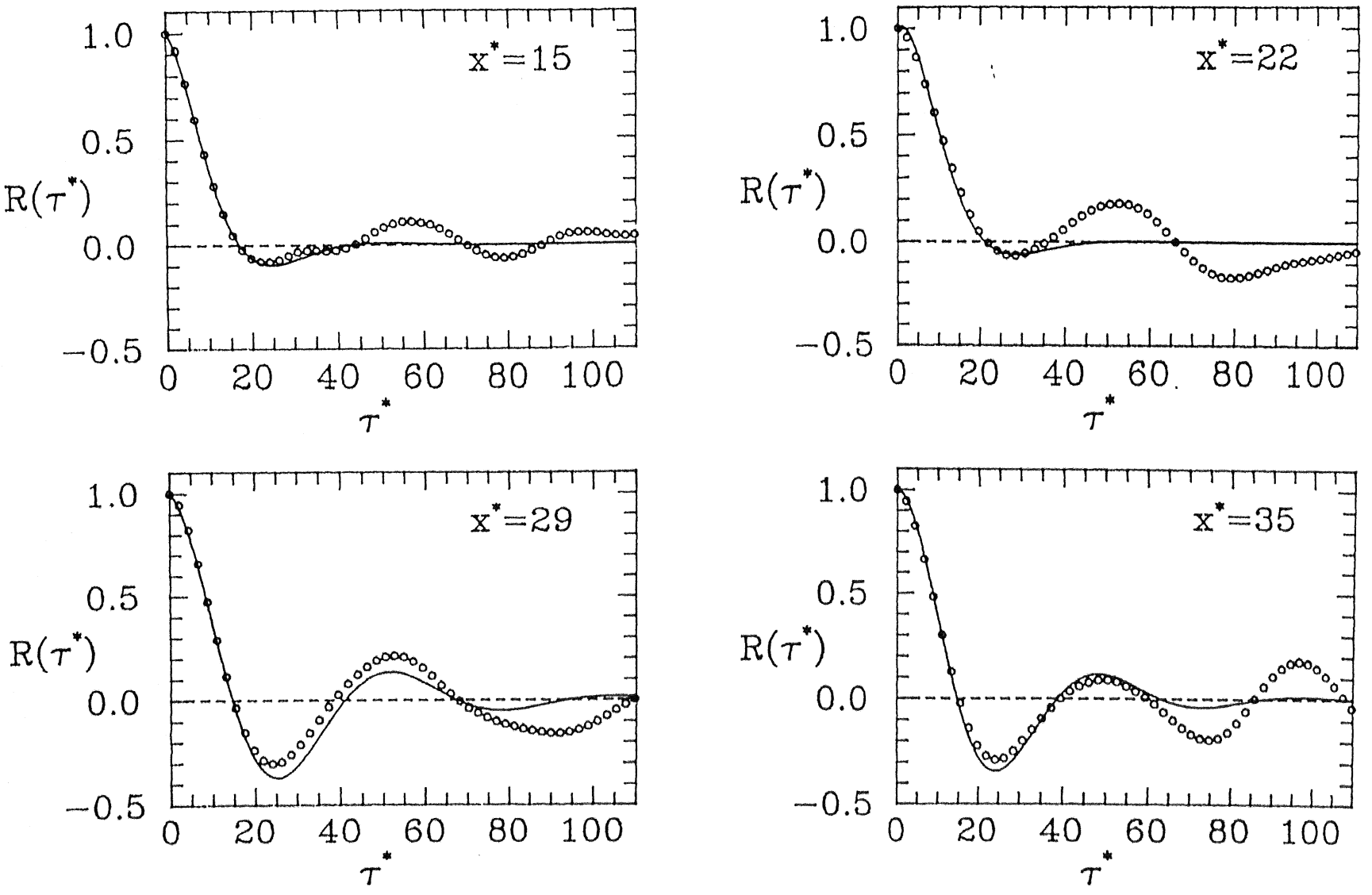

Figure 4.22a : Normalised autocorrelation function of depth signal at $x^* = 15$, 22, 29 & 35 and Fr = 5.49

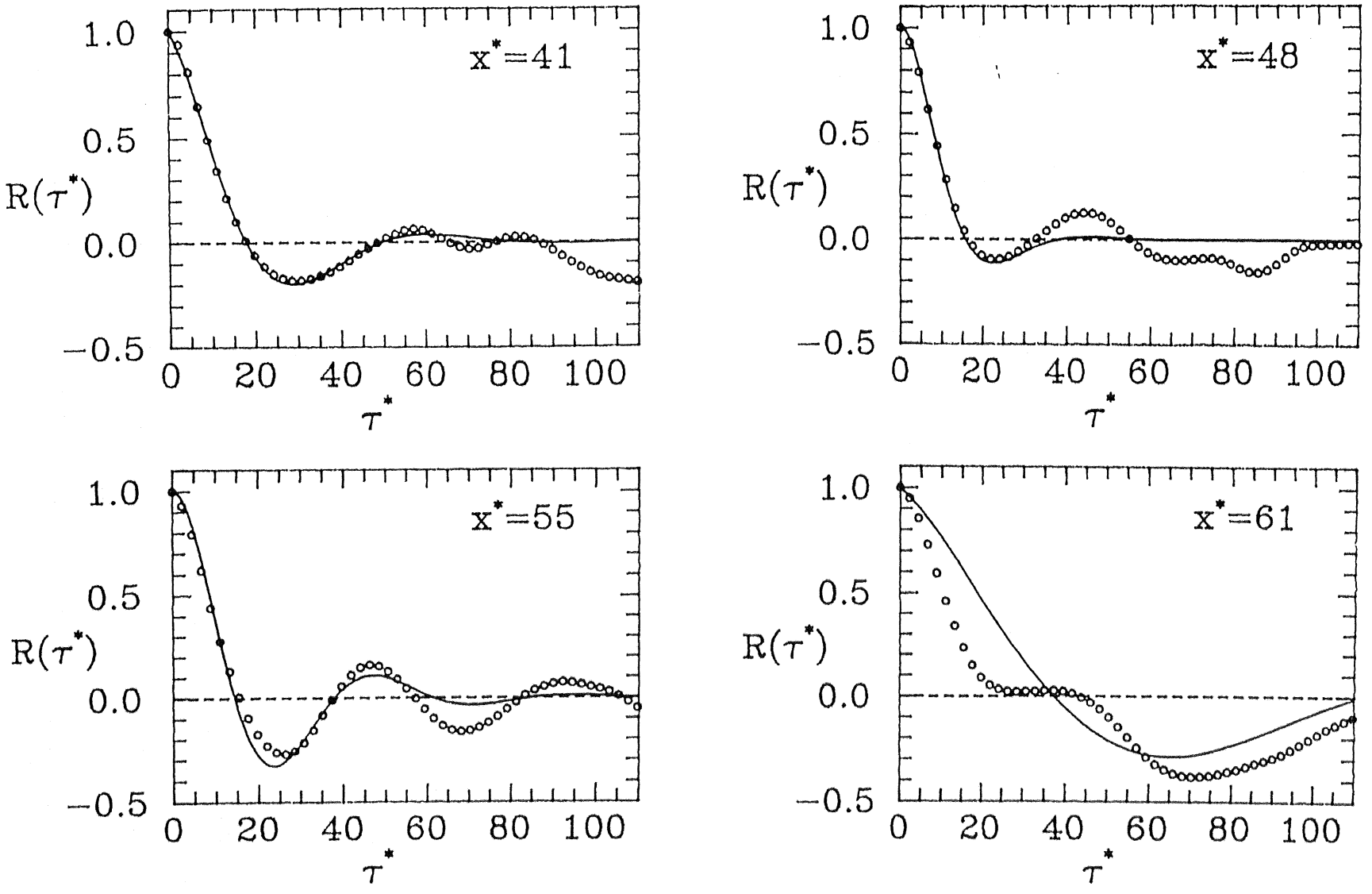

Figure 4.22b : Normalised autocorrelation function of depth signal at $x^* = 41$, 48, 55 & 61 and Fr = 5.49

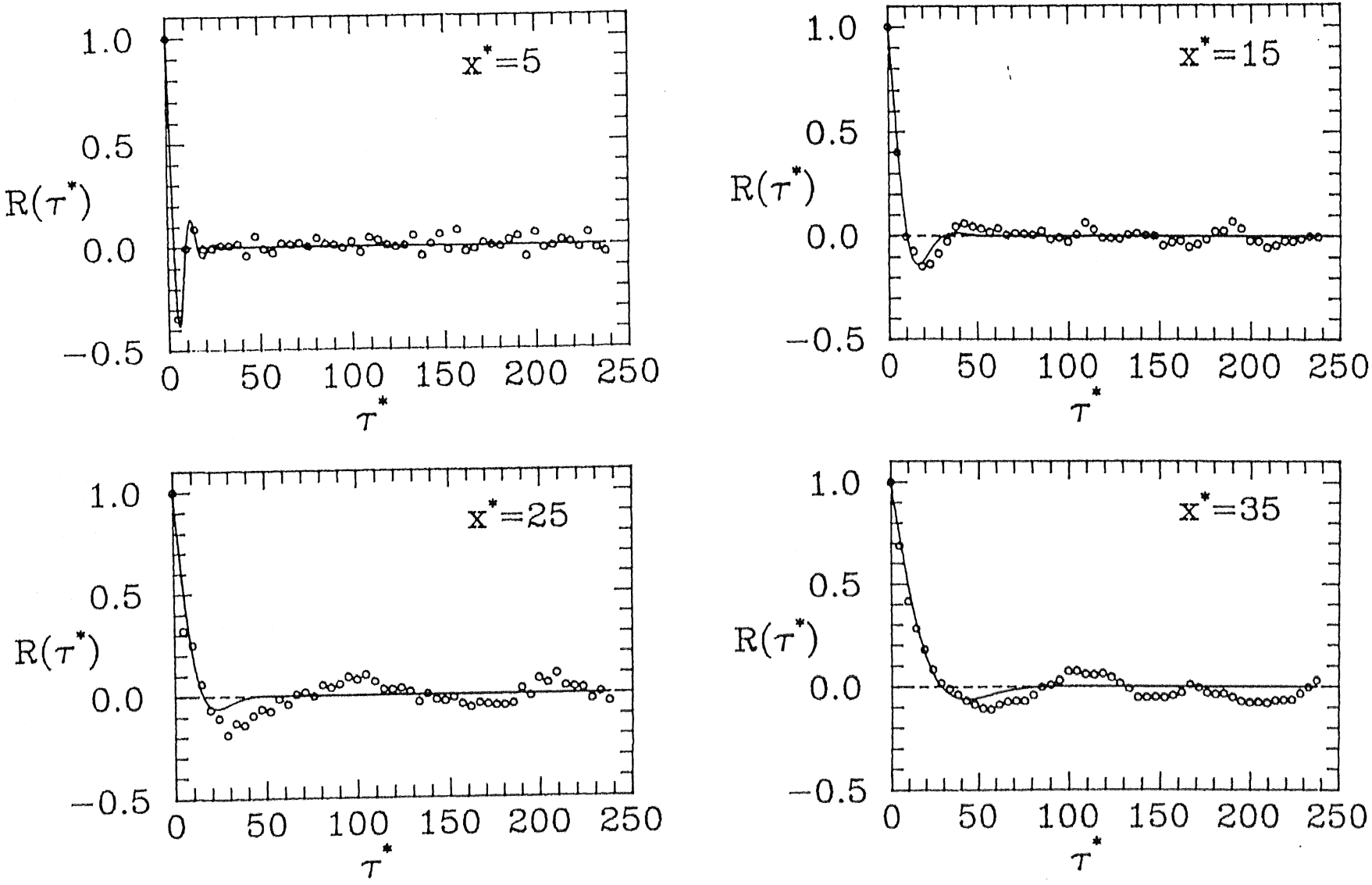

Figure 4.23a : Normalised autocorrelation function of pressure signal at x^*= 5, 15, 25 & 35 and Fr = 9.59

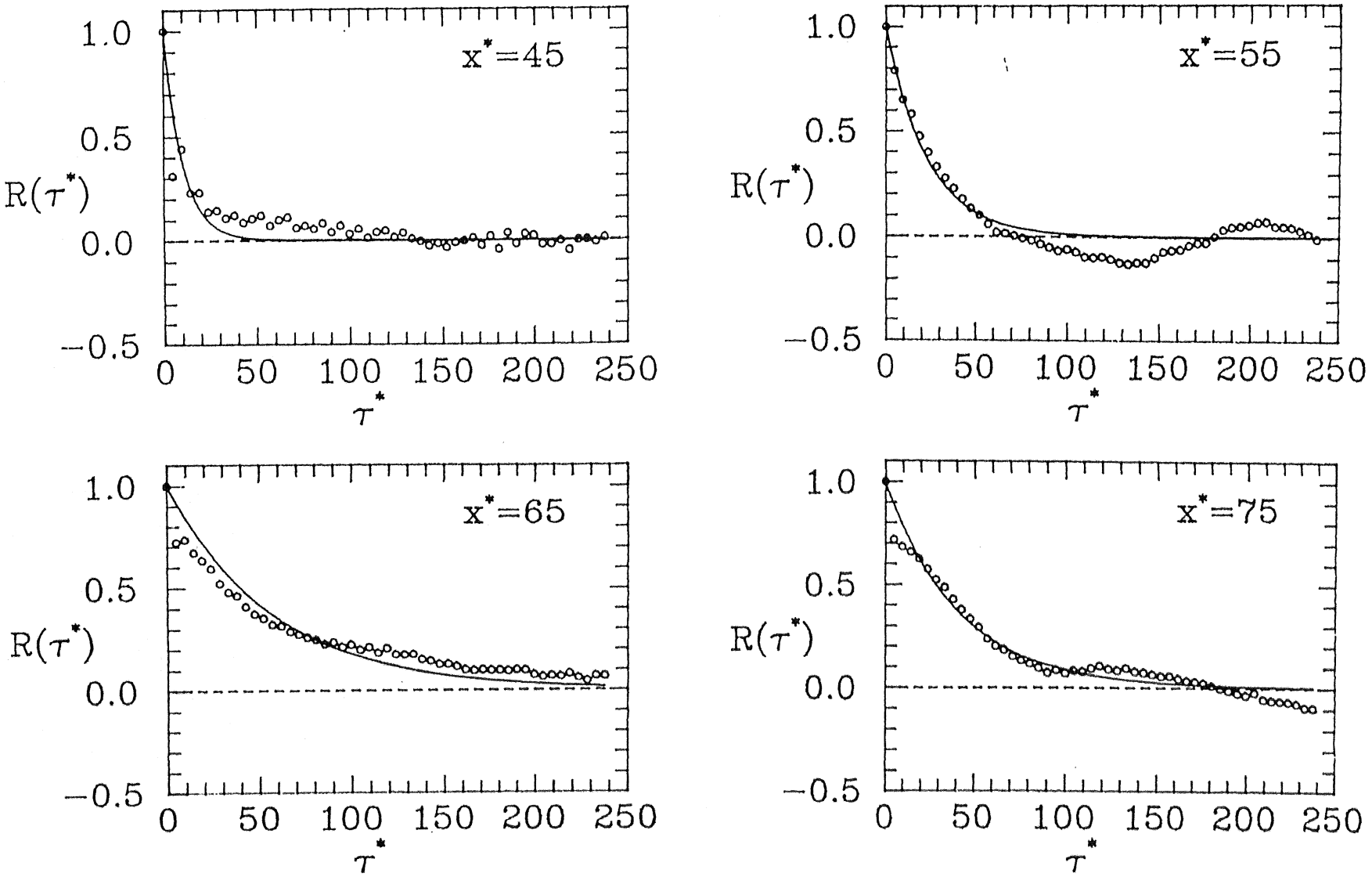

Figure 4.23b : Normalised autocorrelation function of pressure signal at $x^* = 45$, 55, 65 & 75 and Fr = 9.59

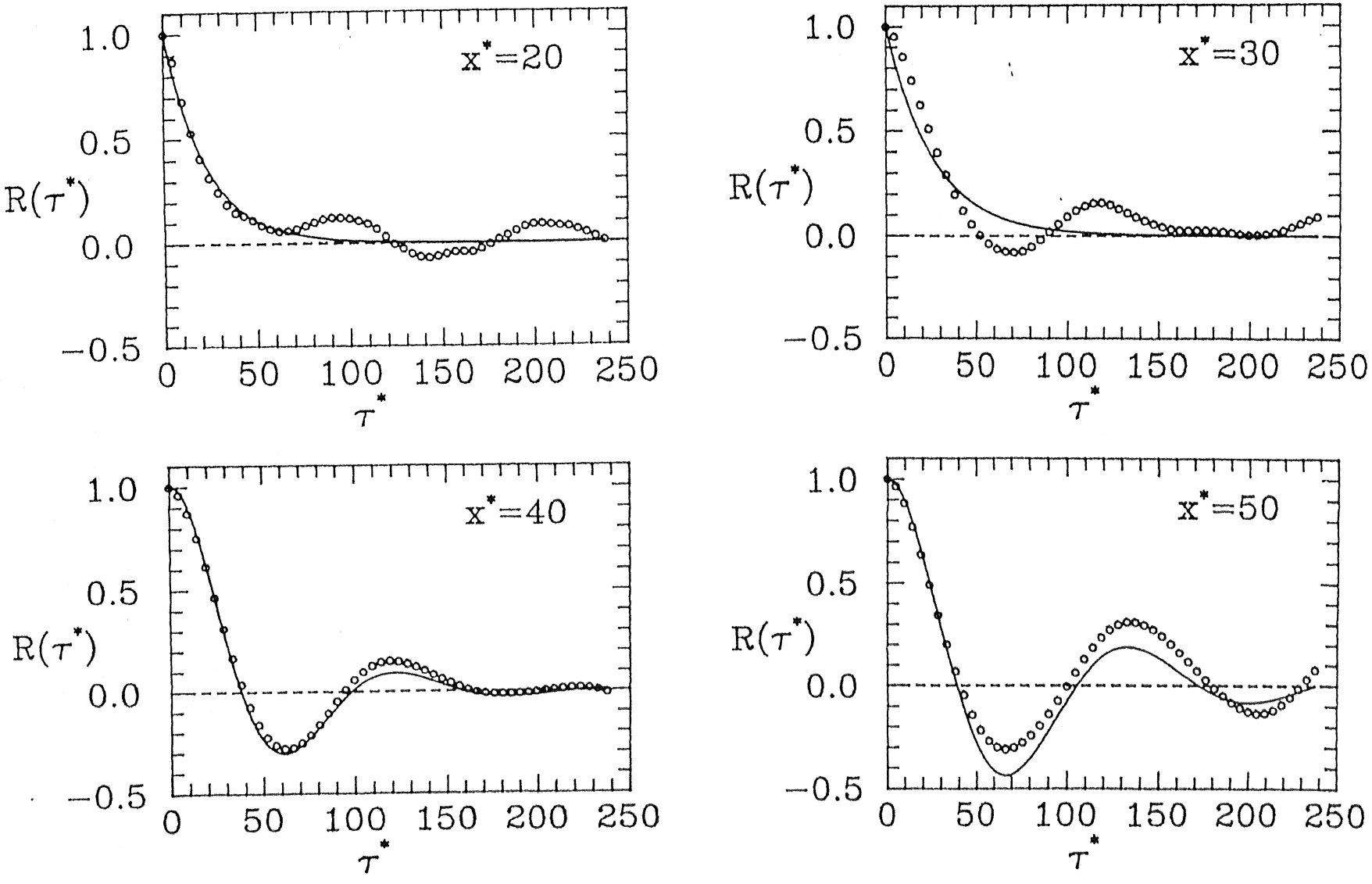

Figure 4.24a : Normalised autocorrelation function of depth signal at $x^* = 20$, 30, 40 & 50 and Fr = 9.59

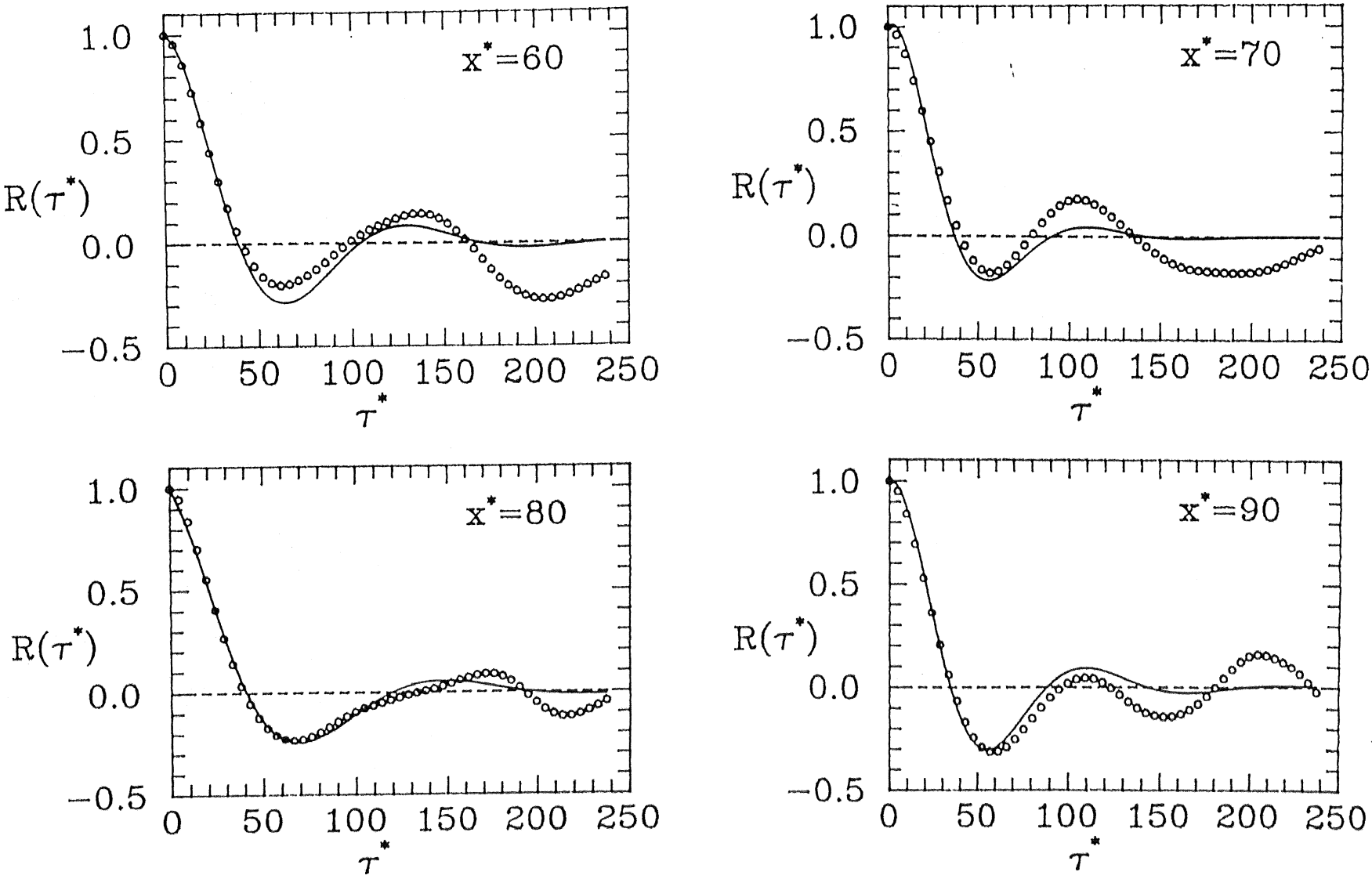

Figure 4.24b : Normalised autocorrelation function of depth signal at x^*= 60, 70, 80 & 90 and Fr = 9.59

autocorrelation function for white noise has a value of unity for zero value of lag time and value of zero at other times. The autocorrelation function for a sinusoidal signal is also sinusoidal with the same frequency. The autocorrelation function for a Gaussian signal have a value of unity for zero value of time lag and decreases gradually to zero. The curve broadens near the origin to a limiting shape corresponding to a fully developed stage. The autocorrelation function for the signals recorded can be seen as a combination of the abovementioned limiting case. The visual observation from figure shows that the pressure signal is comparable to white noise very near the toe. It develops to a Gaussian signal as it goes further downstream. The presence of sinusoidal trend (arising from wave like instability at air water interface) in the signal cannot be ruled out. The autocorrelation function for the pressure signal broadens (near the origin) steadily with the increase of distance from the toe of the jump. The depth signal is seen to be fully developed as compared to the pressure signal. Data is however not available for the depth signal very near the toe.

4.6 Power Spectrum

Power spectra have been obtained by using the Fourier transformation of the experimentally recorded signals. Figure 4.25 - 4.28 shows the spectra for all four cases defined in Section 4.1. The results are shown for 8 different locations in the region of the jump for both pressure and depth.

As in the case of the autocorrelation function power spectra also can be interpreted keeping in mind the spectra of benchmark signals referred in Section 4.5. The power spectra for white noise is a line parallel to the frequency axis indicating equal contribution from all frequencies. The theoretical power spectra of a sinusoidal signal is a Dirac-delta function with a value of infinity at the frequency equal to that of signal and zero for all other frequencies, indicating that the total energy is contributed by the single frequency. The power spectra of a Gaussian signal is a continuously decreasing curve, which is nearly flat at low frequency

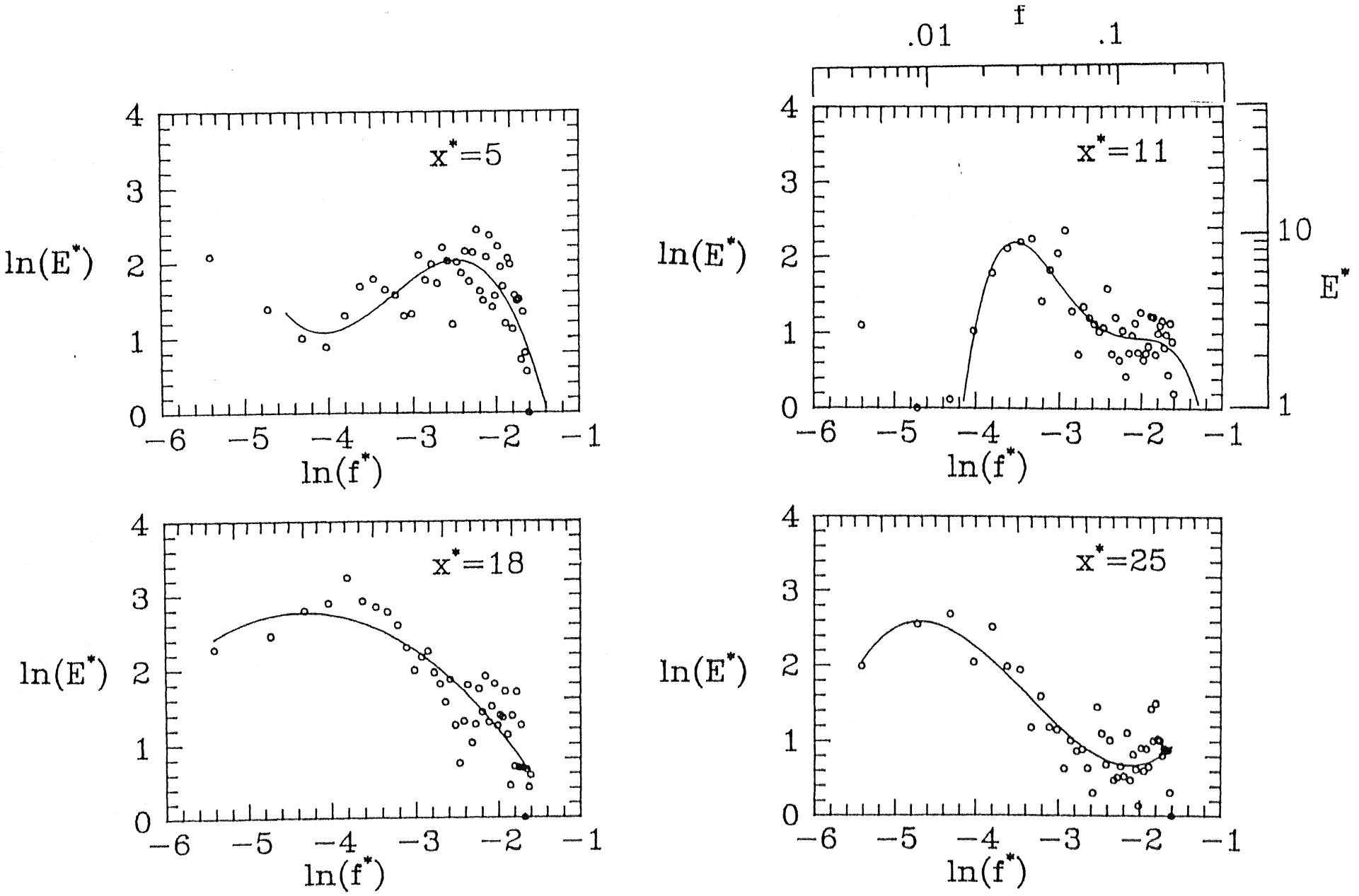

Figure 4.25a : Spectra of pressure signal at x^* = 5, 11, 18 & 25 and Fr = 5.49

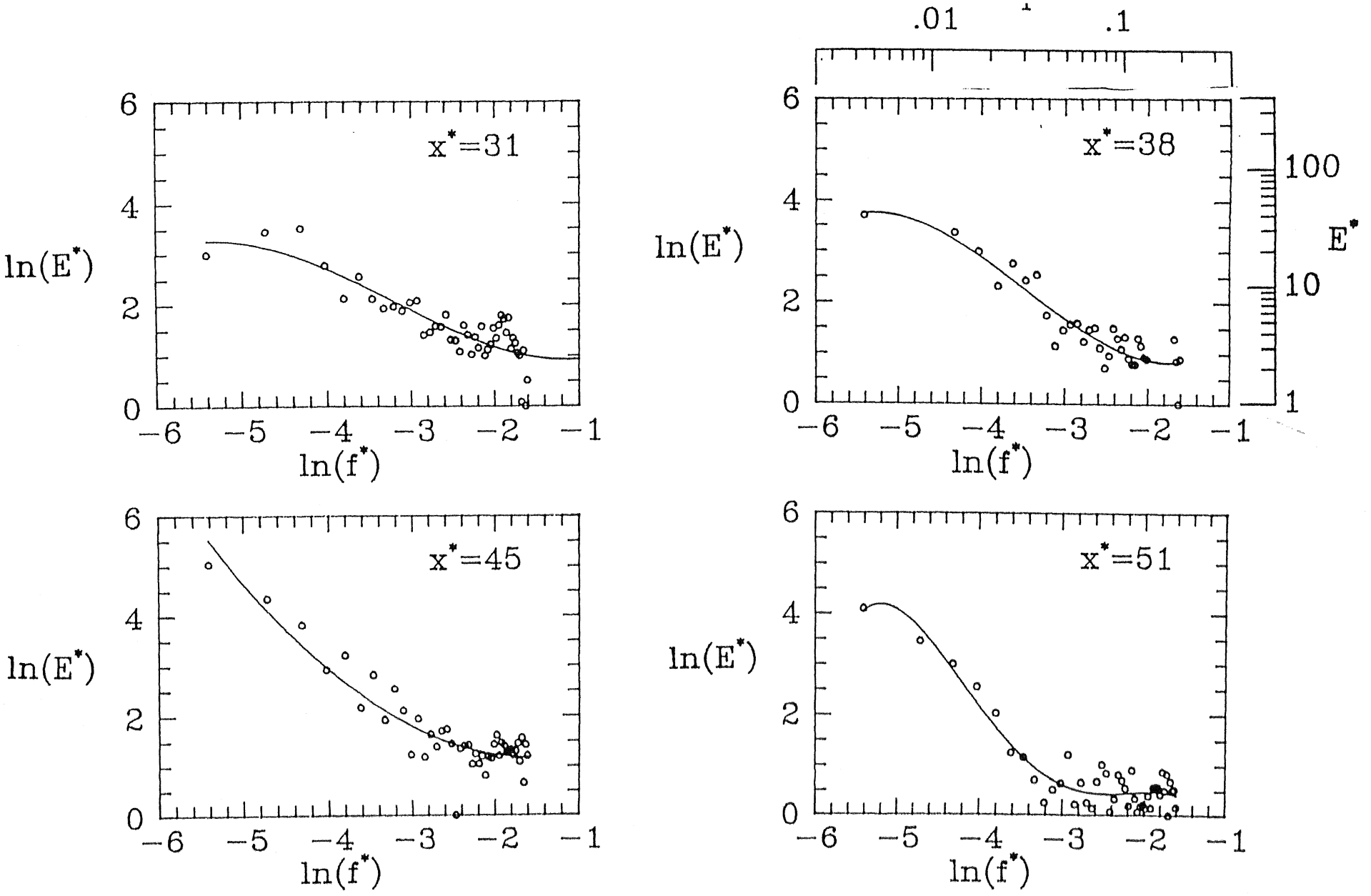

Figure 4.25b : Spectra of pressure signal at x^*= 31, 38, 45 & 50 and Fr = 5.49

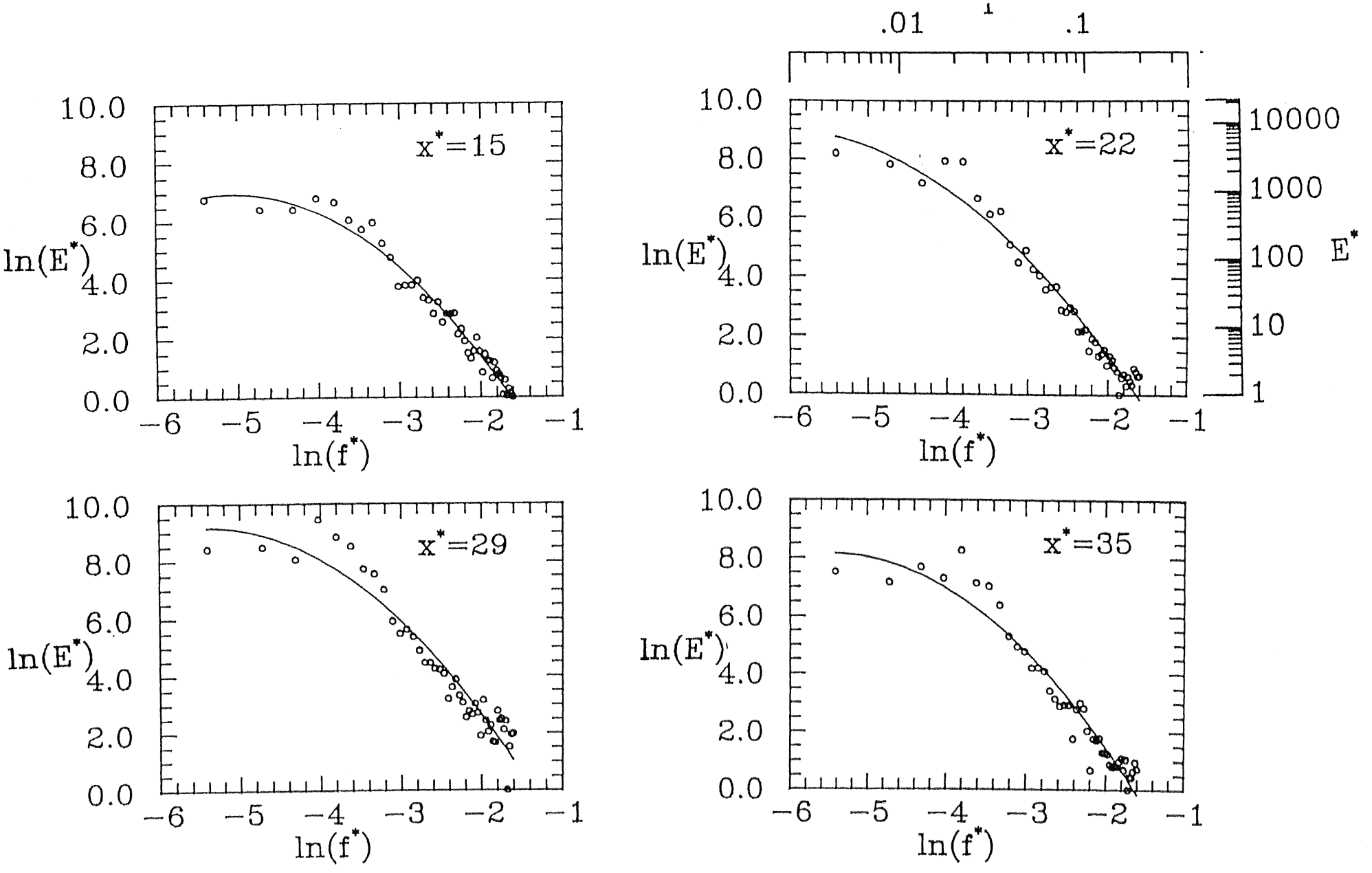

Figure 4.26a : Spectra of depth signal at x^* = 15, 22, 29 & 35 and Fr = 5.49

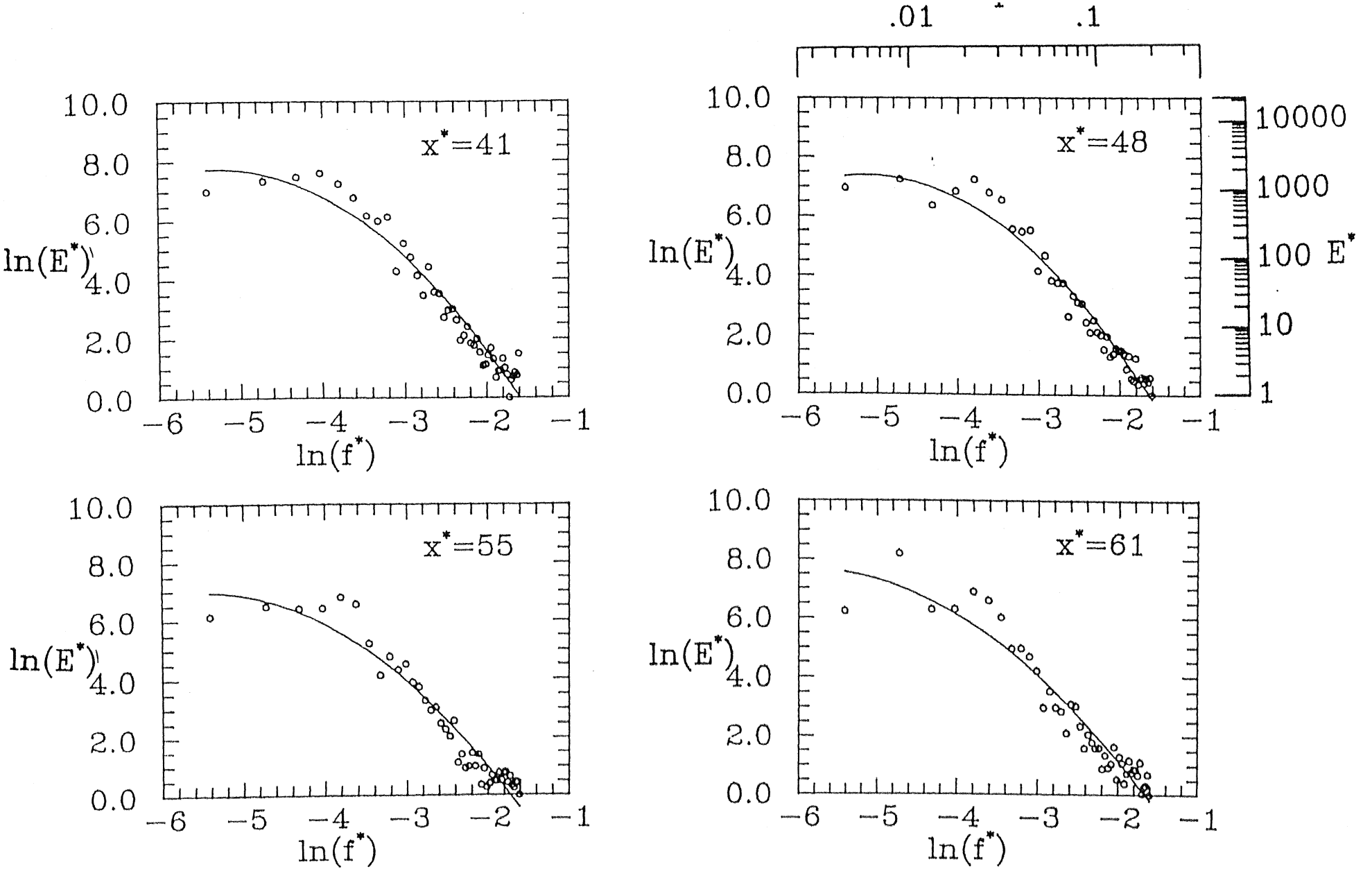

Figure 4.26b : Spectra of depth signal at x^*= 41, 48, 55 & 61 and Fr = 5.49

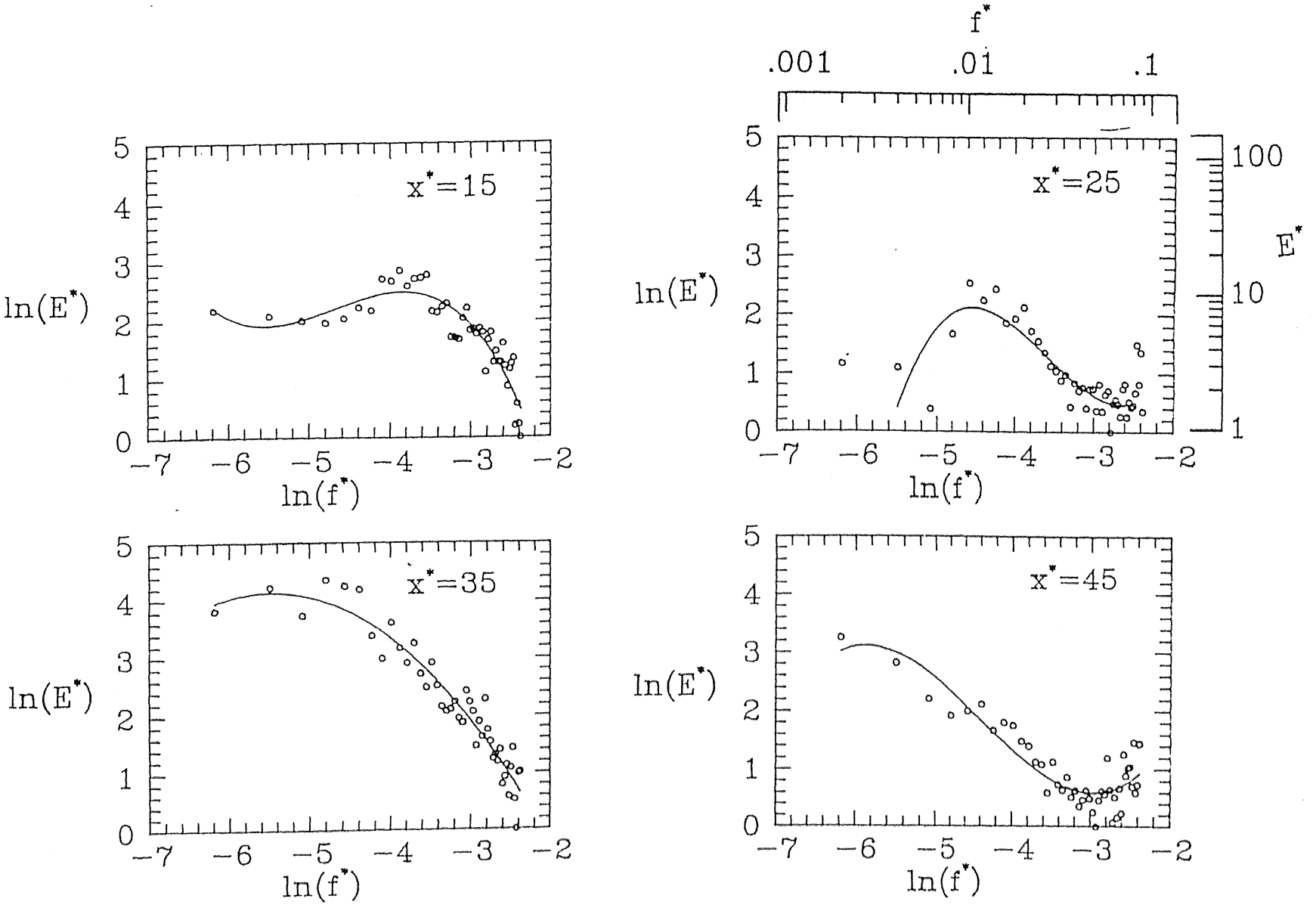

Figure 4.27a : Spectra of pressure signal at x^*= 15, 25 , 35 & 45 and Fr = 9.59

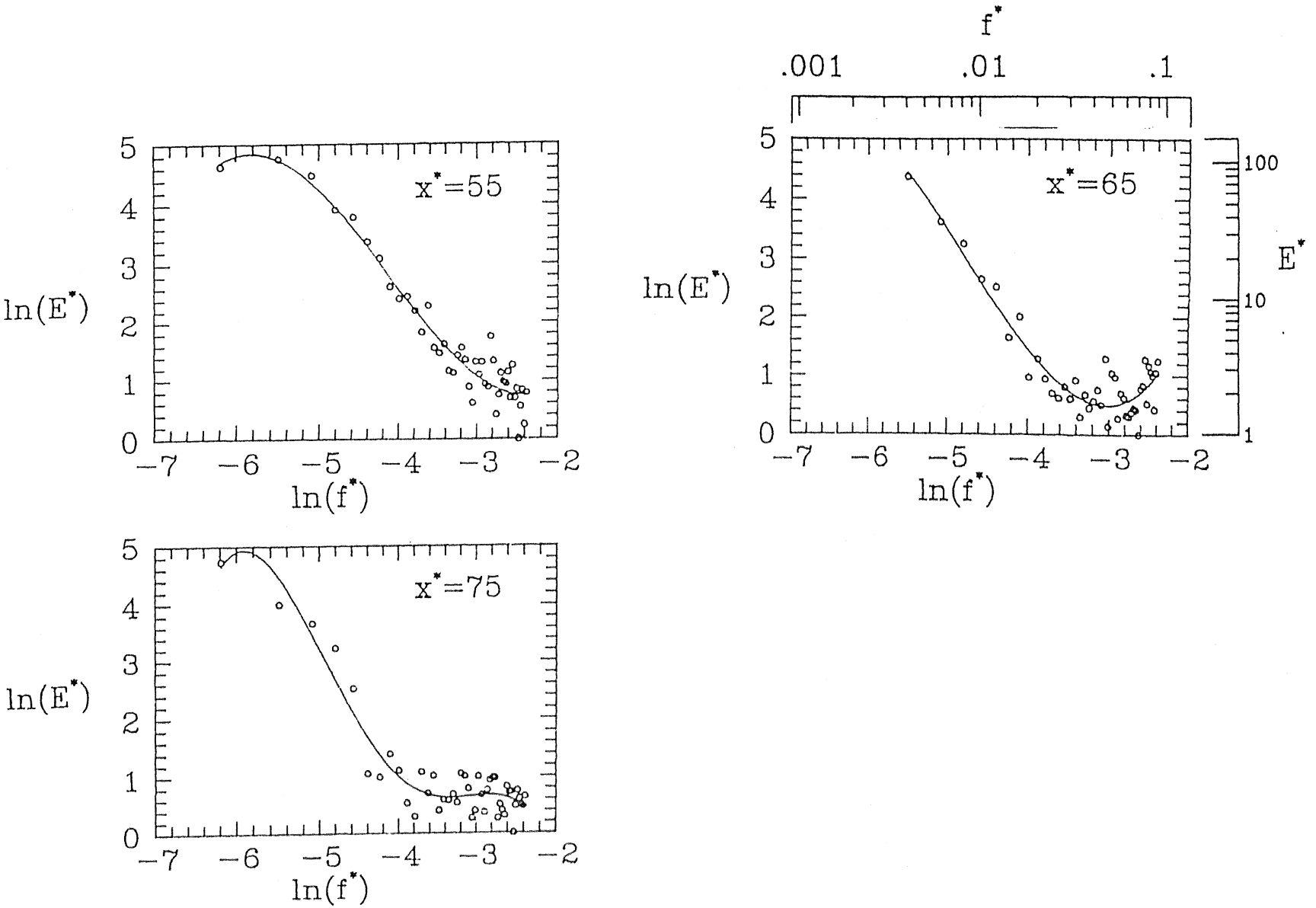

Figure 4.27b : Spectra of pressure signal at x^*= 55, 65 & 75 and Fr = 9.59

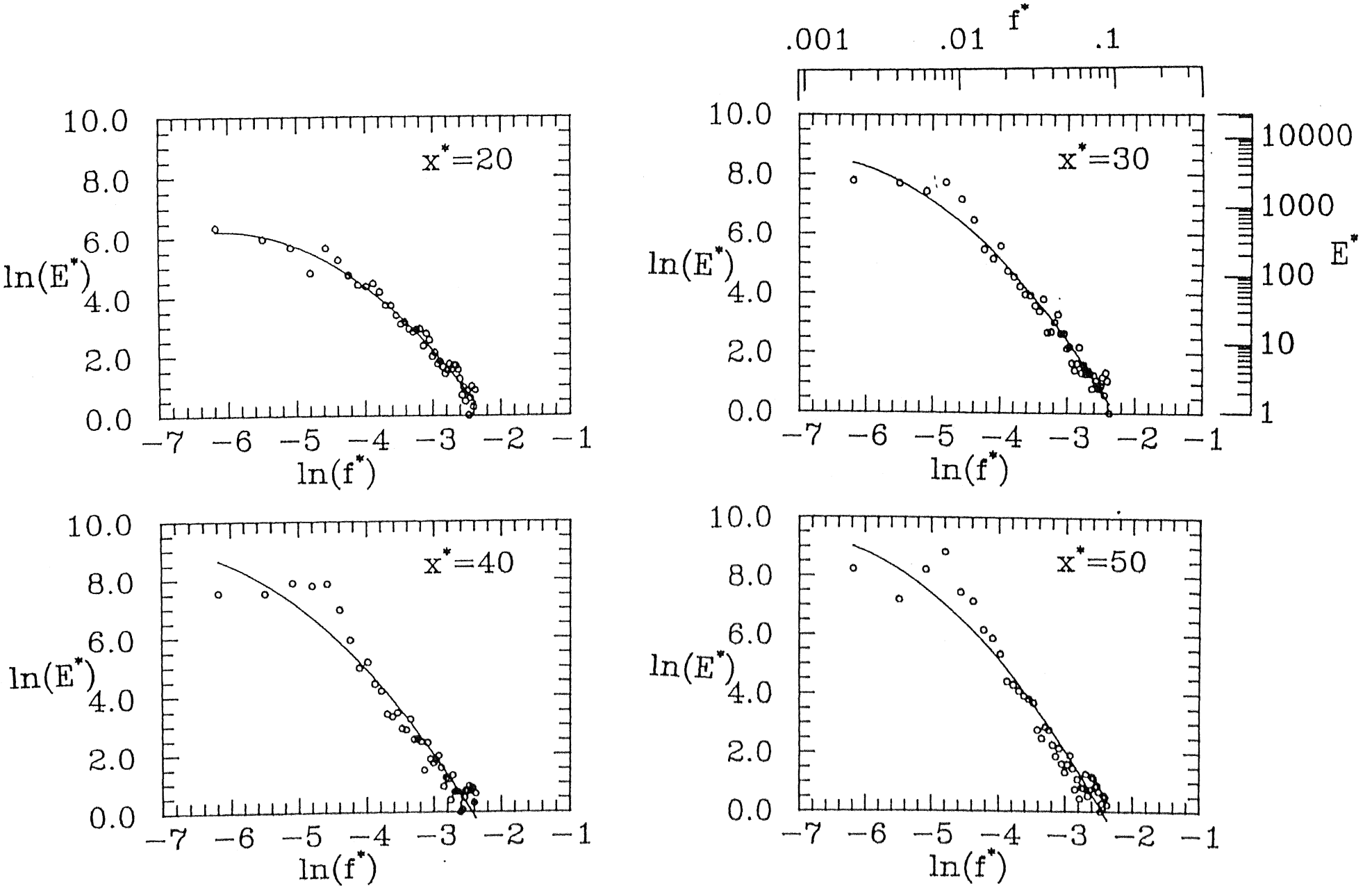

Figure 4.28a : Spectra of depth signal at x^* = 20, 30, 40 & 50 and Fr = 9.59

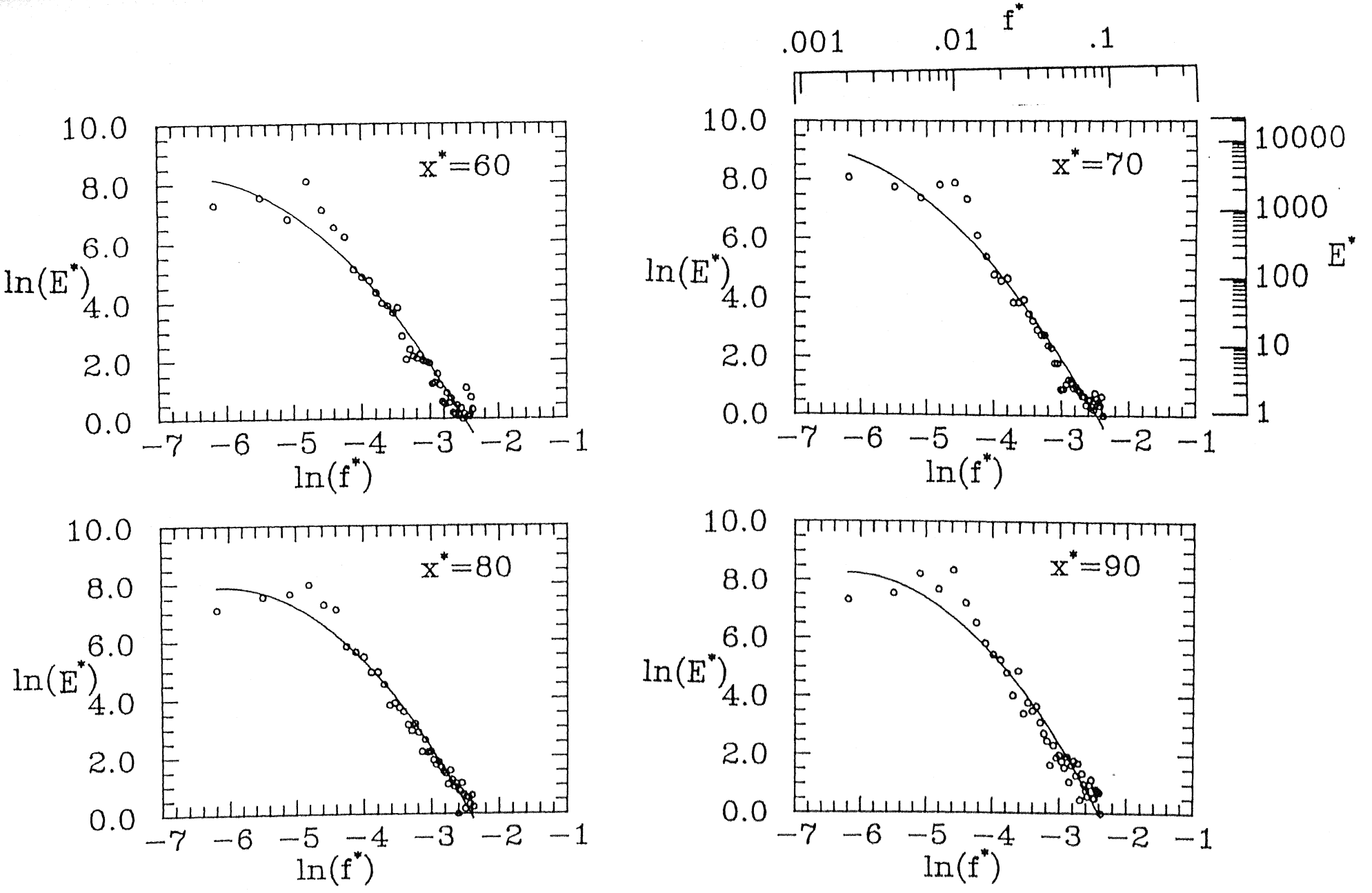

Figure 4.28b : Spectra of depth signal at x^*= 60, 70, 80 & 90 and Fr = 9.59

and decays monotonically at higher values. It is well known that in fully developed turbulence, the slope of the spectrum in the intermediate (inertial) range is -5/3, independent of the problem being studied. It is also to be noted that turbulence cannot be truly Gaussian. At very low frequencies, the spectra should show an increasing trend since energy has to be fed from the mean flow (zero frequency) to the fluctuating quantities. This trend of spectra increasing initially with frequency and falling off later is correctly seen in the present work.

The spectra obtained for the signals recorded in the present work were not smooth. To find the dominant trend in the spectra, the amplitude of spectra was smoothed by averaging. The details of this process are discussed in Section 3.3.4 . The spectra obtained after averaging shows a definite trend. The spectra for pressure signal near the toe is comparable to white noise and does not fall-off at higher frequencies. But as the distance increases, it develops to a shape comparable to a Gaussian one. Similar trends were seen for the pressure signal at both Froude numbers. Because of experimental difficulties the signal for depth very near the toe was not measured. The recorded depth signal spectra at a later distances shows a definite trend and is comparable to that of a Gaussian signal. similar trend were observed at both the Froude numbers.

The slope of the spectra in the intermediate range 5 -20 Hz as a function of distance are summarized in Tables 4.2a to 4.2d. The approach towards a fully developed state can be seen to be rapid in all the cases.

4.7 Cross-Correlation

The cross-correlation between the depth and pressure signals was computed at 7 different locations for each Froude number. Figure 4.29 shows variation of the correlation coefficient with distance from the toe of the jump. The calculation have been carried out using a sample space of 1024 points. From Figure 4.29 it is clear that the correlation coefficient increases with distance from

Table 4.2a : Slope of power spectra for pressure fluctuation at Fr = 5.49

x^*	5	15	18	25	31	38	45	51
slope	-2.00	-0.96	-0.88	-0.73	-0.67	-0.90	-1.10	-1.65

Table 4.2b : Slope of power spectra for depth fluctuation at Fr = 5.49

x^*	15	22	29	35	41	48	55	61
slope	-2.06	-2.41	-2.50	-2.35	-2.26	-2.18	-2.03	-2.11

Table 4.2c : Slope of power spectra for pressure fluctuation at Fr = 9.59

x^*	15	25	35	45	55	65	75
slope	-1.36	-0.90	-1.16	-0.83	-1.33	-1.50	-1.86

Table 4.2d : Slope of power spectra for depth fluctuation at Fr = 9.59

x^*	20	30	40	50	60	70	80	90
slope	-1.68	-2.22	-2.36	-2.41	-2.28	-2.43	-2.19	-2.27

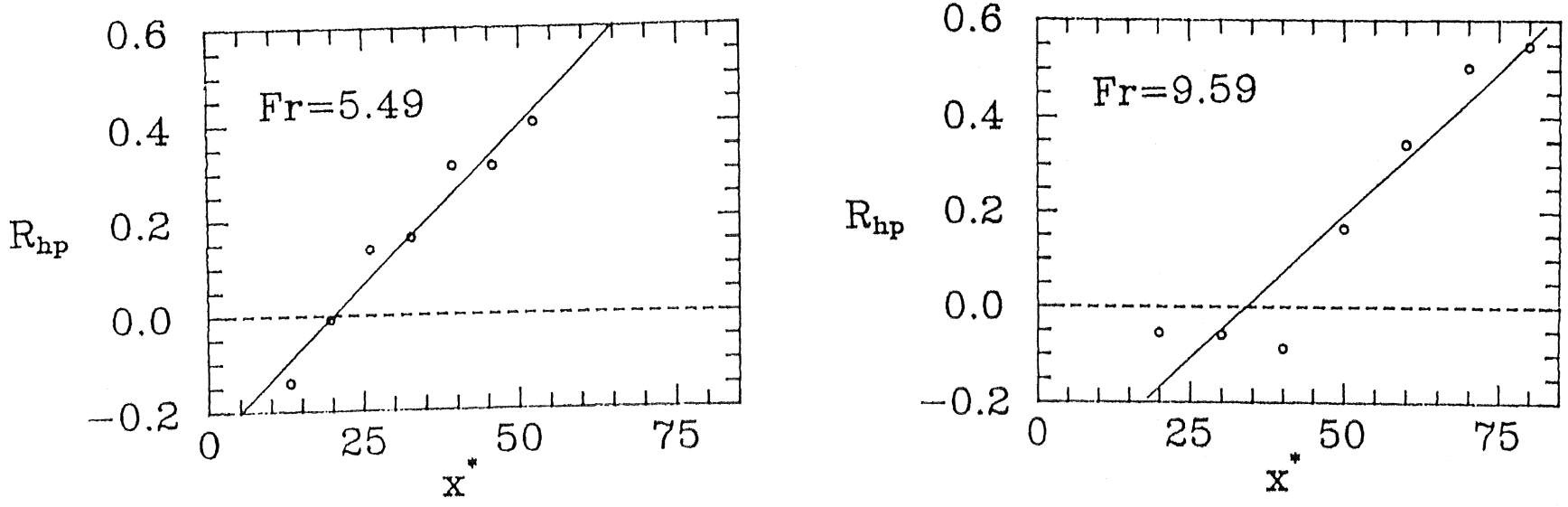

Figure 4.29 : Variation of crosscorrelation coefficient between pressure and depth signal with distance at Fr = 5.49 & 9.59

the toe at each Froude number. It is also obvious that the signals are almost uncorrelated near the toe. The variation of correlation with distance is predominantly linear. The visual inspection of the results shows that the rate of increase of correlation coefficient is almost the same at both Froude numbers. However the correlation coefficient at a point is smaller at higher Froude number.

4.8 Scales of Fluctuation

The results obtained from correlation analysis can be discussed quantitatively by calculating the scales of fluctuation. These are shown in terms of the nondimensional scale as a function of distance from the toe of the jump, Figure 4.30a. By inspection of this plot it is clear that for pressure fluctuation, the scales near the toe are different for longitudinal and transverse correlation functions. The scales are comparable for the right and left side transverse correlations. At some points the scale becomes negative but this error is due to errors in curve fitting. The scale at points far from the toe for both longitudinal and transverse correlation function are close to one another. One can summarize that the pressure fluctuation is anisotropic near the toe of the jump and develops gradually to an isotropic condition with the increase of distance.

The scales calculated for the depth signal at Froude number 4.59 for both the longitudinal and transverse correlation functions are close to each other. This depicts that the signal is isotropic at all points. The scales at the higher Froude number shows a trend which is very similar to that of the pressure fluctuation.

Figure 4.30b shows the length scales of both pressure and depth fluctuation nondimensionlised with respect to local depth. It gives an account of ratio of length scale and local depth. The most likely value of the ratio is 0.5 and it varies between 0 to 1.

Figure 4.31 shows the variation of the integral scale calculated for the autocorrelation function for the four cases. The

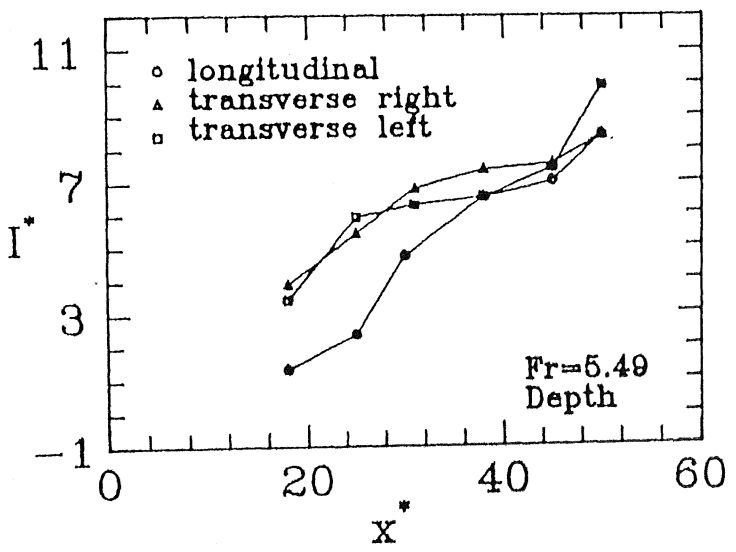

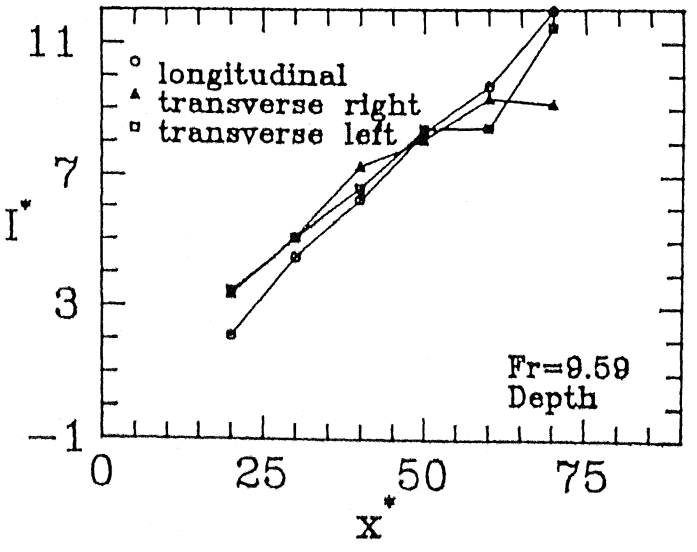

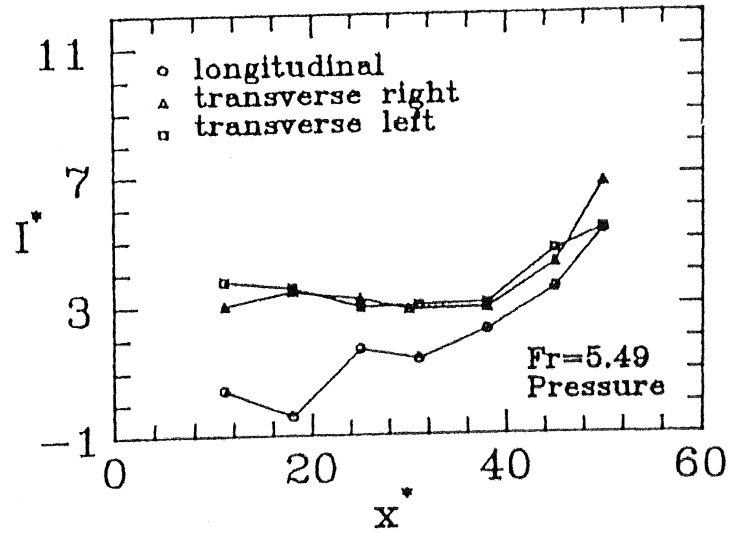

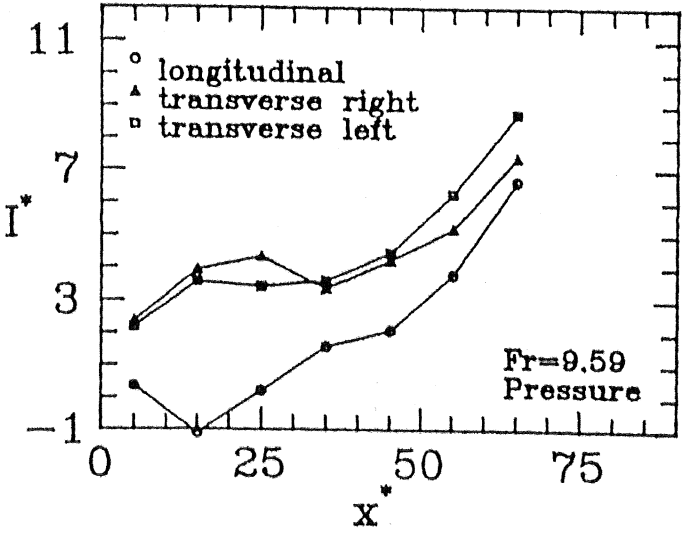

Figure 4.30a : Variation of nondimensional integral length scale (I/h_1), for pressure and depth fluctuation, with distance at Fr =5.49 & 9.59

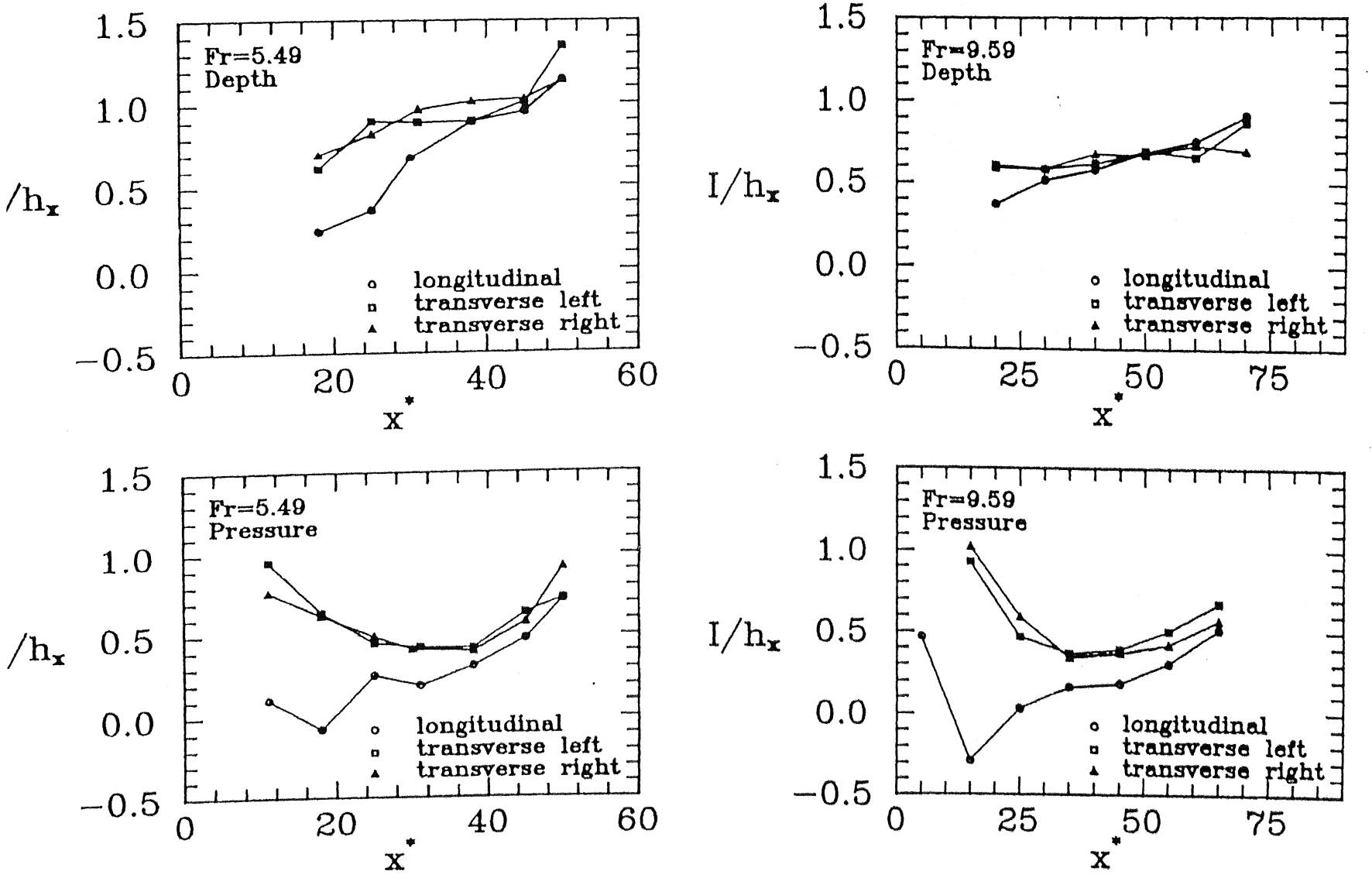

Figure 4.30b : Variation of nondimensional integral length scale (I/h_2), for pressure and depth fluctuation, with distance at Fr =5.49 & 9.59

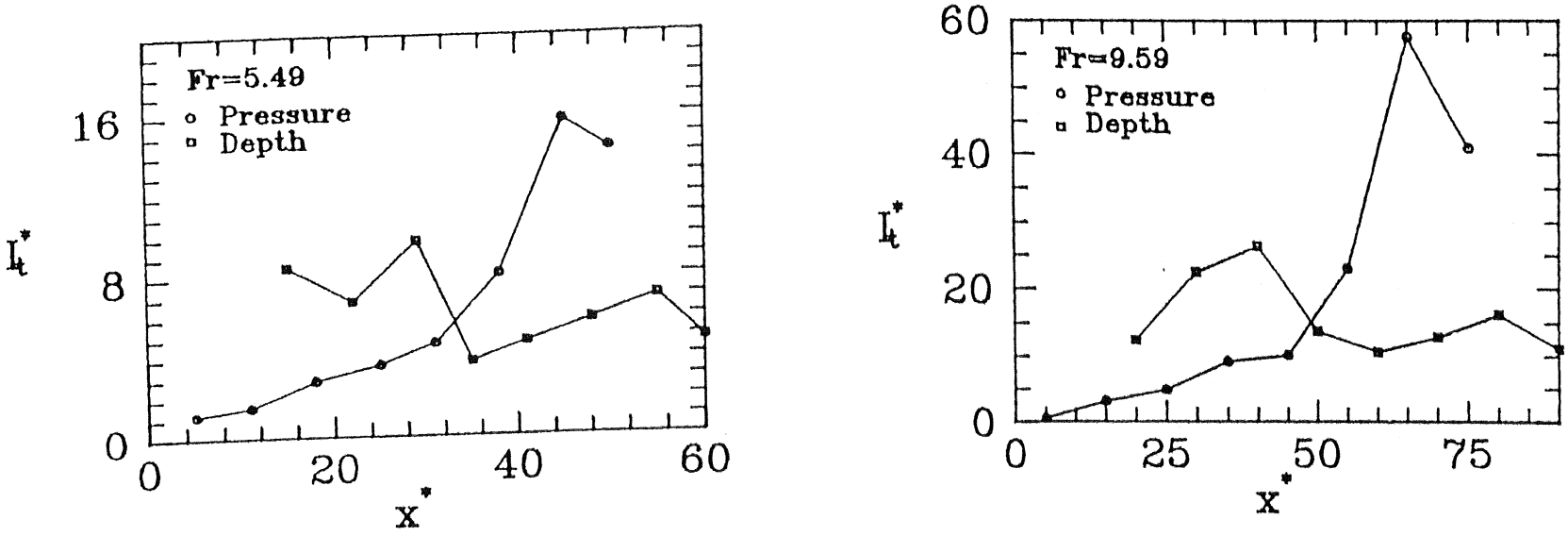

Figure 4.31 : Variation of nondimensional integral time scale, for pressure and depth fluctuation, with distance at Fr =5.49 & 9.59

figure shows that the pressure scale increases at a slow rate near the toe, but far away, it increases steadily. The same trend is seen at both Froude numbers. For the depth signal it shows no significant change but remains almost unchanged.

4.9 Air Content and Apparent Unit Weight

The air entrained in the jump decreases the unit weight of the airwater mixture. Therefore the magnitude of depth is greater as compared to the pressure. The air content has been calculated in the present work using the best fit value of pressure and depth at different location. Figure 4.32 shows the variation of air content and the apparent unit weight for both Froude numbers. The air content decreases with the increasing distance, this is easily explained since air entrainment gets reduced downstream of the jump. Thus the apparent unit weight increases with the increasing distance and finally it reaches the value equal to that of water. It is also clear that the air content increases with increasing Froude number since the jump becomes more turbulent and entrains more air.

4.10 Comparison of Result with Previous work

The results obtained in the present work compared well with the work, of similar nature, done in past. Shape of the PDFs of fluctuation of pressure were following the shape of PDF of a Gaussian signal, as described by Abdul Khader and Elango and Rinaldo and Fiorotto. The trend of skewness and kurtosis for fluctuation in pressure signals were same as described by Rinaldo and Fiorotto.

The results obtained for spatial correlation of fluctuation of pressure signals were compared to that, obtained by Rinaldo and Fiorotto, in terms of the minimum lag distance for which the value of correlation coefficient becomes zero. Tables 4.3a and 4.3b shows the comparison. The shape of the transverse correlation functions also were same as obtained by Rinaldo and Fiorotto.

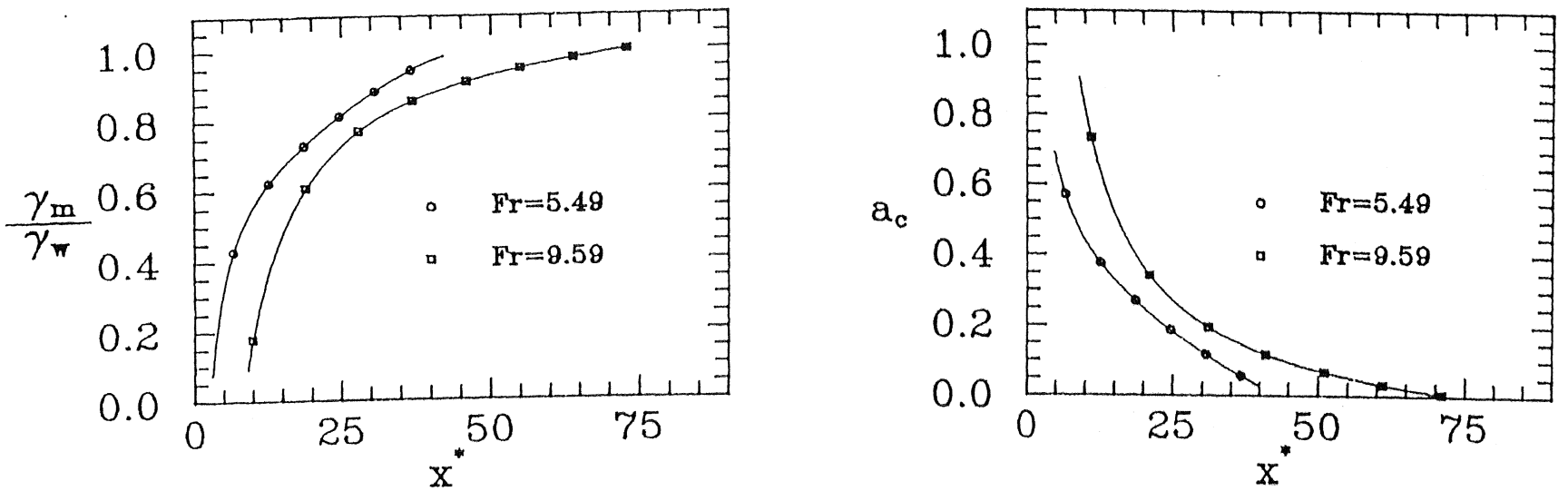

Figure 4.32 : Variation of γ_m / γ_w and air content (a_c) with with distance

Table 4.3a : Comparison of spatial correlation function at a Froude number of about 5.5

Present study		Rinaldo & Fiorotto	
Fr=5.49		Fr=5.7	
x^*	ξ^*	x^*	ξ^*
7	2.00	5	1.40
11	2.25	11	2.00
18	3.40	18	3.00

Table 4.3b : Comparison of spatial correlation function at a Froude number of about 9.5

Present study		Rinaldo & Fiorotto	
Fr=9.59		Fr=9.5	
x^*	ξ^*	x^*	ξ^*
15	5.0	15	2.2
25	6.0	25	3.8
35	7.0	35	7.8
43	9.0	45	10.0

The autocorrelation function is compared to the results obtained by Vasiliev and Bukreyev and Abdul Khader and Elango. It is also compared in terms of value of dimensionless lag time for which the correlation coefficient become zero. Table 4.4 shows the comparison.

Table 4.4 : Comparison of autocorrelation function at a Froude number of about 5.5

Present Study		Khader & Elango		Vasiliev & Bukreyev	
Fr= 5.49		Fr=5.9		Fr=5.74	
x^*	τ^*	x^*	τ^*	x^*	τ^*
5.0	4.50	5.0	3.00	-	-
9.5	5.50	11.0	5.50	10	5
13.5	6.25	18.0	10.00	-	-
22.0	12.00	25.0	20.00	-	-
31.0	24.00	31.0	28.00	-	-

The spectra obtained had some noise added to it, but the averaged spectra shows the trend which is discussed in the result obtained by Khader and Elango.

CHAPTER - 5

CONCLUSIONS AND SCOPE OF FURTHER STUDIES

5.1 Conclusions

The following conclusions have been drawn in the present study :

(1) Decay rate of standard deviation are greater for the pressure signal than for the depth signal with respect to distance from toe of the jump, i.e., the pressure fluctuations although more intense initially near the toe, subsequently become small.

(2) The probability density function (PDF) of the pressure and depth signals are comparable to the PDF of a Gaussian signal at all locations.

(3) The spatial correlation between pressure and depth increases with distance from the toe. Depth signals are more correlated in space as compared to the pressure signals at a given point and Froude number.

(4) The transverse correlation is greater than the longitudinal correlation near the toe of the jump in most cases. In other words, the turbulent fluctuations are initially anisotropic and subsequently decay to become isotropic.

(5) The left and the right side transverse correlations were almost equal thus depicting that the flow is symmetric and one dimensional.

(6) The autocorrelation plots show that the degree of correlation of the pressure signal increases with distance from the toe. For the depth signal it remains almost unchanged. The integral scale based on autocorrelation function also confirms this trend.

(7) Both autocorrelation and spectra indicate that the pressure signal is comparable to white noise near the toe, but develops to a Gaussian signal at greater distances. In contrast, the depth signal is close to Gaussian in the entire range over which data is collected.

(8) The cross-correlation between the pressure and depth signals was negligible near the toe of the jump and increases linearly with distance. The rate of increase is identical for the two Froude numbers studied.

(9) The effect of air entrainment is clearly seen in data. Air content decreases with the increase of distance.

4.2 Scope for Further Studies

(1) The present work can be carried out at different Froude numbers and the trends can be explained with greater reliability.

(2) The air content can be measured independently by a suitable instrument and compared to the result obtained in the study.

(3) The study for fluctuations can be carried out separately using longer record lengths so that the effect of data size and sampling rates on the turbulence statistics can be ascertained.

REFERENCE

1. **ABDUL KHADER, M. H. and ELANGO, K.** (1974), Turbulent Pressure Field beneath a Hydraulic Jump, Journal of Hydraulic Research, Vol. 12(4), 469-489.

2. **BOWER, E. C. and TOSO, J.** (1988), Extreme Pressure in Hydraulic Jump Stilling Basin, Journal of Hydraulic Engineering ASCE, Vol. 114(8), 829-843.

3. **FIOROTTO, V. and RINALDO, A.** (1992), Turbulent Pressure Fluctuation under Hydraulic Jump, Journal of Hydraulic Research, Vol. 30(4), 499-520.

4. **LEUTHEUSSER, H. J. and KARTHA, V. C.** (1972), Effect of Inflow Condition on Hydraulic Jump, Journal of Hydraulic Division ASCE, Vol. 98(HY8), 1367-1385.

5. **LOPARDO, R. A. and HENNING, R. E.** (1985), Experimental Advances on Pressure Fluctuation beneath Hydraulic Jump, Proceedings, 21st Congress, International Association of Hydraulic Research, Melbourne, Australia, Vol. 3, 633-638.

6. **ROUSE, H., SIAO, T. T. and NAGARATNAM, S.** (1955), Turbulence Characteristics of Hydraulic Jump, Transactions of ASCE, Vol. 124, 926-950.

7. **VASILIEV, O. F. and BUKREYEV, V. I.** (1967), Statistical Characteristics of Pressure Fluctuation in the Region of Hydraulic Jump, Proceedings, 12th Congress, International Association of Hydraulic Research, Colorado, Vol. 2, 1-8.

APPENDIX

1. Algorithm for calculation of Power Spectrum and Auto Correlation

Step 1. Split the data in 8 equal parts of 1024 points.

Step 2. Select one set of data point and convert it to actual value of quantity (x_i).

Step 3. Find the mean of quantity (x_m).

Step 4. Remove the mean from the quantity, i.e., $x_i' = x_i - x_m$.

Step 5. Find the Fourier Transformation of the mean removed signal through FFT algorithm

Step 6. Repeat step (2) to step (5) for each set of data point

Step 7. Find the average of real and imaginary, at each frequency, of transformed quantity of 8 set

Step 8. Find the amplitude as square root of sum of square of real and imaginary part at each frequency.

Step 9. Find the Nyquist frequency ($f_{ny} = 1 / 2\Delta$, Δ = time interval of record).

Step 10. Find the Fourier transformation of amplitude.

Step 11. Auto correlation function ordinate are calculated as real part of transformed quantity.

2. Algorithm for Calculation of PDF and Statistical Quantity

Step 1. Read the signal and convert it to actual value (x_i).

Step 2. Find the mean of the signal (x_m).

Step 3. Remove the mean from the signal, i.e., $x_i' = x_i - x_m$.

Step 4. Find the absolute maximum and minimum value of the mean removed signal.

Step 5. Divide the whole range of signal in 50 equal part.

Step 6. Find the relative frequency of each.

Step 7. Find the range on the minimum side of data such that the area under PDF for this range is 0.1 of the total area of PDF

Step 8 The statistical minimum is the average of value in this range

Step 9. Find the range on the maximum side of data such that the area under PDF for this range is 0.1 of the total area of PDF

Step 10. The statistical maximum is the average of value in this range

Step 11. Find the skewness, kurtosis and standard deviation using appropriate integral as discussed in text.

Step 12 Find the PDF of Gaussian signal with the same standard deviation value.

Step 13 Find the kurtosis of the Gaussian signal calculated in Step-12.

3. Algorithm for Space Correlation

Step 1 Read the signal for reference point and convert it to actual value, i.e., x_{1i} , where x is either p or h

Step 2 Read the signal for second point and convert it to actual value, i.e., x_{2i} .

Step 3 Find the mean of the either signal (x_{1m} and x_{2m}).

Step 4 Remove the mean from the respective signal, i.e.,

$$x'_{1i} = x_{1i} - x_{1m}, \text{ and}$$

$$x'_{2i} = x_{2i} - x_{2m}.$$

Step 5 Find the sum as $S = \sum_{i=1}^{N} x'_{1i} \cdot x'_{2i}$, N = total number of points.

Step 6 Find the RMS value of mean removed signal, i.e., σ_1 and σ_2 .

Step 7 Find the correlation coefficient as,

$$R = \frac{S}{N \cdot \sigma_1 \cdot \sigma_2}$$

4. Algorithm for Cross Correlation

Step 1 Read the pressure signal at a point and convert it to actual value, P_i , i = 1, N. N is total of points in sample space.

Step 2 Read the depth signal at the same point and convert it to actual value, h_i , i = 1, N.

Step 3 Find the mean of either signal, i.e., P_m and h_m .

Step 4 Remove the mean from either signal, i.e.,

$$P'_i = P_i - \underline{P}_m \text{ , and}$$

$$h'_i = h_i - \underline{h}_m \text{ .}$$

Step 5 Find the RMS value of either mean removed signal, i.e. σ_p and σ_h

Step 6 Find the sum as, $S = \sum_{i=1}^{N} P'_i \cdot h'_i$.

Step 7 Find the correlation coefficient as,

$$R_{Ph} = \frac{S}{N \cdot \sigma_p \cdot \sigma_h}$$